

---

# Self-assembly of Artificial DNA Nano and Microscale Motifs

Thomas L. Sobey

---



Munich 2010



---

# Self-assembly of Artificial DNA Nano and Microscale Motifs

Thomas L. Sobey

---

Dissertation  
at the Faculty of Physics  
Ludwig-Maximilians-Universität  
Munich, Germany

authored by  
Thomas L. Sobey  
from Albury, Australia

15.07.2010

Supervisor: Professor Friedrich C. Simmel  
Co-supervisor: Professor Philip Tinnefeld  
Date of Examination: 19.08.2010

## Abstract

Nanotechnology attempts to control matter at the nanometer scale so that new types of materials, components and devices for a wide variety of applications can be developed. There are two approaches possible. The first stems from semiconductor technology in which improvements in processing small structures have led to a drastic reduction in the size of electronic components. The inverse approach – which is used in this work – orientates itself around structures based on biological systems, in which highly dynamic nanometer size components assemble themselves.

In this thesis it is shown how defined structures with sizes ranging from nanometers to micrometres and made up of DNA molecules can self assemble. Self-assembly has four defining features: structured particles, a suitable environment, a driving force and reversible binding. DNA molecules are relatively stable and can be synthesised with arbitrary sequences of four units, diffuse freely in an aqueous buffer under Brownian motion, and can bind and unbind (using hydrogen bonding) with one another in the practical temperature range between 0 and 100°C. They are thus useful building blocks for self-assembly.

A review is provided of some physical properties of DNA, and of self-assembled DNA ‘motifs’ and devices developed to date, along with examples that have been demonstrated here in the laboratory. Such examples include DNA nanotubes, lattices, and ‘origami’ structures.

The idea of assembling structures – not by creating and breaking hydrogen bonds using temperature changes – but rather by changing the concentration of small molecules known as denaturants is introduced. The denaturants also form hydrogen bonds and can occupy the binding sites of the DNA molecules. Decreasing the concentration of denaturants frees the binding sites and allows the self-assembly of structures. This is demonstrated with successful motifs, and provides an isothermal assembly technique that allows the use of many temperature-sensitive components in DNA self-assembly.

It is shown that self-assembled motifs are useful as templates for nanoscale objects such as fluorescent molecules, which can be set out in defined geometries. Moreover, using newly developed optical super-resolution techniques, such geometries are resolved below the optical diffraction limit, providing the possibility for nanoscale optical calibration standards.

And finally the intrinsic stability of three-dimensional structures as compared to two-dimensional structures is investigated, in that the assembly and ‘melting’ of DNA nanotubes is shown to be fundamentally different to that of DNA lattices, with the closed form of the tubes providing a natural and significantly higher stability. This will be useful for designing and building stronger structures in DNA nanotechnology.



# Zusammenfassung

Nanotechnologie strebt die Kontrolle von Materie auf der Nanometerskala an, wovon man sich die Erzeugung von neuartigen Materialien und Werkstoffen für verschiedenste technologische Anwendungen erhofft. Grundsätzlich gibt es hierfür zwei unterschiedliche Ansätze. Der eine leitet sich von der Halbleitertechnologie ab, in der die Verfeinerung von Strukturierungsprozessen in den letzten Jahrzehnten zu einer drastischen Verkleinerung von elektronischen Bauelementen geführt hat. Der umgekehrte Ansatz - der in der vorliegenden Arbeit verfolgt wird - orientiert sich an der Strukturbildung in biologischen Systemen, in denen nanometerskalige Strukturen durch hochdynamische, molekulare Selbstanordnungs- und Selbstorganisationsprozesse erzeugt werden.

Im Folgenden wird gezeigt, wie mit Hilfe von Selbstanordnungsprozessen aus DNA-Molekülen definierte Strukturen im Nanometer- bis Mikrometer- Bereich erzeugt werden können. Selbstanordnungsphänomene treten auf, wenn folgende vier Voraussetzungen erfüllt sind: die sich organisierenden Einheiten haben eine spezielle Struktur; sie befinden sich in einer geeigneten Umgebung; es existiert eine Triebkraft für die Organisation und die Bindungen zwischen den Einheiten sind reversibel. DNA Moleküle erfüllen diese Bedingungen. Sie sind chemisch relativ stabil und können mit beliebigen Sequenzen aus vier „DNA-Basen“ synthetisiert werden, sie diffundieren in wässriger Umgebung unter dem Einfluss Brown'scher Bewegung und sie können bei moderaten Temperaturen Bindungen (Wasserstoffbrücken) eingehen und wieder lösen.

In der vorliegenden Arbeit wird zunächst ein Überblick über die physikalischen Eigenschaften von DNA-Moleküle gegeben und danach Beispiele von bisher entwickelten selbstanordnenden „DNA-Motiven“ und DNA-Maschinen vorgestellt. Daraufhin werden mehrere strukturelle DNA-Motive vorgestellt, die im Rahmen dieser Arbeit erzeugt wurden, z.B. DNA-basierte Nanoröhren, zweidimensionale DNA-Gitter und DNA-„Origami-Strukturen“. Insbesondere wird dabei gezeigt, dass man solche DNA-Strukturen auch herstellen kann, indem man die Bildung von Wasserstoffbrückenbindungen nicht nur durch Temperaturänderungen beeinflusst, sondern durch Konzentrationänderungen von sogenannten „Denaturierungsmitteln“. Die Denaturierungsmittel formen ebenfalls Wasserstoffbrücken und können die Bindungen der DNA besetzen. Fortwährende Verdünnung der Denaturanten setzt die Bindungen wieder frei, und führt daher zur kontrollierten Selbstanordnung der DNA-Strukturen.

Selbstanordnende DNA-Motive haben sich als geeigneten Vorlagen für die Erzeugung nanoskaliger Strukturen erwiesen. Zum Beispiel können fluoreszierende Moleküle in definierten Geometrien an DNA-Origami-Vorlagen angebunden werden. In dieser Arbeit wird mit den neuartigen optischen Methoden der Superresolutionsmikroskopie gezeigt, wie man solche Molekülmuster auch unterhalb der Beugungsgrenze auflösen kann. Aufgrund ihrer Nanometerpräzision könnten solche Strukturen auch als „Eichstandards“ für die Superresolutionsmikroskopie verwendet werden.

Im abschließenden Teil der Arbeit wird die intrinsische Stabilität dreidimensionaler Strukturen im Vergleich zu zweidimensionalen Strukturen untersucht. Dabei wird demonstriert, dass die thermisch getriebene Dissoziation (der „Schmelzübergang“) von dreidimensionalen DNA-Nanoröhren wesentlich anders ist, als die von zwei dimensionaler DNA-Gittern. Dies liegt an kooperativen Wechselwirkungen aufgrund der geschlossenen Form der Röhren, wodurch diese eine erhebliche höhere Stabilität erhalten.



# Contents

<b>1</b>	<b>Introduction</b>	<b>v</b>
1.1	Motivation for this thesis . . . . .	v
1.2	Outline of this thesis . . . . .	vii
<b>I</b>	<b>Self-assembly and DNA</b>	<b>1</b>
<b>2</b>	<b>Self-assembly itself</b>	<b>3</b>
2.1	Introduction . . . . .	3
2.1.1	Structured particles . . . . .	5
2.1.2	Reversible binding forces . . . . .	5
2.1.3	Environment . . . . .	6
2.1.4	Driving forces . . . . .	7
2.1.5	Boundaries . . . . .	7
2.1.6	Types of self-assembly . . . . .	7
2.1.7	Equilibrium . . . . .	7
2.1.7.1	Static . . . . .	7
2.1.7.2	Dynamic . . . . .	7
2.1.8	Information content . . . . .	8
2.1.8.1	Templated . . . . .	8
2.1.8.2	Algorithmic . . . . .	8
2.1.9	Level . . . . .	9
2.1.9.1	Single level . . . . .	9
2.1.9.2	Multi-level . . . . .	9
2.2	Other aspects of self-assembly . . . . .	9
2.2.1	Energy minimisation . . . . .	9
2.2.2	Nucleation. . . . .	9
2.3	Engineered self-assembly . . . . .	9
2.3.1	Forward and backward problems . . . . .	10
2.3.2	Yield . . . . .	10
2.3.3	Defects . . . . .	10

<b>3</b>	<b>DNA as a structured particle for self-assembly</b>	<b>11</b>
3.1	Some physical properties of DNA . . . . .	12
3.1.1	DNA as a molecule and polymer . . . . .	12
3.1.2	Secondary structure . . . . .	13
3.1.3	Mechanical properties . . . . .	15
3.1.3.1	Freely Jointed Chain . . . . .	15
3.1.3.2	Worm-Like Chain . . . . .	18
3.1.4	Hybridisation and denaturation . . . . .	19
3.1.5	DNA melting . . . . .	19
3.1.6	Optical properties . . . . .	21
3.1.7	DNA as a polyelectrolyte . . . . .	23
3.1.7.1	Number of counterions . . . . .	24
3.1.7.2	Distribution of counterions . . . . .	25
3.2	Kinetics and thermodynamics of DNA molecules and reactions . . . . .	25
3.2.1	Kinetics . . . . .	25
3.2.1.1	First order reaction . . . . .	26
3.2.1.2	Second order reaction . . . . .	27
3.2.1.3	Two-step reaction . . . . .	28
3.2.1.4	Hybridisation and branch migration . . . . .	29
3.2.2	Thermodynamics . . . . .	30
3.2.2.1	Gibbs energy and the van't Hoff equation . . . . .	30
3.2.2.2	Enthalpy and entropy . . . . .	31
3.2.2.3	Thermal stability . . . . .	32
3.2.2.4	Secondary structure . . . . .	33
3.2.2.5	Melting . . . . .	35
3.3	Summary . . . . .	38
3.4	Examples of DNA self-assembly from the literature . . . . .	38
3.4.1	The beginning of the field . . . . .	38
3.4.2	Quasi one dimensional . . . . .	38
3.4.3	Two dimensional . . . . .	38
3.4.4	Three dimensional . . . . .	39
<b>II</b>	<b>Equipment and Methods</b>	<b>45</b>
<b>4</b>	<b>Assembly and measurement techniques [1]</b>	<b>47</b>
4.1	Equipment and techniques . . . . .	49
4.1.1	Absorption spectroscopy . . . . .	49
4.1.2	Gel electrophoresis . . . . .	50
4.1.3	Fluorescence microscopy . . . . .	53
4.1.4	Total internal reflection fluorescence microscopy . . . . .	55
4.1.5	Super-resolution microscopy . . . . .	57
4.1.6	Atomic force microscopy . . . . .	60

---

4.2	Materials . . . . .	66
4.2.1	Absolute concentration by UV absorption . . . . .	69
4.2.2	Relative concentration by polyacrylamide gel electrophoresis . . . . .	69
4.2.3	Thermal annealing . . . . .	70
4.2.4	Fluorescence microscopy . . . . .	71
4.2.5	Atomic force microscopy in fluid . . . . .	72
4.3	Steps . . . . .	72
4.3.1	Absolute concentration by UV absorption . . . . .	72
4.3.2	Relative concentration by polyacrylamide gel electrophoresis . . . . .	75
4.3.3	Thermal annealing . . . . .	79
4.3.4	Fluorescence microscopy . . . . .	80
4.3.5	Atomic force microscopy in fluid . . . . .	81
 <b>III Results &amp; Discussion</b>		 <b>87</b>
<b>5</b>	<b>DNA nanodevices [2]</b>	<b>89</b>
5.1	Using DNA as an intermediary between information processing and mechanical action . . . . .	89
5.2	Characterising DNA nanodevices experimentally . . . . .	90
5.3	Towards molecular motors based on DNA . . . . .	90
5.4	DNA walkers . . . . .	94
5.5	Novel DNA biosensors . . . . .	95
5.6	DNA nanodevices controlled using genetic mechanisms . . . . .	97
<b>6</b>	<b>Examples of DNA self-assembly demonstrated</b>	<b>101</b>
6.1	DNA lattices . . . . .	101
6.2	DNA nanotubes . . . . .	103
6.3	Stretched and aligned DNA . . . . .	105
6.4	DNA-wrapped carbon nanotubes with quantum dots . . . . .	108
6.5	DNA-wrapped carbon nanotubes with origami rectangles . . . . .	109
<b>7</b>	<b>Isothermal assembly of DNA origami structures using denaturing agents [3]</b>	<b>111</b>
<b>8</b>	<b>DNA origami as a nanoscopic ruler for super-resolution microscopy [4]</b>	<b>115</b>
<b>9</b>	<b>Assembly and melting of DNA nanotubes from single-sequence tiles [5]</b>	<b>121</b>
<b>10</b>	<b>Conclusion and outlook for self-assembly with DNA and self-assembly itself. . .</b>	<b>131</b>
10.1	Overview . . . . .	131
10.2	Future experiments . . . . .	133
10.3	The future of understanding self-assembly . . . . .	135

Bibliography	137
Acknowledgements	147
Résumé	148

# Chapter 1

## Introduction

### Contents

---

1.1	Motivation for this thesis . . . . .	v
1.2	Outline of this thesis . . . . .	vii

---

### 1.1 Motivation for this thesis

As a child, I often wondered why things in the natural world are as they are. And why are they not different? Why are leaves the size they are? And the shape they are? And why are there so many different leaves? Are any two identical? And how do they grow to be like that? What about trees, animals, rocks, stars...

Scientists are beginning to be able to answer these questions. But the answers aren't coming just from biologists. Or from physicists, chemists, mathematicians or any of the other natural science disciplines. They are coming from work from all of these together, in a gradual merging of the disciplines. And to find the answers, scientists are having to look at finer and finer details, and at each level they find answers which bring new questions that require them to look at even finer (smaller) details for new answers. Scientists finally now think that they may have reached the appropriate level of detail (size), so that they can begin to give real answers. This level of detail is the nanometer. One billionth of a meter. Small, but that is where the answers seem to lie.

The surprising thing is, that this is true not just for leaves, but for many examples in the natural world: us for example, as we grow and live.

This level is the level of atoms and molecules.

People are asking questions, and scientists are working on answering them. But there another facet to this. Engineers are building smaller and smaller 'things'. Whether it's computer chips, sensors for airbags in cars, or medical devices that help our body recover from injury or sickness, to name a few. And engineers are reaching limits. They have been using big blocks of 'stuff' and 'carving' them up and molding them into shapes and

machines and circuits. Somewhat like artists carve statues. Top-down – starting from the ‘top’ and carving ‘down’.

There is another approach – the opposite – bottom-up – starting with small building blocks and building up. And this may become an increasingly important way in the future. The building blocks are atoms and molecules, and the results are what we can build from these.

However, there is still another facet to all this. No one ‘puts’ leaves together. And it is difficult to ‘put’ atoms and molecules together. Which is where self-assembly comes in. Self-assembly is about how things put themselves together. Magnets in a row for example that snap together. The processes of self-assembly are found throughout nature: in living beings, plants, mineral and crystal formation, and the universe itself, to name a few examples. It occurs from the smallest atomic scales up to scales between galaxies. And it is what might allow engineers to use ‘bottom-up’ approaches to small-scale technology: nanotechnology. By understanding self-assembly scientists may better be able to answer the questions we ask.

There is one last ingredient that needs to be added to this story, and that is deoxyribonucleic acid, or DNA. The molecular carrier of genetic information that allows copying of characteristics from one living generation to the next. And a unique molecular structure that has properties found nowhere else in natural or synthetic chemistry. It is these properties that make it a perfect building block for self-assembly at the nanoscale.

This thesis is not about leaves. Or the other examples. But to understand them, one needs to understand this new discipline of self-assembly. These factors come together in this thesis, and are discussed either directly or indirectly throughout it. To improve our understanding of self-assembly we ‘play’ with it scientifically to develop small defined structures. And in the future we may be able to assemble these to develop longer and more complicated structures in a multi-level assembly process. And by doing so begin to understand how ‘nature’ assembles beautiful and complicated structures such as leaves.

## 1.2 Outline of this thesis

In the following a brief outline of this thesis is given:

- Chapter two – an introduction to self-assembly.
- Chapter three – an introduction to the physical properties of DNA.
- Chapter four – a description of some of the experimental techniques used.
- Chapter five – a review of self-assembled DNA nanostructures from the literature.
- Chapter six – examples of DNA self-assembly demonstrated in this work.
- Chapter seven – proof that DNA complex structures can be assembled at constant temperature.
- Chapter eight – use of self-assembled DNA structures as molecular platforms for super-resolution microscopy.
- Chapter nine – verification that three-dimensional DNA nanostructures can be more stable than two-dimensional nanostructures.
- Chapter ten – a view of what might be done in the future.



# Part I

## Self-assembly and DNA



# Chapter 2

## Self-assembly itself

### Contents

---

<b>2.1</b>	<b>Introduction</b>	<b>3</b>
2.1.1	Structured particles	5
2.1.2	Reversible binding forces	5
2.1.3	Environment	6
2.1.4	Driving forces	7
2.1.5	Boundaries	7
2.1.6	Types of self-assembly	7
2.1.7	Equilibrium	7
2.1.8	Information content	8
2.1.9	Level	9
<b>2.2</b>	<b>Other aspects of self-assembly</b>	<b>9</b>
2.2.1	Energy minimisation	9
2.2.2	Nucleation.	9
<b>2.3</b>	<b>Engineered self-assembly</b>	<b>9</b>
2.3.1	Forward and backward problems	10
2.3.2	Yield	10
2.3.3	Defects	10

---

## 2.1 Introduction

Self-assembly is about how things put themselves together. There are many examples in the world around us, indeed our bodies and the universe are products of self-assembly. And so are trees, diamonds, schools of fish, galaxies, DNA molecules, the list goes on...



Figure 2.1: Examples of self-assembly: *a)* bubbles on a liquid surface *b)* galaxy M81 *c)* a Bismuth crystal *d)* a Ferrofluid in a magnetic field.

Scientists are interested in understanding how such complexity, order and patterns can arise. There are several reasons for this. Humans are fascinated by the origins of the universe and life. Self-assembly appears to be important from the very smallest to the very largest scales that we know of. The intricate structures and processes that occur within living creatures might be partially explained with self-assembly. Mimicking nature, we might use self-assembly techniques to build artificial systems, this may be especially important in nanotechnology, where the parallel arrangement of atoms and molecules is important. And finally, the understanding of the spontaneous development of patterns connects the studies of individual components and many interacting components. It thus links scientific reductionism to complexity and emergence.

Researchers from many disciplines have been, and continue to work on understanding self-assembly. Some examples of natural and artificial self-assembled systems are shown in and a brief history of some important advances in this field are listed in Table 2.1 on page 6.

Physicists are pursuing galaxy formation, chemists are coaxing out larger and complexer molecules and crystals, biologists are busy measuring cell processes, mathematicians are modelling pattern formation, and computer scientists are developing algorithms that engineers can use to take advantage of self-assembly. The question arises as to whether those that concentrate their research on self-assembly really belong to any one traditional discipline, perhaps they belong to a new emerging discipline?

How exactly do we define self-assembly? There have been many attempts, I freely borrow from Professor John Pelesko's (University of Delaware) recent comprehensive and precise definition:

*Self-assembly refers to the spontaneous formation of organised structures through a stochastic process that involves pre-existing structured components, binding forces that are reversible, an environment, and a driving force.*

Let us examine the terms in this definition. Spontaneous formation occurs, given that the conditions in the rest of the definition are met. Organised structures allow us to differentiate from simple aggregated structures (for example: precipitates in chemistry). Stochastic processes indicate that there are some random as well as predictable elements that occur during formation. A discussion of the particularly important factors: structured particles, reversible binding forces, an environment, and a driving force, is given in the following.

### 2.1.1 Structured particles

These are the building blocks of self-assembled structures. Simple examples include atoms and molecules that form crystals and bubbles that form bubble rafts. Structure is particularly important in lipids that form micelles, the detailed shape of 'head' and 'tail' of the lipid molecule determines the shape of the micelle formed. Similarly, the type of side chain in amino acids determines to some extent how a protein folds together. We can see from these examples that structure plays a crucial role.

### 2.1.2 Reversible binding forces

These are the forces that hold the structured particles together. They can be forces between the structured particles themselves, or interactions between the structured particles and their environment. Examples of the first include ionic bonds in metallic crystals and capillary forces between bubbles. Examples of the second are hydrophobic and hydrophilic interactions of lipid molecules with water molecules, these minimise/maximise the interaction with water molecules. By reversible we mean that the binding can be broken allowing

---

1930s	Alan Turing develops the theory of universal computation.
1950s	John von Neumann develops a theory of automata replication.
1953	James Watson and Francis Crick analyse the structure of DNA.
1955	H. Fraenkel-Conrat and R. Williams self-assemble the tobacco mosaic virus in a test tube.
1957	Penrose and Penrose construct a simple self-replicating system.
1961	Hau Wang develops “Wang Tiles” demonstrating the equivalence of tiling problems and computation.
1991	Nadrian Seeman and Junghuei Chen self-assemble a cube from DNA.
1994	Leonard Adleman launches the field of DNA computation by using DNA to solve a Hamiltonian path problem.
1996	Kazuo Hosokawa’s group demonstrates microscale self-assembly using surface tension.
2000	George Whiteside’s group self-assembles electrical networks from millimetre scale polyhedra.
2000	Yurke, Simmel, Neumann and colleagues self-assemble a DNA-fuelled molecular machine
2004	William Shih adapts the methods of Seeman to self-assemble a DNA octahedron.
2004	Eric Winfree and Paul Rothemund self-assemble a Sierpinski triangle from DNA demonstrating that self-assembly may be used for computation.
2009	Liedl, Dietz and Shih demonstrate three dimensional self-assembly using origami techniques.
2010	Self-assembly research continues to expand and draw the interest of scientists from many fields.

---

Table 2.1: Landmarks in Self-assembly

particles that initially bind in a wrong position to unbind and move around to a correct position. Binding forces can thus be defined as those forces that hold a system in an ordered state.

### 2.1.3 Environment

The structured particles are confined in some way and/or something. For lipid molecules it is the surrounding water molecules, for the carbon atoms forming a natural diamond crystal it is the surrounding molten rock. Both of these examples of environments are fluids, and this is the general case. There is a good reason for this, we noted in the definition that organisation and reversible binding are important: the structured particles must be able to move around and create and break bonds (the binding forces) with one another until they are in a position that fits in the organisation of the structure. This can generally only

occur in fluids. Properties of the environment can also play an important role: the rate that the temperature of the molten rock falls determines the size of diamond crystals, the salt concentration in the solution can affect the shape of the micelle formed.

### 2.1.4 Driving forces

As mentioned in the previous section on the environment, the structured particles need to be able to move around to find a position in the organised structure. The force that moves them could be called the driving force. This is often - but not always - forces that are involved in Brownian motion. That is, the forces that 'jostle' the particles in their environment, for example lipid molecules interacting with water molecules. For bubbles sitting on a curved liquid surface forming a bubble raft, the driving force is gravity.

The structured particles move around until bound into position by the binding forces. Sometimes they are subsequently removed from their position by the driving force, and either rebind, are replaced by another structured particle, or the position is left empty.

### 2.1.5 Boundaries

The boundaries between these four components - structured particles, binding forces and driving forces, and the environment - is not always clear. At intermediate distances binding and driving forces can blur. The environment or its properties may change the structure of the particle, and the driving force may be provided by the environment. The four components provide a means of analysing, understanding and classifying self-assembly, but they are not rigid. For reference, a summary of the components is provided in Table 2.2 on page 8.

### 2.1.6 Types of self-assembly

Three different classes might be suggested for identifying types of self-assembly. These are based on equilibrium characteristics, information content, or level.

#### 2.1.7 Equilibrium

##### 2.1.7.1 Static

Those processes that lead to structures in either local or global equilibrium.

##### 2.1.7.2 Dynamic

Those processes that lead to non-equilibrium structures. These structures exist only so long as the system is dissipating energy.

---

Structured particles	These are the components that actually do the assembling. The inherent structure of the particles determines the complexity of the final self-assembled system. Tailoring the structure of the particles provides the first means of control of the self-assembling system. Examples of structured particles include magnets, lipids, proteins and DNA.
Reversible binding forces	This is what holds the particles together. Usually, this binding is reversible, allowing the system to move from local equilibria to a global equilibrium. Altering the binding force provides a second means of control of a self-assembling system. The interaction of the particles or external stimuli may activate or alter binding forces in the system. Examples of binding forces include capillary forces, electromagnetic forces, and chemical bonds.
Environment	The particles are embedded in an environment. The proper environment is necessary in order for the binding force to act. For example, capillary forces are only useful when the particles live at the surface of a liquid. Tailoring of the environment or dynamically changing the environment provides an important means of control of a self-assembling system. The environment can be manipulated to change the confirmation of particles or alter the binding forces in the system.
Driving force	In order for self-assembly to occur the particles must interact stochastically. This driving force in the system is usually thought of as noise. This may be thermal noise, physical oscillation of the system, or driving via electromagnetic fields.

---

Table 2.2: Nature's four key components of a self-assembling system [6].

## 2.1.8 Information content

### 2.1.8.1 Templated

The environment carries significant information about the final structure e.g. assembly of molecules on a patterned surface.

### 2.1.8.2 Algorithmic

There are multiple types of structured particles and they carry information about the final structure.

### 2.1.9 Level

#### 2.1.9.1 Single level

Structured particles self-assemble into a structure which is the final product e.g. atoms self-assembling into a crystal.

#### 2.1.9.2 Multi-level

Structured components self-assemble into structures, these structures are then components that self-assemble into higher-order structures, and so on, e.g. self-assembly of DNA, RNA, proteins, lipids etc that self-assemble into complete cells, the cells then self-assemble into organs, and so on.

## 2.2 Other aspects of self-assembly

### 2.2.1 Energy minimisation

In static self-assembly, we have said that structures form at a local or global equilibrium. This equilibrium is at a local or global total energy minimum. Examples of the include crystals minimising a chemical potential, lipids minimising their interaction with water molecules, and proteins folding into a lower energy state.

This principle only applies for static self-assembly - dynamic self-assembly dissipates energy.

### 2.2.2 Nucleation.

We have discussed the structured particles moving around in their environment, responding to the driving force and binding with one another. The point at which two particles begin to bind to one another is known as nucleation. Once two particles are bound together in an energy minimising structure, they form what is known as a 'seed' to which other particles can bind and form larger structures. Alternatively, there may be particular structured particles with particular properties that act as seeds by themselves.

Thermodynamically seen, nucleation is a localised first-order phase transition.

## 2.3 Engineered self-assembly

Designing artificial self-assembled systems present four problems. These are forward problems, backward problems, yield and defects.

### 2.3.1 Forward and backward problems

The first two present a choice for the designer. One can take a given set of structured particles, an environment, and binding and driving forces, and thus analyse what structures will form. This is known as the forward problem.

The other possibility is to decide on a structure, and then design the structured particles, an environment and binding and driving forces so that this structure will form. This is known as the backward (or inverse problem).

### 2.3.2 Yield

The stochastic (random) nature of self-assembly results in some of the structures not forming completely. The percentage of complete structures is called the yield.

### 2.3.3 Defects

The reversibility of bond formation in self-assembly allows the correct positioning of the structured particles in the self-assembled structure. However, it also allows correctly positioned particles to be set free, leaving a gap for structures to assemble around before another structured particle can bind into the position. Gaps within self-assembled structures are known as defects.

---

Now that we understand some of the essential ideas of self-assembly, we can go on to discuss DNA, and in particular some of the physical properties of DNA molecules which make them ideal for use in self-assembly.

# Chapter 3

## DNA as a structured particle for self-assembly

### Contents

---

<b>3.1</b>	<b>Some physical properties of DNA</b>	<b>12</b>
3.1.1	DNA as a molecule and polymer	12
3.1.2	Secondary structure	13
3.1.3	Mechanical properties	15
3.1.4	Hybridisation and denaturation	19
3.1.5	DNA melting	19
3.1.6	Optical properties	21
3.1.7	DNA as a polyelectrolyte	23
<b>3.2</b>	<b>Kinetics and thermodynamics of DNA molecules and reactions</b>	<b>25</b>
3.2.1	Kinetics	25
3.2.2	Thermodynamics	30
<b>3.3</b>	<b>Summary</b>	<b>38</b>
<b>3.4</b>	<b>Examples of DNA self-assembly from the literature</b>	<b>38</b>
3.4.1	The beginning of the field	38
3.4.2	Quasi one dimensional	38
3.4.3	Two dimensional	38
3.4.4	Three dimensional	39

---

Here we give an introduction to some of the physical properties of DNA molecules that make them ideal candidates for self-assembly.

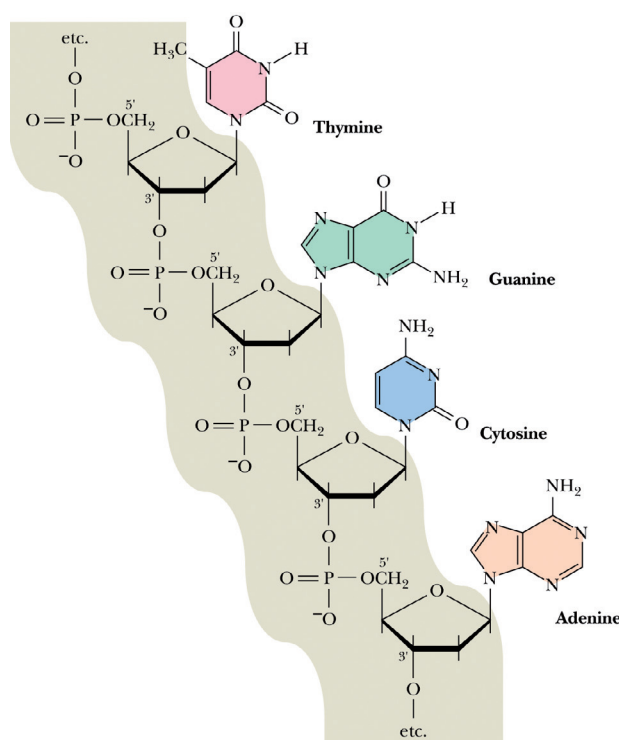


Figure 3.1: The chemical structure of single-stranded DNA [7]<sup>1</sup>.

## 3.1 Some physical properties of DNA

### 3.1.1 DNA as a molecule and polymer

DNA comes in single-stranded and multi-stranded forms. The single-stranded form is a heteropolymer of nucleoside units bound to one another via phosphates. The nucleosides consist of a particular deoxyribose with one of four ‘bases’ adenine, cytosine, guanine or thymine attached to their 1' carbon atoms (Figure 3.1 on page 12). Adenine and guanine are purine molecules with four nitrogen atoms, thymine and cytosine are pyrimidine molecules with two nitrogen atoms. The polymer can be assigned a direction based on its end units: one end terminates with a hydroxyl group at the 3' C atom (the 3' end), the other end terminates with a phosphate group at the 5' C atom (the 5' end). DNA sequences are written from the 5' end to the 3' end. Many enzymes work in one direction or the other.

Two single-strands can bind (hybridise) together using Watson-Crick base pairing. This is a way the bases use hydrogen bonds to bind to each other. Adenine and thymine (often written as A and T) can pair with two hydrogen bonds, cytosine and guanine (often written as C and G) can pair with three hydrogen bonds (Figure 3.2 on page 13). This results in a cytosine-guanine pair being more stable than an adenine-thymine pair. In general, only these pairs can form, other combinations are not possible (in special conditions there are

<sup>1</sup>From GARRETT/GRISHAM. Biochemistry, 4E. © 2009 Brooks/Cole, a part of Cengage Learning, Inc. Reproduced by permission. [www.cengage.com/permissions](http://www.cengage.com/permissions)

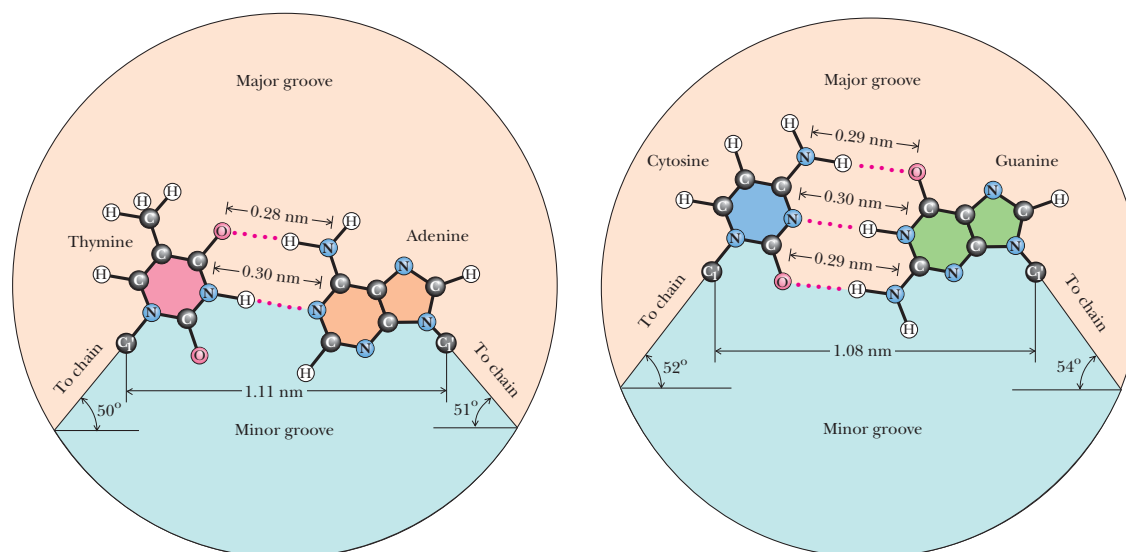


Figure 3.2: Watson-Crick base pairing: thymine can bind to adenine with two hydrogen bonds, cytosine can bind to guanine with three hydrogen bonds [7]<sup>2</sup>.

exceptions, but this is unusual). This pairing brings about the concept of complementarity, two single strands that have the correct sequences in the correct directions to pair with one another are known as complementary. Note that the strands bind in an anti-parallel configuration.

Two single-strands bound together are known as double-stranded DNA, and under physiological conditions this takes on the form of a right-handed helix, with 10.5 base pairs per helical turn, and one helical turn has a length of 3.4 nm and diameter of 2 nm. This form is known as the ‘B’ form (there are two other forms taken on in different environmental conditions). The helix is not symmetric but has a major groove and minor groove. The orientation of the base pairs can be described by a set of six parameters roll, slide, tilt, shift, twist, and rise, as shown in Figure 3.5 on page 16.

The structural parameters of the B form DNA double helix can be found in Table 3.1 on page 15.

### 3.1.2 Secondary structure

Single-stranded DNA can often interact with itself through base pairing interactions. This results in ‘secondary’ structure forming within the molecule, and can often be uniquely decomposed into stems and loops. Frequently these elements, or combinations of them,

<sup>2</sup>From GARRETT/GRISHAM. Biochemistry, 4E. © 2009 Brooks/Cole, a part of Cengage Learning, Inc. Reproduced by permission. www.cengage.com/permissions

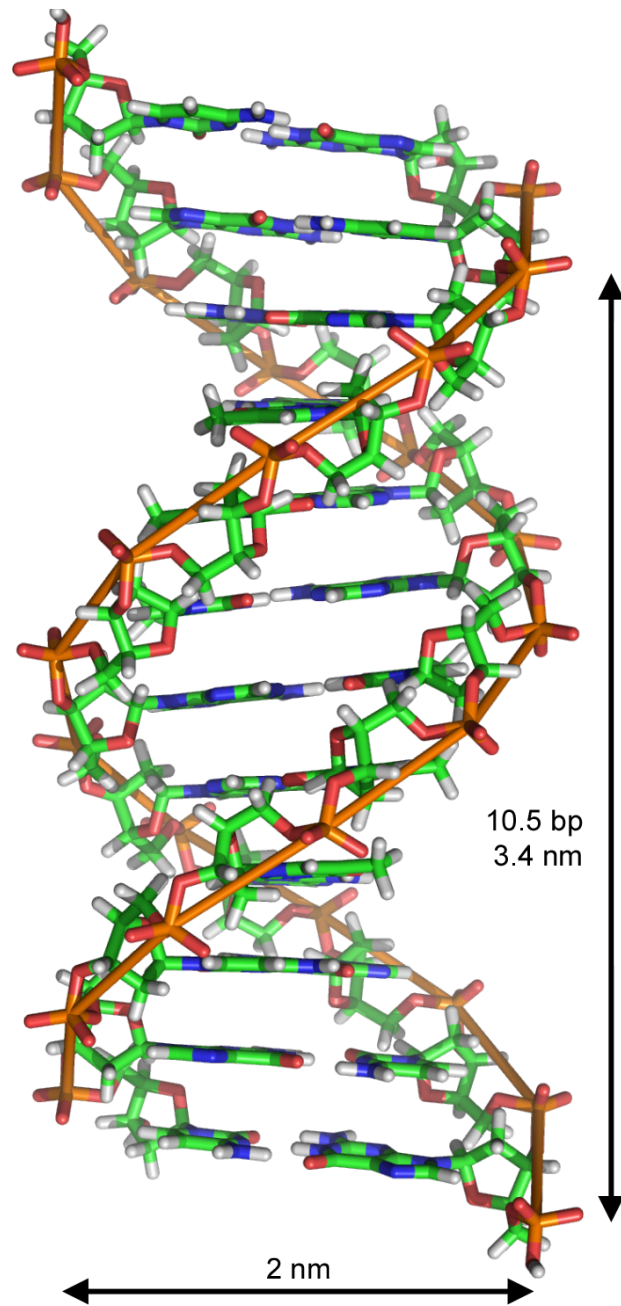


Figure 3.3: Depiction of a B-form DNA double helix [8].

<i>Structural Parameter</i>	<i>B-DNA</i>
Direction of helix rotation	Right handed
Residue per helical turn	10.5 $\text{\AA}$
Axial rise per residue	3.4 $\text{\AA}$
Pitch (length) of the helix	34 $\text{\AA}$
Base pair tilt	$-6^\circ$
Rotation per residue	$34.3^\circ$
Diameter of helix	20 $\text{\AA}$

Table 3.1: Structural parameters of B form DNA.

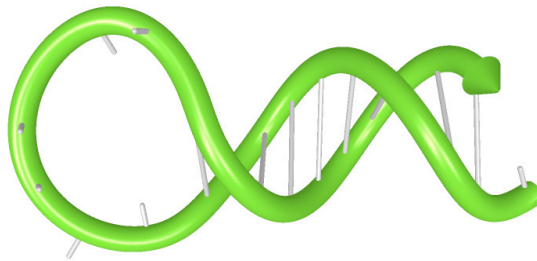


Figure 3.4: Depiction of an example of secondary structure within single stranded DNA: a stem and loop forming a so-called hairpin [9].

can be further classified, for example, tetraloops, pseudoknots and stem-loops. Examples of how secondary structure can theoretically be predicted are given in Section 3.2.2.4.

### 3.1.3 Mechanical properties

There are various models to describe polymers of different flexibilities. Double-stranded DNA is somewhat inflexible and described by a Worm-Like Chain model. Single-stranded DNA is quite flexible and often described using a Freely Jointed Chain model.

#### 3.1.3.1 Freely Jointed Chain

Each monomer in the chain is at point  $\mathbf{x}_i$  in space for  $i = 0, 1, \dots, N$ . We can define the bonds (see Figure 3.6a on page 18) that connect these monomers

$$\mathbf{r}_i = \mathbf{x}_i - \mathbf{x}_{i-1} \quad (3.1)$$

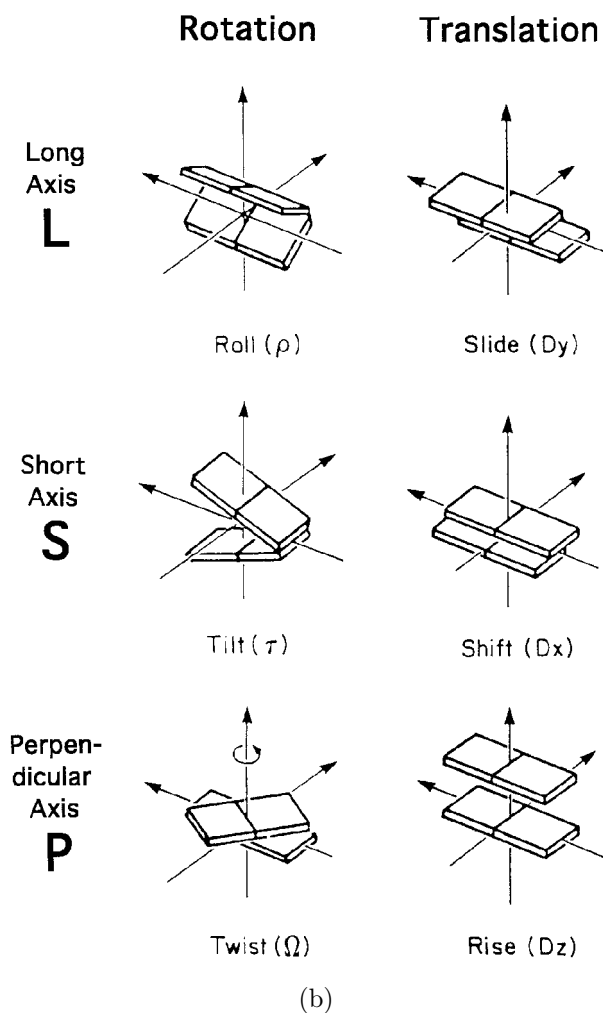
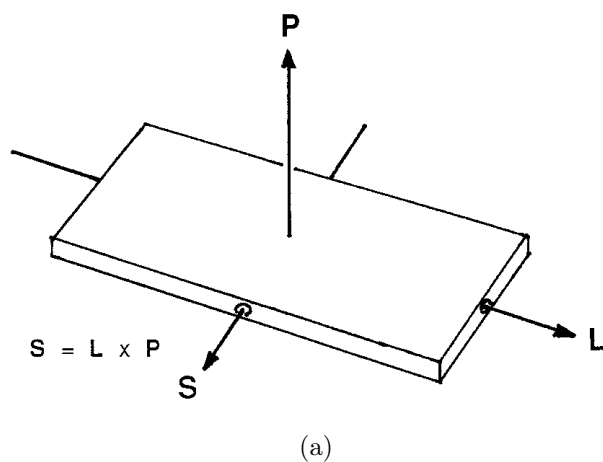


Figure 3.5: *a)* Definitions of local axes  $L$ ,  $P$ ,  $S$  for a DNA double helix.  $L$  is a unit vector along the long axis of the base pair between purine C8 and pyrimidine C6 atoms.  $P$  is the unit normal vector.  $S$  is the base pair short axis, defined by:  $S = L \times P$ . *b)* The six local helix parameters for adjacent base pairs [10].

To construct a probabilistic model for the polymer, we say that  $\mathbf{x}_i$  must be a distance  $b$  away from  $\mathbf{r}_{i-1}$ , and each direction in space has the same probability. To formulate this mathematically, we write down the following distribution for the bond vectors

$$\psi(\mathbf{r}_i) = \frac{1}{4\pi b_0} \delta(|\mathbf{r}| - b_0) \quad (3.2)$$

The delta function says that the length of the bond must be  $b_0$ , and the fraction gives the correct normalisation factor in three dimensional space. Each bond is statistically independent from every other bond, so

$$\psi(\mathbf{r}_i, \mathbf{r}_j) = \psi(\mathbf{r}_i) \psi(\mathbf{r}_j) \quad (3.3)$$

the joint probability distribution can be factored into single bond probability distributions. For a chain of  $N$  bonds, we have a joint probability distribution of

$$\psi(\mathbf{r}_1, \mathbf{r}_2, \dots, \mathbf{r}_N) = \prod_{i=1}^N \psi(\mathbf{r}_i) \quad (3.4)$$

for the set of  $N$  bonds (note no excluded volume). This is equivalent to a random walk of  $N$  steps. The end-to-end vector is

$$\mathbf{R} = \mathbf{R}_N - \mathbf{R}_0 = \sum_{i=1}^N \mathbf{r}_i \quad (3.5)$$

Because

$$\langle \mathbf{r}_i \rangle = \int \mathbf{r}_i \psi(\mathbf{r}_i) d\mathbf{r}_i = 0 \quad (3.6)$$

then the expected value of end-to-end vector  $\mathbf{R}$  is

$$\langle \mathbf{R} \rangle = \sum_{i=1}^N \langle \mathbf{r}_i \rangle = 0 \quad (3.7)$$

There is no preferred direction for any bond, so the average vector for each bond is the zero vector.

$$\langle \mathbf{R}^2 \rangle = \left\langle \left( \sum_i \mathbf{r}_i \right)^2 \right\rangle = \sum_i \langle \mathbf{r}_i^2 \rangle + \sum_{i \neq j} \langle \mathbf{r}_i^2 \cdot \mathbf{r}_j \rangle = N b_0^2 \quad (3.8)$$

All cross terms vanish because the distribution of the individual bonds are statistically independent. There are  $N$  remaining terms that each give a factor of  $b^2$ . This implies that  $\sqrt{\langle \mathbf{R} \cdot \mathbf{R} \rangle} = b N^{1/2}$ , or the root mean square distance of a polymer grows as  $N$  to the 1/2 power.

Single-stranded DNA may be modelled with this, experimental results give a persistence length of  $< 1$  nm. An extension of this model is the Freely-Rotating Chain [11].

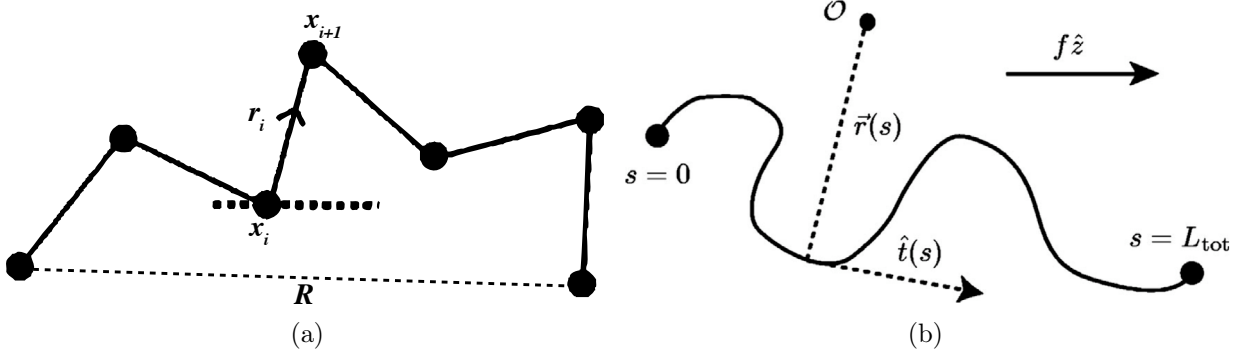


Figure 3.6: *a)* Freely Jointed Chain model of a polymer, used to describe single-stranded DNA. *b)* Worm-Like Chain model of a polymer, used to describe double-stranded DNA [12].

### 3.1.3.2 Worm-Like Chain

This is also known as the Semiflexible Chain or Kratky Porod model [13].

The polymer is treated as a filament that follows some path in space,  $\mathbf{r}(s)$ , where  $s$  measures the distance along the backbone, see Figure 3.6b on page 18. Introduce the tangent vector  $\mathbf{t}(s) = \partial\mathbf{r}/\partial s$ . For a given conformation, we assign a Boltzmann weight  $e^{-E_{elast}/k_B T}$ .

$$E_{elast} = \frac{\kappa}{2} \int_0^L \left( \frac{d\mathbf{t}}{ds} \right)^2 ds \quad (3.9)$$

is the bending energy,  $|\partial\mathbf{t}/\partial s|$  is the curvature and  $\kappa$  is the elastic modulus. Many properties of the worm-like chain can be solved exactly, one can show the tangent correlation function (bond correlation function) decays exponentially

$$\langle \cos \theta \rangle = \langle \mathbf{t}(0) \cdot \mathbf{t}(s) \rangle = e^{-\frac{s}{L_p}} \quad (3.10)$$

$$L_p = \frac{\kappa}{k_B T} \quad (3.11)$$

with  $L_p$  being the persistence length - the distance along the backbone over which the chain loses the memory of orientation. Under normal conditions, 100 mM monovalent salt, 20 °C, the persistence length of double-stranded DNA is 50 nm or 150 base pairs. Further

$$R = \int_0^L \mathbf{t}(s) ds \quad (3.12)$$

$$\langle R^2 \rangle = \langle (R(L) - R(0))^2 \rangle \quad (3.13)$$

$$= \int_0^L ds \int_0^L ds' \langle \mathbf{t}(s) \mathbf{t}(s') \rangle \quad (3.14)$$

$$= \int_0^L ds \int_0^L ds' e^{-\frac{(s-s')}{L_p}} \quad (3.15)$$

$$= 2LL_p \left( 1 - \frac{L_p}{L} \left( 1 - e^{-\frac{L}{L_p}} \right) \right) \quad (3.16)$$

$$\langle R^2 \rangle = \begin{cases} 2LL_p & (L \gg L_p) \text{ ideal chain limit} \\ 2LL_p(1 - L_p/L) & (L > L_p) \\ L^2 & (L_p \gg L) \sim \text{rigid rod} \end{cases} \quad (3.17)$$

This results in a Kuhn length of  $\langle R^2 \rangle = 2L_p$ , twice the persistence length [14]. Kuhn lengths can be thought of as if they are freely jointed with each other.

### 3.1.4 Hybridisation and denaturation

The binding of two single-stranded DNA molecules to each other via Watson-Crick base-pairing is known as hybridisation. This can occur if the sequences are complementary or partially complementary. The rate at which this occurs depends on a number of factors including DNA concentration, salt type and concentration, and temperature. The mathematics describing hybridisation are given in Section 3.2.

If double-stranded DNA molecules are subjected to conditions of pH, temperature, or ionic strength that disrupt the hydrogen bonds, the strands are no longer held together. This is known as denaturation. If increasing temperature is the denaturing agent, the double helix is said to melt. At pH values greater than 10, the bases release protons (deprotonation), and thus lose their ability to form stable hydrogen bonds. Small molecules that readily form hydrogen bonds can also denature DNA if present in sufficiently high concentrations to compete effectively with the hydrogen bonding between base pairs [7].

Denatured DNA will renature to re-form double-stranded DNA if the denaturing conditions are removed (that is, if the solution is cooled, the pH is returned to neutrality, or if the denaturants are diluted out).

Denaturation and renaturation are depicted in Figure 3.7 on page 20.

### 3.1.5 DNA melting

When double-stranded DNA is denatured by heating, it separates into single strands in a process called melting (see Figure 3.8 on page 21). In early studies, DNA was described by an Ising model - that is, a lattice of two-state units (the base pairs), which can be either closed (state 0) or open (state 1). In this approach, a particular state of the molecule is

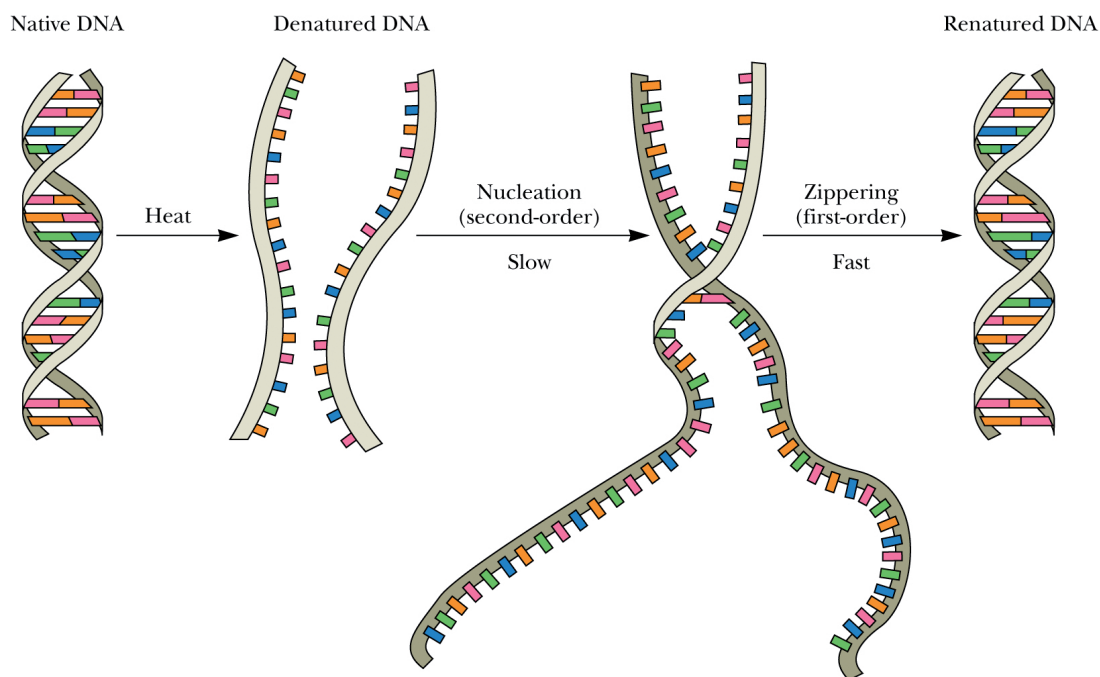


Figure 3.7: Steps in the thermal denaturation and renaturation of DNA. The nucleation phase of the reaction is a second-order process depending on sequence alignment of the two strands. This process takes place slowly because it takes time for complementary sequences to encounter one another in solution and then to align themselves. Once the strands form several initial bonds correctly, the strands then zipper up quickly [7]<sup>3</sup>.

described by a chain of 0s and 1s: ...0011100011... for example. Melting is the transition from ...0000000000... to ...1111111111...

However, the Ising model does not properly describe the entropy of the open states. Open base pairs can occupy many states which requires a phenomenological entropy factor to take account of these, and the entropy term depends on the size of the open 'bubbles'. This calculation imposes demanding constraints on computer programs.

Thus a Hamiltonian model was introduced. This describes the stretching of the base pairs by a real number, instead of simply by 0 or 1. A Hamiltonian can be written for the DNA molecule by adding the kinetic energy of the base-pair fluctuations, the potential energy linking the bases in a pair, and a stacking potential describing the interaction of each base pair with its nearest neighbours. The entropy term is then built into the model because the stretching of the base pairs can take any value, allowing the wandering of the open strands.

This model is one-dimensional so its statistical physics can be studied exactly. The configuration partition function for a DNA molecule of  $N$  base pairs is an  $N$ -dimensional

<sup>3</sup>From GARRETT/GRISHAM. Biochemistry, 4E. © 2009 Brooks/Cole, a part of Cengage Learning, Inc. Reproduced by permission. [www.cengage.com/permissions](http://www.cengage.com/permissions)

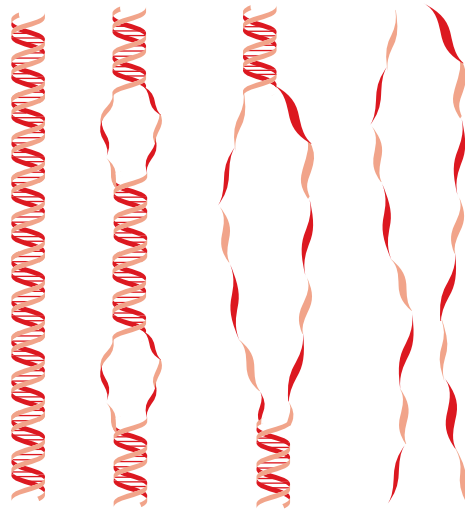


Figure 3.8: The melting of DNA. Below the melting temperature, some ‘bubbles’ appear where the base pairs are broken. As the melting temperature is approached, these bubbles get progressively bigger and eventually invade the full molecule, leading to a complete separation of the two strands [15].

integral. But, as the bases interact only with their nearest neighbours, the function to be integrated is actually a product of functions depending on two variables, and this allows a calculation that proceeds along the chain, using a ‘transfer-integral’. This is difficult for a DNA sequence.

The partition function is needed in order to calculate what is known as the melting temperature. This is the temperature at which half of the total number of base pairs are separated - see Section 3.1.6 for more details.

However, it has been realised that the partition function is not really needed to characterise DNA thermal properties. Instead, from the transfer-integral calculation, one can define a scalar quantity that can be obtained analytically in some approximation, or exactly by a numerical calculation, which is fast. The secret of DNA’s thermal properties lies in the correlations between the positions of the ‘weak’ adenine-thymine base pairs and the ‘strong’ guanine-cytosine base pairs. The scalar quantity provides a simple measure of the influence of the correlations on the thermal properties of DNA - in a single number that can easily be calculated [15].

DNA melting can be tracked by its absorption at ultra-violet wavelengths. Thus this discussion continues in the following section. The kinetics of DNA melting are discussed in 3.2.1.

### 3.1.6 Optical properties

The purines and pyrimidines in DNA absorb strongly at ultra-violet wavelengths. DNA has an absorption maximum at a wavelength of around 260 nm, this results from in-plane

transitions between  $\pi$  electrons of the bases ( $\pi - \pi^*$ ). The exact wavelength maximum is dependent on the sequence. Excitations of out-of-plane transitions are much weaker and can be neglected. Sugars and phosphates contribute to the absorption mostly below 190 nm [16,17].

The amount of absorption for a particular sequence of DNA is described by the molar extinction coefficient. This is described in further detail in 4.1.1. The absorption is dependent on the absorption of the individual bases, and on the interactions between bases and their neighbours. The 260 nm absorption value of a sequence can be calculated from the following equation based on the approximation of nearest-neighbour interactions

$$\epsilon_{260} = 2 \left( \sum_1^{N-1} \epsilon_{Nearest-neighbour} \right) - \sum_2^{N-1} \epsilon_{Individual} \quad (3.18)$$

where *Nearest - Neighbor* is the nearest neighbour coefficient for a pair of bases, *Individual* is the coefficient for an individual base, and  $N$  is the base length of the sequence [18]. The values for the individual and nearest-neighbours have been determined experimentally [19,20] for single-stranded DNA at standard temperature and buffer conditions.

However, these values are only valid for single-stranded DNA without secondary structure, and single-stranded DNA often has secondary structure at room temperature, depending on its sequence. This makes it difficult to calculate an accurate extinction coefficient for DNA with secondary structure, and as we will see, this affects determination of DNA concentration (4.1.1).

Double-stranded DNA in solution absorbs less than the same DNA in single-stranded form. This property is known as hyperchromicity. If some property of the environment (for example temperature - see the following section) is changed so that the DNA changes from one form to the other, then the absorption changes.

By monitoring the optical absorbance at approximately 260 nm while increasing the temperature, and normalising the absorbance change in an appropriate way, a plot of  $\theta_B$ , the fraction of broken base pairs, versus temperature can be calculated. 3.9 illustrates a measurement which might be observed for a short DNA ( $\sim 100$  bp). In the early part of the transition there is a slight linear increase in absorbance. This linear increase is interpreted as a slight linear increase in the average base pair stacking of the double helix. The DNA is still predominantly base paired. Absorption values in this pre-transition linear region are specified by a linear function of temperature,  $A_L(T)$ . As the temperature is raised, hydrogen bonded base pairs between complementary strands begin to open. Opening of the remaining base pairs occurs in a highly cooperative manner causing the strands to completely separate. After strand separation, a linear absorbance is again observed if the temperature is further increased. This absorbance corresponds to the increased unstacking of bases in the single strands and is represented by  $A_U(T)$ . The fraction of broken base pairs  $\theta_B$  vs. temperature is obtained by correcting the observed absorbance change for volume expansion and plotting

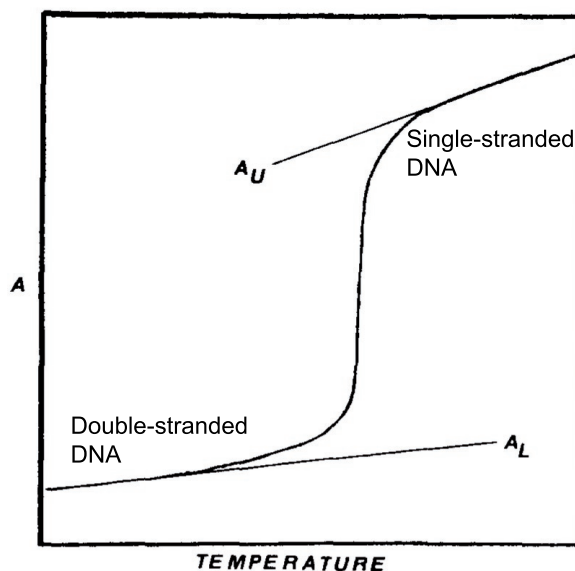


Figure 3.9: A typical plot of absorbance vs. temperature demonstrating the denaturation of a short DNA. Absorbance increase is normally 30—40% from a solution with 0.4 absorbance units at 260 nm [21].

$$\theta_B = \frac{A(T) - A_L(L)}{A_U(T) - A_L(T)} \quad (3.19)$$

The temperature at which 50% of the base pairs are broken (and correspondingly 50% are intact) is known as the melting temperature  $T_m$ . This is dependent on the ionic strength of the solution, the lower the ionic strength, the lower the melting temperature. Ions suppress the electrostatic repulsion between the negatively charged phosphate groups in the complementary strands of the helix, thereby stabilising it. At high concentrations of ions,  $T_m$  is raised and the transition between helix and coil is sharp. Additionally, DNA hybridisation occurs quickly if the temperature is warm enough to promote diffusion but not above  $T_m$  which would cause melting.

### 3.1.7 DNA as a polyelectrolyte

DNA is a polyelectrolyte - a polymer whose repeating units bear an electrolyte group. These groups dissociate in aqueous solutions, making the polymers charged. Each phosphate in the backbone of DNA are deprotonated above pH 1 and carry a negative charge, giving it a very high charge density. This has to be taken into account when investigating interactions with other charged molecules and surfaces.

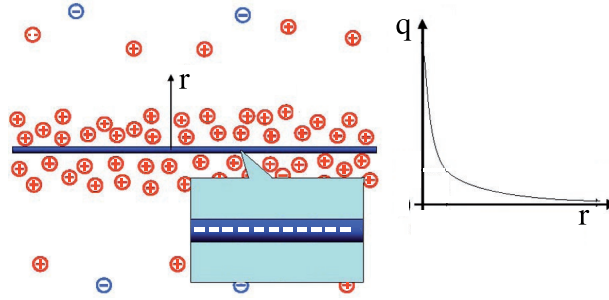


Figure 3.10: A highly charged rod-like polymer in salt solution attracts an oppositely charged condensate [22].

### 3.1.7.1 Number of counterions

The formulation of counterion condensation theory by Oosawa and Manning provides a simple prediction of the number of counterions bound, or ‘condensed’ onto a charged polymer. The central concept is that a charged polymer is unstable if it has linear charge above a critical value. It is neutralised by counterions that condense on to the polymer to increase the average separation between unneutralised charges to the critical value. Assuming the polymer to be a rod, the critical charge  $n_c$  is

$$n_c = \frac{e}{z\lambda_b} \quad (3.20)$$

where  $e$  is the electron charge,  $z$  is the valence, and  $\lambda_b$  is the Bjerrum length.

$$\lambda_b = \frac{e^2}{4\pi\epsilon_r\epsilon_0k_B T} \quad (3.21)$$

$\epsilon_r$  is the dielectric constant and  $\epsilon_0$  is the permittivity of free space. The Bjerrum length is the distance between two unit charges at which the Coulomb’s law free energy equals  $k_B T$ , and is approximately 0.71 nm. The charges themselves are assumed to be arranged linearly with uniform spacing  $b$ . A convenient dimensionless measure of the charge density is  $\lambda_b/b$ , known as the Oosawa-Manning parameter. For double-stranded DNA  $b = 0.17$  nm (two phosphates per 0.34 nm rise from one base pair to the next).

$$\xi = \frac{\lambda_b}{b} = \frac{0.71 \text{ nm}}{0.17 \text{ nm}} = 4.2 \quad (3.22)$$

For DNA in a monovalent electrolyte, counterions are assumed to condense onto the DNA to make its unneutralised charge fraction equal  $\xi^{-1}$  over a broad concentration range. The number of condensed counter ions is then a constant fraction of total DNA charge and is given by  $1-\xi^{-1}$  or 76%, known as the Manning fraction [23, 24].

### 3.1.7.2 Distribution of counterions

The equilibrium distribution of ions around the DNA can be found with the Poisson-Boltzmann equation. A general solution called the Gouy-Chapman model is a simplified form of the famous Debye-Hückel theory. It proposes two layers of ions around the DNA helix. Close to the strand is the condensed counterions (positive ions), called the Stern layer. The outer layer, called the diffuse layer, consists of a cloud of positive and negative ions that still feel the potential of the DNA charges, but being shielded by the Stern layer are not strongly bound. The potential is screened exponentially (see Figure 3.10 on page 24) from its value at the DNA  $V_0$  with distance  $r$ :

$$V = V_0 e^{-r/\kappa^{-1}} \quad (3.23)$$

where  $\kappa^{-1}$  is the Debye screening length

$$\kappa^{-1} = \frac{1}{\sqrt{8\pi\lambda_b N_A I}} \quad (3.24)$$

Here  $N_A$  is Avogadro's constant and  $I$  is the ionic strength. The understanding behind this is that as counterion moves away from the DNA helix it experiences an increase in entropy with  $\ln r$  and a decrease in electrostatic energy with  $\ln r$ .

## 3.2 Kinetics and thermodynamics of DNA molecules and reactions

The rate at which DNA strands hybridise and denature is described by reaction kinetics. The energies involved are described by thermodynamics.

### 3.2.1 Kinetics

One possibility to describe the rates of DNA reactions is to formulate rate equations. One must ensure however, that significant numbers of molecules are present and thus stochastic processes are not significant. For typical concentrations of nanomolar to micromolar and volumes of microlitres to millilitres these conditions are fulfilled.

Rate equations describe the concentration  $X_i$  of species  $i$  as continuous variables, with  $N$  different species, and are composed of a set of  $N$  nonlinear, coupled ordinary differential equations in time  $t$

$$\frac{dX_1}{dt} = f_1(X_1, X_2, \dots, X_N) \quad (3.25)$$

$$\frac{dX_2}{dt} = f_2(X_1, X_2, \dots, X_N) \quad (3.26)$$

$$\dots \quad (3.27)$$

$$\frac{dX_N}{dt} = f_N(X_1, X_2, \dots, X_N) \quad (3.28)$$

These equations can in general not be solved analytically without making use of approximations. Such approximations might include setting reaction rates or species concentration to zero. Alternatively they can be solved numerically.

There are several different reaction types that can be described, as discussed in the following.

### 3.2.1.1 First order reaction

A simple chemical reaction is the reversible change of a species  $X_1$  into another species  $X_2$



where  $k_+$  is the rate of the forward reaction and  $k_-$  is the rate of the reverse reaction. Important to note is that this is a two-state reaction description with no intermediate steps, this will in many cases not be accurate. Such a reaction might be the unfolding of single-stranded DNA with secondary structure into a state with no secondary structure.

The rate equations are thus

$$\frac{dX_1}{dt} = -k_+X_1 + k_-X_2 \quad (3.30)$$

$$\frac{dX_2}{dt} = k_+X_1 - k_-X_2 \quad (3.31)$$

$$= -\frac{dX_2}{dt} \quad (3.32)$$

These can be solved to give:

$$X_1(t) = \frac{k_+X_{1,0} - k_-X_{2,0}}{k_+ + k_-} e^{-(k_++k_-)t} + \frac{k_-(X_{1,0} + X_{2,0})}{k_+ + k_-} \quad (3.33)$$

$$X_2(t) = \frac{k_-X_{2,0} - k_+X_{1,0}}{k_+ + k_-} e^{-(k_++k_-)t} + \frac{k_+(X_{1,0} + X_{2,0})}{k_+ + k_-} \quad (3.34)$$

where  $X_{1,0}$  and  $X_{2,0}$  are the concentrations of  $X_1$  and  $X_2$  respectively at time  $t = 0$ . If the reverse reaction rate is much lower than the forward reaction rate  $k_- \ll k_+$  then these simplify to a decay of species  $X_1$

$$X_1(t) = X_{1,0}e^{-k_+t} \quad (3.35)$$

with half life

$$t_{1/2} = \frac{\ln 2}{k_+} \quad (3.36)$$

Such a reaction is known as a reaction of first order.

### 3.2.1.2 Second order reaction

A reaction in which two strands hybridise can be written so



which gives a rate equation for species  $X_3$  (the double-stranded product)

$$\frac{dX_3}{dt} = -k_+X_3 + k_-X_1X_2 \quad (3.38)$$

Important to note is that this is a two-state reaction description with no intermediate steps, this will in many cases not be accurate.

With the conditions

$$X_{3,0} + X_{1,0} = X_3 + X_1 \quad (3.39)$$

$$X_{3,0} + X_{2,0} = X_3 + X_2 \quad (3.40)$$

and introduction of the following parameters

$$\alpha := k_- \quad (3.41)$$

$$\beta := -k_+ - k_-(X_{3,0} + X_{1,0} + X_{2,0}) \quad (3.42)$$

$$\gamma := k_-(X_{3,0} + X_{1,0})(X_{3,0} + X_{2,0}) \quad (3.43)$$

gives the following

$$\frac{dX_3}{dt} = \alpha X_3^2 + \beta X_3 + \gamma \quad (3.44)$$

If the reverse reaction rate is much lower than the forward reaction rate  $k_- \ll k_+$  then  $\alpha \sim 0$  and

$$\frac{dX_1}{dt} = \frac{dX_2}{dt} = -k_+X_1X_2 \quad (3.45)$$

If  $X_1$  and  $X_2$  are present at equal concentrations  $X_1 = X_2$  then

$$\frac{dX_1}{dt} = -k_+dX_1^2 \quad (3.46)$$

This can be integrated to give

$$X_1(t) = \frac{1}{k_+(t_0 + t)} \quad (3.47)$$

$$X_1(t) = \frac{X_{1,0}}{1 + k_+ t X_{1,0}} \quad (3.48)$$

The half life is then

$$t_{1/2} = \frac{1}{k_+ X_1} \quad (3.49)$$

Such a reaction is known as a reaction of second order.

### 3.2.1.3 Two-step reaction

For a two-step reaction that involves an intermediate equilibrium



there are three rate equations

$$\frac{dX_1}{dt} = -k_+ X_1 + k_- X_2 \quad (3.51)$$

$$\frac{dX_2}{dt} = -k_+ X_1 - (k_- + k_f) X_2 \quad (3.52)$$

$$\frac{dX_3}{dt} = k_f X_2 \quad (3.53)$$

This reaction series describes DNA hybridisation more accurately than because it captures the nucleation and zipping steps.

There are three assumptions one could make to solve these equations.

The first is the Steady-State Approximation that assumes that the concentration of  $X_2$  does not alter. An alternative approach to solving the rate equations is to use the Pre-equilibrium Approximation. This is that  $X_1$  and  $X_2$  are always present in their equilibrium ratios, which is equivalent to assuming that  $k_f$  is much slower than both  $k_+$  and  $k_-$ . Neither of these approximations reproduces the gradual increase and decrease in the concentration of  $X_2$  that occurs for many choices of  $k_+$ ,  $k_-$  and  $k_f$ . Another approximation is to assume that  $k_-$  is zero. This may appear a drastic approximation, but it leads to rate equations which can be solved analytically

$$X_1(t) = X_{1,0} e^{-k_+ t} \quad (3.54)$$

$$X_2(t) = \frac{k_+}{k_f - k_+} X_{1,0} (e^{-k_+ t} - e^{-k_f t}) + X_{2,0} (e^{-k_f t}) \quad (3.55)$$

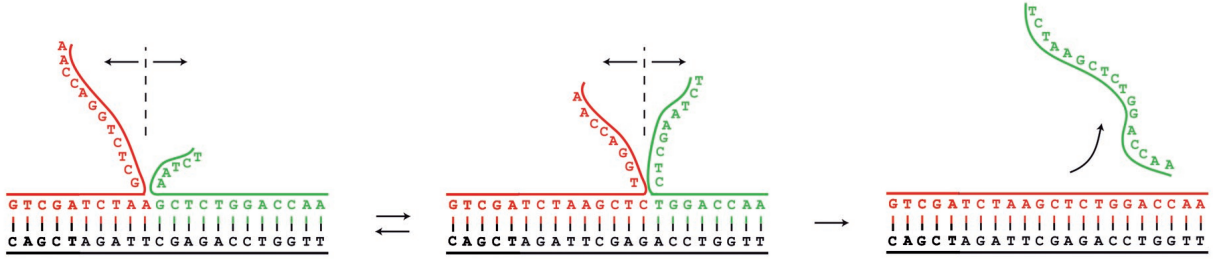


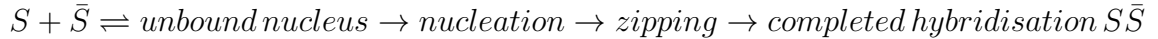
Figure 3.11: Branch migration. The red strand (left upper) is longer than the green strand (right upper) and has more bases complementary to the black strand (below). During branch migration a one dimensional random motion of the intersection of the strands takes place. Three snapshots are shown as the red strand displaces the green strand completely [25].

$$X_3(t) = X_{1,0} + X_{2,0} + X_{3,0} - X_1 - X_2 \quad (3.56)$$

This approximation gives curves which are of the same general form as the numeric results. However because  $k_-$  is not zero,  $X_2$  forms too quickly.

### 3.2.1.4 Hybridisation and branch migration

The hybridisation of two complementary single-stranded DNA molecules can be written with simplifications as the following reaction cascade:



By the hybridisation of two strands, the building of a nucleus is the rate limiting step. Only after the binding of a critical number of base pairs does the rate of binding significantly increase and become higher than the rate at which they can dissociate from one another. From experimental measurements it is known that - dependant on the surrounding environment - values of  $5 \pm 1$  base pairs for AT pairs and 2-3 base pairs for GC - are typical for building a nucleus [26]. The rate of association of every extra base pair is of order  $10^6 \text{ s}^{-1} \leq k_+ \leq 10^7 \text{ s}^{-1}$ . Typical hybridisation rates are of order  $10^5 \text{ M}^{-1}\text{s}^{-1}$ .

In a strand displacement (branch migration) reaction, a strand A, after a nucleation step with strand B, displaces strand C. Such processes are much slower than normal hybridisation. To model the strand displacement process, a one dimensional stepwise random motion from A to B is used. For rate  $k$ , with which strand A displaces strand C, the following is valid

$$k = \frac{2k_+}{N - 2n + 2} e^{(-\frac{\Delta G_n}{RT})} \quad (3.57)$$

with a hybridisation rate  $k_+$ , a strand length of  $N$ , a critical nucleation length  $n$  and an enthalpy difference  $\Delta G_n$  for opening the double strand at one end [27].

A significant increase in the speed of strand displacement occurs when a single-stranded extension (toehold) is available. If the double strand is short ( $<100$  base pairs) and the toehold is longer than 8 base pairs, then the rate of strand displacement is almost as high as pure hybridisation of two single strands [28]. In this case it is adequate to describe the strand displacement process as a one-step reaction with a rate constant of order  $10^5 - 10^7 M^{-1}s^{-1}$ . However, the rate constant can be influenced by many factors, including sequence, and mono and divalent salt (e.g.  $Na^+$ ,  $Mg^{2+}$ ) concentration.

Secondary structure within single strands can significantly affect the hybridisation rate between two strands. A systematic examination of hairpin structures with stem lengths between 7 and 16 base pairs and loop lengths of between 7 and 40 bases found several results [29]<sup>1</sup>. Hairpins with loop length of 12 bases, stem length of 16 base pairs gave  $k_+ = 50 M^{-1}s^{-1}$ ; with loop length 21 bases, stem length of 16 base pairs gave  $k_+ = 500 M^{-1}s^{-1}$ ; and loop length of 16 bases, stem length of 12 bases gave  $k_+ = 10\,000 M^{-1}s^{-1}$ . These are several orders of magnitude below the typical values. If one wishes to accelerate the hybridisation without altering the hairpin loop itself, then one can add a toehold to one of the stem ends, this allows a nucleus to form for a complementary strand. With such a toehold of 3 to 6 bases, the hybridisation can be accelerated by one to two orders of magnitude [25, 29].

## 3.2.2 Thermodynamics

### 3.2.2.1 Gibbs energy and the van't Hoff equation

A chemical reaction is often assumed to occur at constant temperature (isothermal) and pressure (isobaric). The thermodynamic potential for such an ensemble is the Gibbs energy

$$G(T, p, N) = -k_B T \ln \Omega(T, p, N) \quad (3.58)$$

where  $\Omega(T, p, N)$  is the partition function of the system. The probability  $p_j$  that a freely chosen particle has a Gibbs energy of  $g_j$  is then

$$p_j \propto e\left(-\frac{g_j}{k_B T}\right) \quad (3.59)$$

For a large number of particles  $N_0$  this means that on average there are  $N_j = p_j N_0$  particles that have the Gibbs energy  $g_j$ . For this reason the ratio of occupancy of two states  $j$  and  $k$  is

$$\frac{N_j}{N_k} = \frac{p_j}{p_k} = \frac{e\left(-\frac{g_j}{k_B T}\right)}{e\left(-\frac{g_k}{k_B T}\right)} = e\left(-\frac{g_j - g_k}{k_B T}\right) =: e\left(\frac{\Delta G}{k_B T}\right) \quad (3.60)$$

In dynamic equilibrium the reversible change of one species into another via

---

<sup>1</sup>In 100 mM NaCl at 25 °C



with concentrations  $X_1, X_2$ , has a constant concentration ratio - and thus also a constant particle number ratio

$$K := \frac{X_1}{X_2} = \frac{N_1}{N_2} = \frac{k_+}{k_-} \quad (3.62)$$

where  $K$  is called the equilibrium constant. The particles of each species can be assigned the Gibbs energies  $g_1$  and  $g_2$ . Thus a relationship between the equilibrium constant and the Gibbs energy of the corresponding states can be written

$$K := \frac{k_+}{k_-} = \frac{X_1}{X_2} = \frac{N_1}{N_2} = e^{\left(-\frac{g_1 - g_2}{k_B T}\right)} = e^{\left(\frac{\Delta G}{k_B T}\right)} \quad (3.63)$$

This relationship is known as the van't Hoff relation.  
From this

$$\Delta G = -k_B T \ln K \quad (3.64)$$

*Note:* This equation is often written in terms of  $R$ , the gas constant. The Boltzmann constant  $k_B$  is used in place of the gas constant by working in pure particle count, rather than number of moles, since

$$R = N_A k_B \quad (3.65)$$

### 3.2.2.2 Enthalpy and entropy

The Gibbs energy can also be defined in terms of a change in enthalpy  $\Delta H$  and entropy  $\Delta S$

$$\Delta G = \Delta H - T \Delta S \quad (3.66)$$

Thus one can derive

$$\ln K = -\frac{\Delta H}{k_B T} + \frac{\Delta S}{k_B} \quad (3.67)$$

Therefore, a plot of the natural logarithm of the equilibrium constant versus the reciprocal temperature gives a straight line. The slope of the line is equal to minus the enthalpy change divided by the Boltzmann constant,  $-\Delta H/k_B$  and the intercept is equal to the entropy change divided by the gas constant,  $\Delta S/k_B$ .

<i>Propagation sequence</i>	$\Delta H^\circ(kcal\ mol^{-1})$	$\Delta S^\circ(e.u.)$	$\Delta G_{37}^\circ(kcal\ mol^{-1})$
AA/TT	-7.6	-21.3	-1.00
AT/TA	-7.2	-20.4	-0.88
TA/AT	-7.2	-21.3	-0.58
CA/GT	-8.5	-22.7	-1.45
GT/CA	-8.4	-22.4	-1.44
CT/GA	-7.8	-21.0	-1.28
GA/CT	-8.2	-22.2	-1.30
CG/GC	-10.6	-27.2	-2.17
GC/CG	-9.8	-24.4	-2.24
GG/CC	-8.0	-19.9	-1.84
Initiation	+0.2	-5.7	+1.96
Terminal AT penalty	+2.2	+6.9	+0.05
Symmetry correction	0.0	-1.4	+0.43

Table 3.2: Nearest-neighbour thermodynamic parameters for DNA Watson-Crick pairs in 1 M NaCl. The slash indicates the sequences are given in anti-parallel orientation. The symmetry correction applies to only self-complementary duplexes. The terminal AT penalty is applied for each end of a duplex that has a terminal AT [30].

### 3.2.2.3 Thermal stability

The thermal stability of double-stranded DNA is described by the standard (that is, per mole) Gibbs energy  $\Delta G^\circ$ . Its value at 37 °C can be calculated from

$$\Delta G_{37}^\circ = \sum_i n_i \Delta G^\circ(i) + \Delta G^\circ(init) + \Delta G^\circ(sym) + \Delta G^\circ(term) \quad (3.68)$$

where  $n_i \Delta G^\circ(i)$  are nearest neighbour parameters,  $\Delta G^\circ(init)$  is an initiation parameter,  $\Delta G^\circ(sym)$  is a penalty for symmetry or self-complementary strands, and  $\Delta G^\circ(term)$  is a penalty for AT terminals, and all values are for  $T = 37^\circ C$ . These values have been measured empirically and are given in Table 3.2 on page 32. An example calculation is given in Figure 3.12 on page 33. The  $\Delta H^\circ$  and  $\Delta S^\circ$  are calculated analogously with the corresponding parameters in Table 3.2. At a different temperature  $T$  the following equation is used to predict  $\Delta G_T^\circ$

$$\Delta G_T^\circ = \Delta H^\circ - T \Delta S^\circ \quad (3.69)$$

The average Gibbs energy change associated with the hybridisation of a complementary base pair is -78 meV at 20 °C. In comparison, this temperature has a thermal energy  $k_B T \sim 26$  meV.

$$\begin{aligned}
5'\text{-CGTTGA-3}' &= \Delta G_{37}^{\circ}{}_{\text{initiation}} + \Delta G_{37}^{\circ}{}_{\text{symmetry}} \\
3'\text{-GCAACT-5}' &+ \text{CG} + \text{GT} + \text{TT} + \text{TG} + \text{GA} + \text{AT}_{\text{terminal}} \\
&\quad \text{GC} \quad \text{CA} \quad \text{AA} \quad \text{AC} \quad \text{CT} \\
\Delta G_{37}^{\circ} \text{ (predicted)} &= 1.96 + 0 - 2.17 - 1.44 - 1.00 - 1.45 - 1.30 + 0.05 \\
\Delta G_{37}^{\circ} \text{ (predicted)} &= -5.35 \text{ kcal mol}^{-1}.
\end{aligned}$$

Figure 3.12: An example of the application of nearest neighbour parameters in Table 3.2 [31].

### 3.2.2.4 Secondary structure

The Gibbs energy of a secondary structure  $a$  is estimated as the sum of the empirically determined Gibbs energies of the constituent loops

$$\Delta G(s) = \sum_{\text{loop} \in a} \Delta G(\text{loop}) \quad (3.70)$$

each defined with respect to the free energy of the unpaired reference state. Secondary structure models have enabled the development of efficient dynamic programming algorithms for characterising the equilibrium properties of a DNA molecule. For algorithmic purposes, it is convenient to represent a secondary structure as a polymer graph, with the strand drawn along the circumference of a circle and base pairs depicted as straight lines joining complementary bases.

The class of secondary structures that are considered in dynamic programs is usually defined to exclude pseudoknots, which correspond to polymer graphs with crossing lines. Initially dynamic programming algorithms were developed for predicting the minimum free energy of a DNA single strand over an ensemble of unspseudoknotted secondary structures  $A$ . Then programs were developed for calculating the partition function  $\Omega$

$$\Omega = \sum_{a \in A} e^{-\Delta G(a)/k_B T} \quad (3.71)$$

This can be used to calculate the equilibrium probability of any secondary structure  $a \in A$

$$p(a) = \frac{1}{\Omega} e^{-\Delta G(a)/k_B T} \quad (3.72)$$

and has thus had profound influence on the development of rigorous sequence design methods. Adaptions of the partition function algorithm allow the calculation of other important equilibrium properties including the probability of any base pair, thermodynamically representative samplings of secondary structures in the ensemble  $A$ , and the average number of incorrectly paired bases relative to a design target. The exclusion of pseudoknots from  $A$  is founded on both modelling and algorithmic considerations. Energy models of pseudoknots are difficult to formulate due to the increased significance of

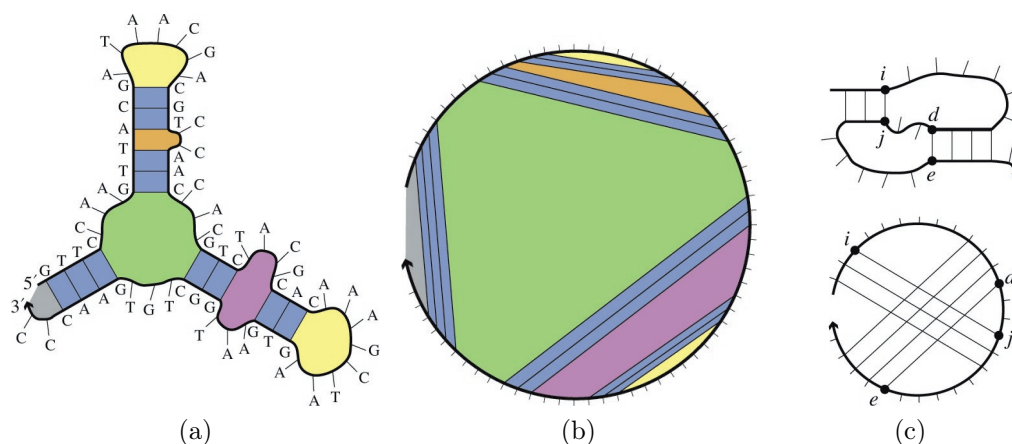


Figure 3.13: Secondary structure model for a single-stranded DNA molecule. *a)* A sample secondary structure with the strand depicted as a directed thick line (an arrow marks the 3' end), base pairs depicted as thin lines joining complementary bases, and unpaired bases depicted as thin protruding lines. This structure can be decomposed into different loop types: hairpin loops (a stretch of unpaired bases closed by one base pair; yellow), stacked base pairs (two consecutive base pairs with no unpaired bases between them; blue), an interior loop (two base pairs separated by unpaired bases on both sides of the loop; purple), a bulge loop (two base pairs separated by unpaired bases on only one side of the loop; orange), a multiloop (three or more base pairs; green), and an exterior loop (the loop containing the two ends of the strand; grey). *b)* An equivalent polymer graph representation, with the strand depicted as a directed thick circular arc, bases depicted as protruding tick marks, base pairs depicted as straight lines joining complementary bases, and loops coloured as in *a)*. *c)* A sample pseudoknot yielding crossing lines in the corresponding polymer graph [32].

geometric issues and tertiary interactions. Furthermore, if the ensemble is augmented to include all possible pseudoknots, the problem can be NP-hard.

Dynamic programs calculate the subsequence partition function  $\Omega_{i,j}$  for each subsequence  $[i, j]$ , starting from short subsequences and iteratively considering longer subsequences until the full partition function  $A$  is obtained.

An example output for the sequence

ACCGTTACCGTTTACGGTTTACGGT

(((((.((((.....))))))..))))))

is shown in Figures 3.14-3.15.

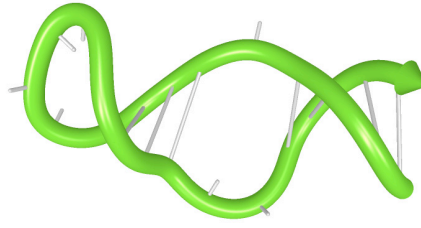


Figure 3.14: Depiction with helical geometry of sequence ACCGTTACCGTTTACGGTTTACGGT at 65 °C in standard buffer conditions. See also Figures 3.15-3.16 [9].

### 3.2.2.5 Melting

As the temperature of a solution containing double-stranded DNA increases, the hydrogen bonds between base pairs begin to break and the double-stranded DNA separates into single-stranded DNA. As previously discussed, the temperature at which 50% of the bonds are broken is known as the melting temperature  $T_M$ . The melting reaction can be written as



The total strand concentration  $c_T$  is

$$c_T = S + \bar{S} + 2S\bar{S} \quad (3.74)$$

At the melting temperature

$$S = \bar{S} = \frac{c_T}{2} \quad (3.75)$$

thus the equilibrium constant  $K$  is

$$K = \frac{4}{c_T} \quad (3.76)$$

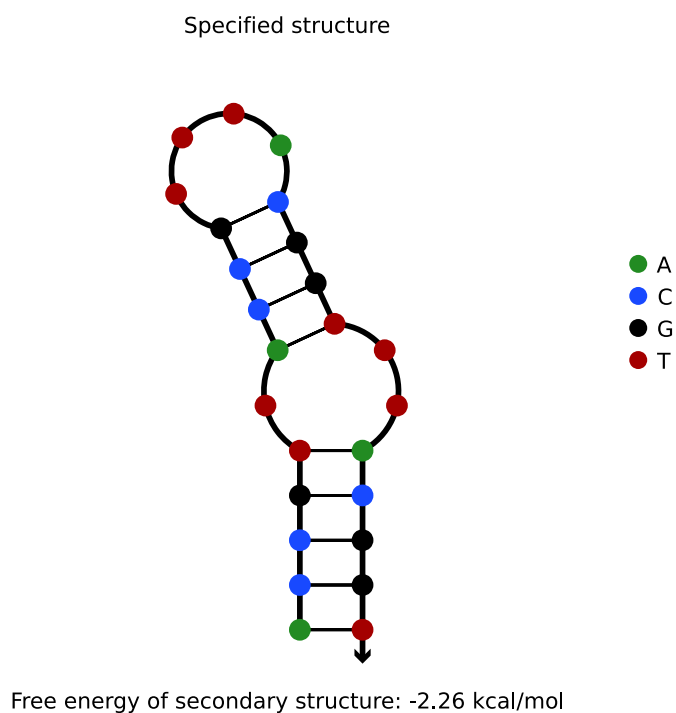
From equations (3.64) and (3.66) we can then derive

$$T_M = \frac{\Delta H}{\Delta S + k_B \ln \frac{c_T}{4}} \quad (3.77)$$

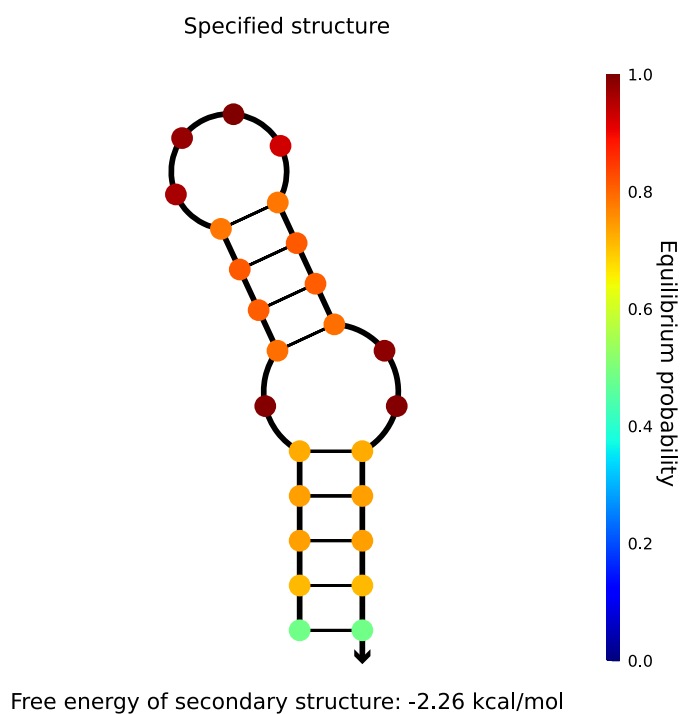
Some sequences however are self-complementary, they are their own complement, and in this case



The total strand concentration  $c_T$  is



(a)



(b)

Figure 3.15: Depiction of the sequence given in Figure 3.14 on page 35 *a)* Each base in the target structure is shaded by the probability that it adopts the depicted state at equilibrium. *b)* Each base in the target structure is colour-coded according to standard sequencing conventions: A = green, T = red, G = black, C = blue [9].

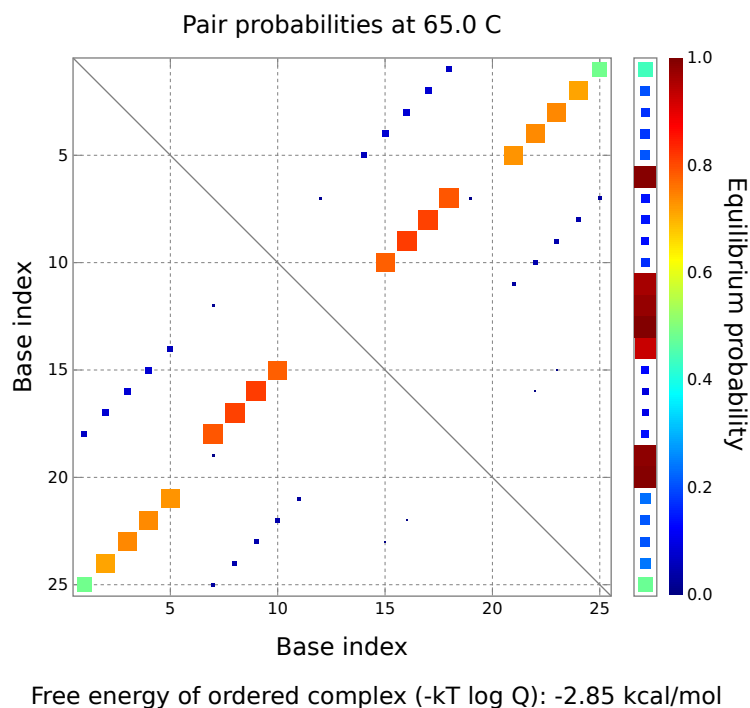


Figure 3.16: Depiction of the sequence given in Figure 3.14 on page 35. Depicts equilibrium base-pairing probabilities. The area and colour of each dot scale with the equilibrium probability of the corresponding base pair. With this convention, the plot is symmetric, with the upper and lower triangles separated by a diagonal line. The area and colour of each dot in the column at right scale with the equilibrium probability that the corresponding base is unpaired [9].

$$c_T = S + 2SS \quad (3.79)$$

At the melting temperature

$$S = \frac{c_T}{2} \quad (3.80)$$

thus the equilibrium constant  $K$  is

$$K = \frac{1}{c_T} \quad (3.81)$$

and so

$$T_M = \frac{\Delta H}{\Delta S + k_B \ln c_T} \quad (3.82)$$

Thus self-complementary sequences have a lower melting temperature.

### 3.3 Summary

We now have an understanding of some of the physical properties of DNA. In its single-stranded form it is a flexible polymer with a persistence length of  $\sim 1$  nm, and often occurs with secondary structure. In its double-stranded B form, it is a right handed helix joined by hydrogen bonds between base pairs and somewhat stiffer with a persistence length of 50 nm. The base sequence plays an important aspect in many properties of DNA. The process of two single-strands joining is known as hybridisation, and separation is known as denaturation - if the agent of separation is increasing temperature then it is known as melting. Typical hybridisation rates are of order  $10^5 \text{ M}^{-1}\text{s}^{-1}$ . DNA absorbs in the ultraviolet wavelengths and its absorption changes between single-stranded and double-stranded forms. Its absorption can be related to its concentration. The thermal stability and minimum free energy of a DNA structure can be calculated by thermodynamic methods, and there are differences when sequences are self-complementary.

Given this background knowledge we can go on in the next section to look at several different examples of self-assembled DNA structures in one, two and three dimensions.

### 3.4 Examples of DNA self-assembly from the literature

#### 3.4.1 The beginning of the field

In nature there exists a DNA structure known as a Holiday Junction. This is a mobile junction between four strands of DNA, as depicted in Figure 3.17 on page 39. In the early 1980's Professor Ned Seeman came up with the idea of using these junctions to build artificial structures such as cubes and lattices (Figure 3.17 on page 39). However, at the time molecular imaging technologies were limited and demonstrations were indirect using gel electrophoresis.

However, this launched the field of DNA self-assembly which has advanced significantly since then. Following is a description of some important examples. Many other examples can also be found in the literature.

#### 3.4.2 Quasi one dimensional

Yan and colleagues have demonstrated a chain of two parallel junctions building on Seeman's ideas, as shown in Figure 3.18 on page 40. Mao and colleagues took advantage of the idea of tensegrity, fusing the concepts of tension and integrity, with flexible junctions and rigid arms to assemble chains of triangular structures.

#### 3.4.3 Two dimensional

Mao and colleagues then went on to develop two important concepts. Firstly, they showed that instead of using single helical junctions one could interlink two double helices on each arm to make the structure significantly more stable (Figure 3.19 on page 41). Secondly,

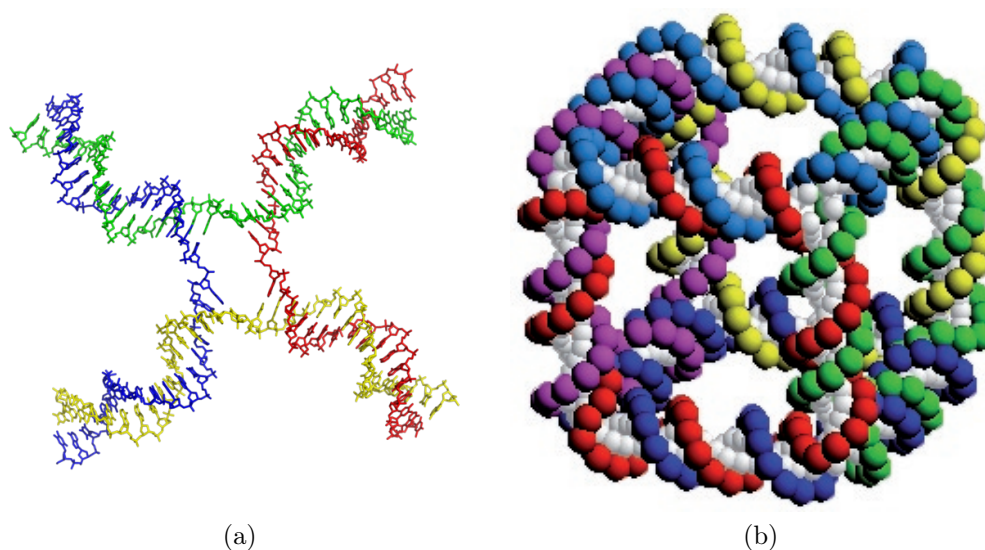


Figure 3.17: *a)* Molecular structure of a Holliday junction [33]. *b)* A depiction of the DNA cube from artificial Holliday junctions that Prof. Ned Seeman demonstrated using gel electrophoresis in 1992 [34].

instead of using 8 different sequences to form a junction, they showed that using sequence symmetry (the same sequence in multiple parts of the structure) they could reduce this to just three different sequences.

With this, they were able to demonstrate large two dimensional arrays as shown in Figure 3.20a on page 41.

Winfree and colleagues used the concept of Wang Tiles (beyond the scope of this work, see [38]) to demonstrate the assembly of a Sierpinski Triangle structure (Figure 3.20b on page 41).

### 3.4.4 Three dimensional

Gothelf and colleagues have introduced the idea of using nets. A net is a two-dimensional (planar) figure that can be folded into a geometric solid. For example, we know that a cube has six sides. Each side of a cube is a square. So if we arrange six squares into a figure that can be folded into a cube, we have a net for a cube. Gothelf did exactly this with the DNA origami technique (see Chapter 7) to fold a long single strand with many short strands into six connected squares, which in turn folded into a box [39].

Mao and colleagues further extended their ideas of multiple double helices, sequence symmetry and tensegrity. By adding a flexible loop into the centre of junctions (Figure 3.22 on page 42), the junction arms are able to bend out of the plane and join to form symmetric three dimensional polyhedra such as buckyballs.

Liedl and colleagues have developed prestressed tensegrity structures. In the top row of Figure 3.23 on page 43 there are images of a tensegrity prism constructed from wood

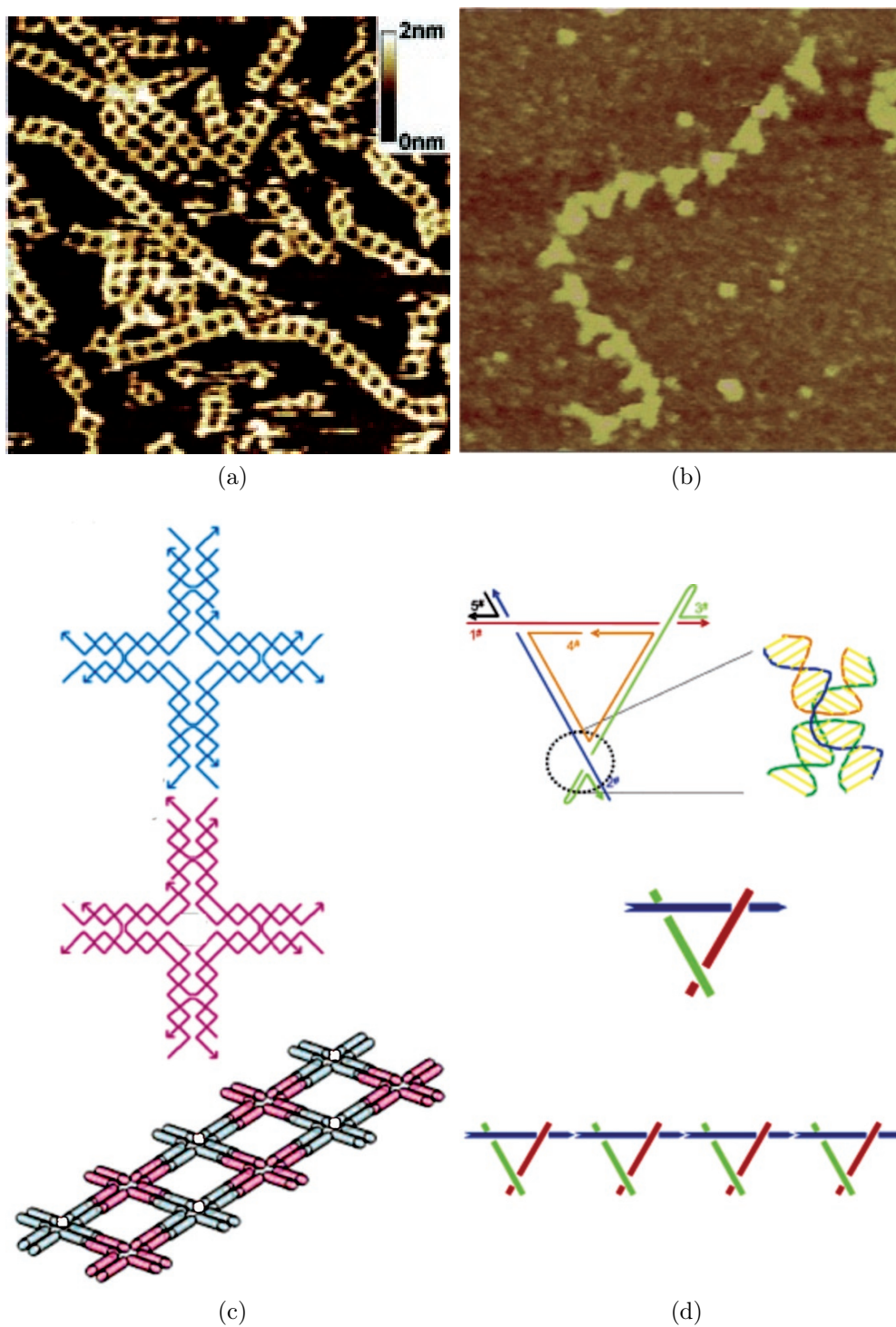


Figure 3.18: *a,c*) Yan and colleagues have demonstrated a chain of two parallel junctions [35] *b,d*) Mao and colleagues took advantage of the idea of tensegrity, fusing the concepts of tension and integrity, with flexible junctions and rigid arms to assemble chains of triangular structures [36].

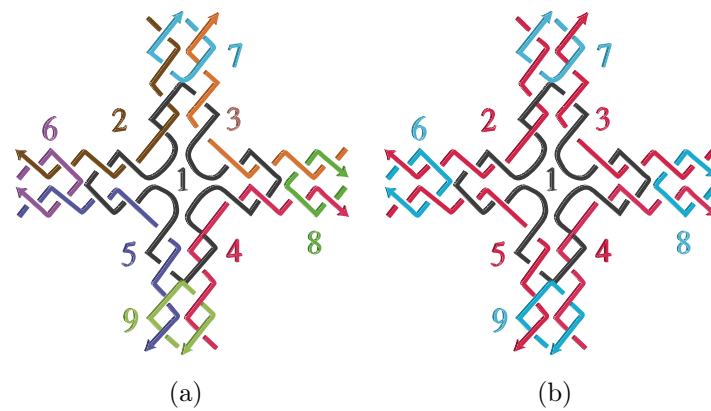


Figure 3.19: Mao and colleagues developed two important concepts. *a*) Firstly, they showed that instead of using single helical junctions one could interlink two double helices on each arm to make the structure significantly more stable. Secondly, instead of using 8 different sequences to form a junction, they showed that using sequence symmetry (use of the same sequence in multiple parts of the structure) they could reduce this to just three different sequences [37].

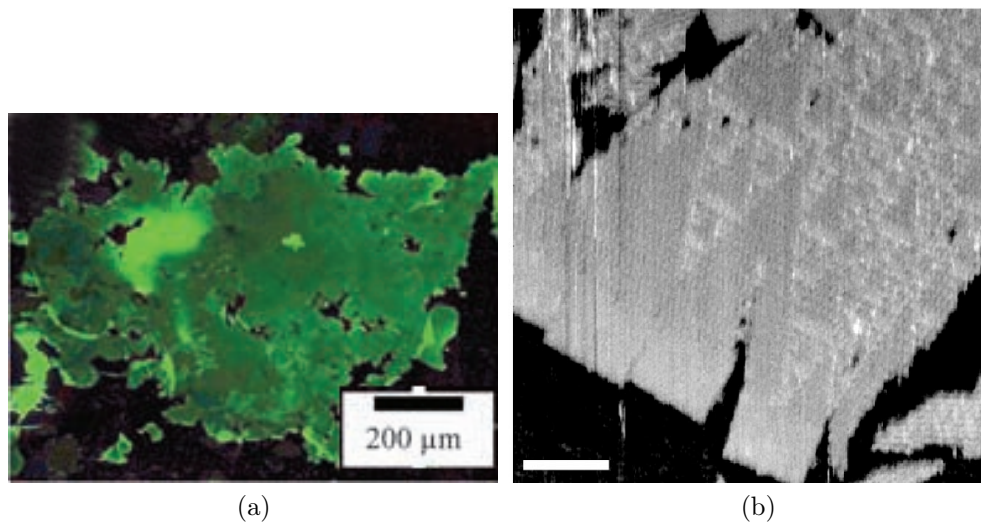


Figure 3.20: *a*) Mao and colleagues demonstrated large ( $\sim$ mm) area arrays using double arm junctions and sequence symmetry [37]. *b*) Winfree and colleagues used the concept of Wang Tiles to demonstrate the assembly of a Sierpinski Triangle structure [38].

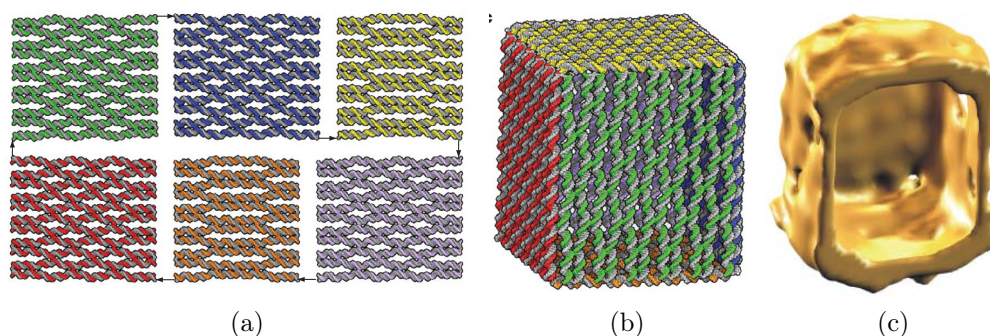


Figure 3.21: Gothelf and colleagues used the DNA origami technique to fold a long single strand with many short strands into a box [39].

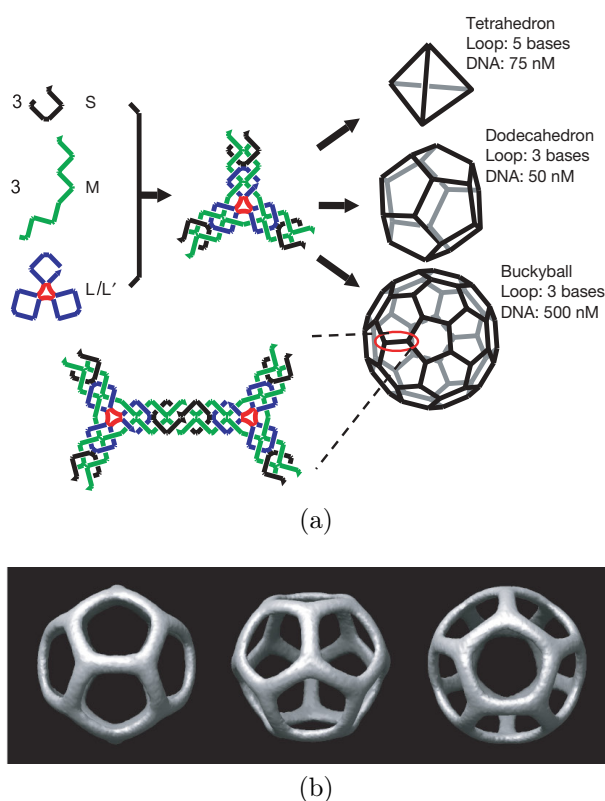


Figure 3.22: Three dimensional structures from Mao and colleagues. *a)* Three different types of DNA single strands stepwise assemble into symmetric three-point-star motifs (tiles) and then into polyhedra. There are three single-stranded loops (coloured red) in the centre of the complex. The final structures (polyhedra) are determined by the loop length (3 or 5 bases long) and the DNA concentration. *b)* Three views of the DNA dodecahedron 3D structure [40].

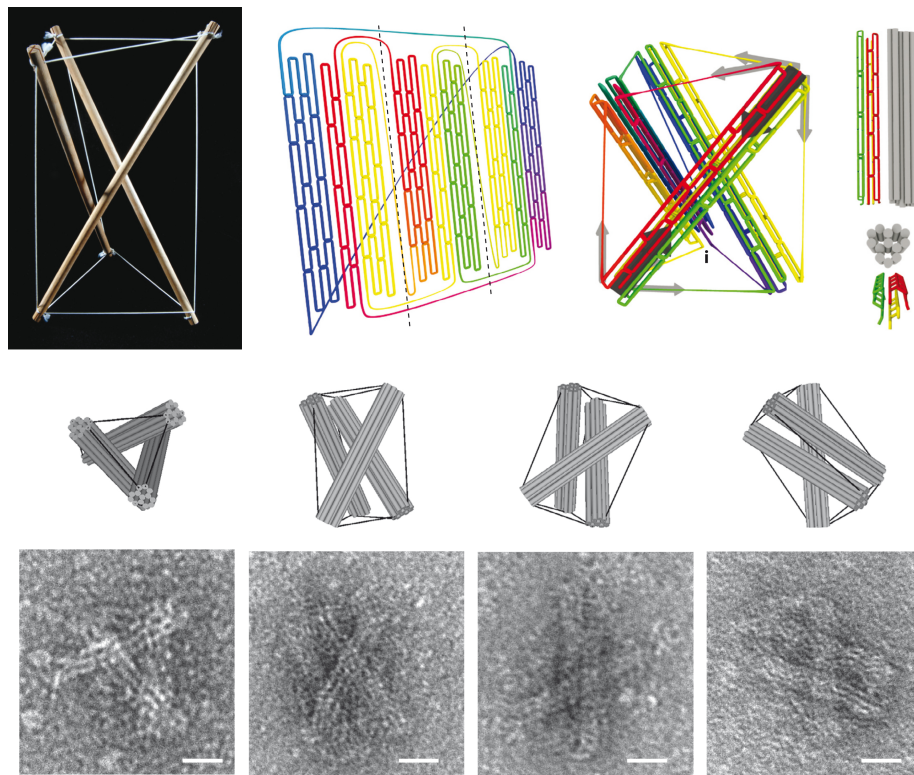


Figure 3.23: Three-dimensional prestressed DNA tensegrity from Liedl and colleagues. Details in text. Electron microscopy image scale bars: 20 nm [41].

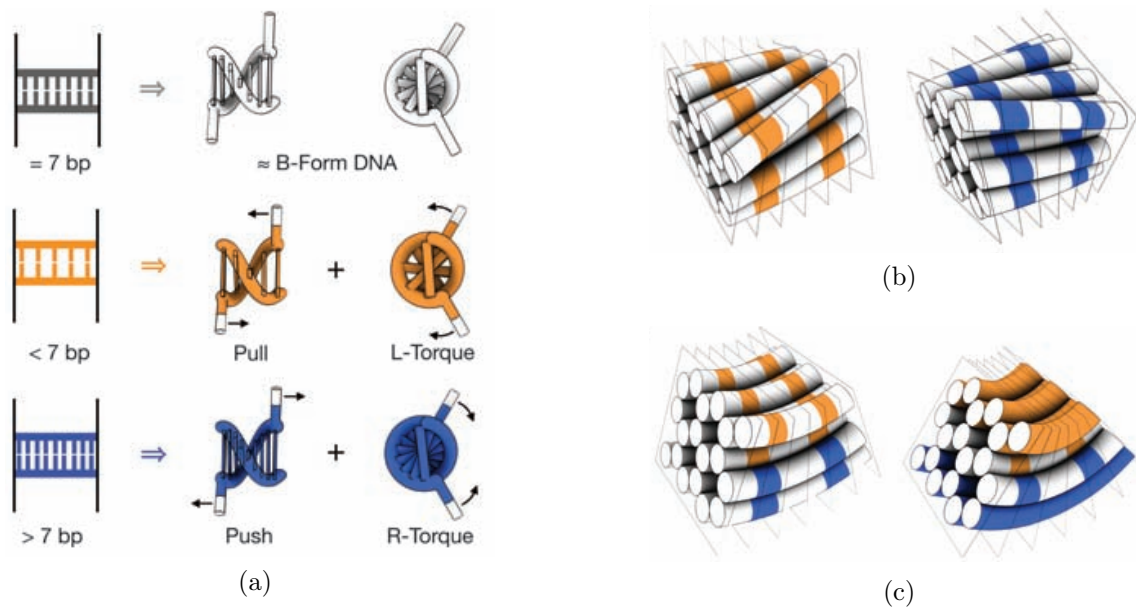


Figure 3.24: Dietz and colleagues have developed methods for controlling twist and curvature in DNA bundles. Details in text [42].

and cord, two-dimensional representation of the pathway through a pre-stressed tensegrity prism, a three-dimensional representation of the backbone pathway for the assembled prism (light grey arrows denote the contractile forces exerted by the single-stranded DNA springs, and dark grey arrows indicate the sum of compressive forces along the axis of the helix bundle) and cylinder and scaffold models of an individual helix bundle (every cylinder represents one double helix). In the bottom two rows are cylinder models and electron microscope images of DNA tensegrity prisms.

Dietz and colleagues have developed methods for controlling twist and curvature in DNA bundles (Figure 3.24 on page 43). Double helices are constrained to a honeycomb arrangement by strand crossovers between helices. Strand crossovers between neighbouring helices are spaced at seven base-pair intervals along the helical axis. By designing intervals with less than seven base-pairs – shown in orange – they create a left-handed torque which pulls on its neighbours. And by designing intervals with more than seven base-pairs – shown in blue – they create a right-handed torque which pushes on its neighbours. Thus they were able to create twist and bending in their structures.

---

These examples of DNA self-assembly in one, two and three dimensions give us an insight in to what is possible with DNA molecules. The following discussion describes the experimental equipment, materials and methods needed to create such structures in the laboratory.

Part II

Equipment and Methods



# Chapter 4

## Assembly and measurement techniques [1]

### Contents

---

<b>4.1</b>	<b>Equipment and techniques . . . . .</b>	<b>49</b>
4.1.1	Absorption spectroscopy . . . . .	49
4.1.2	Gel electrophoresis . . . . .	50
4.1.3	Fluorescence microscopy . . . . .	53
4.1.4	Total internal reflection fluorescence microscopy . . . . .	55
4.1.5	Super-resolution microscopy . . . . .	57
4.1.6	Atomic force microscopy . . . . .	60
<b>4.2</b>	<b>Materials . . . . .</b>	<b>66</b>
4.2.1	Absolute concentration by UV absorption . . . . .	69
4.2.2	Relative concentration by polyacrylamide gel electrophoresis . . . . .	69
4.2.3	Thermal annealing . . . . .	70
4.2.4	Fluorescence microscopy . . . . .	71
4.2.5	Atomic force microscopy in fluid . . . . .	72
<b>4.3</b>	<b>Steps . . . . .</b>	<b>72</b>
4.3.1	Absolute concentration by UV absorption . . . . .	72
4.3.2	Relative concentration by polyacrylamide gel electrophoresis . . . . .	75
4.3.3	Thermal annealing . . . . .	79
4.3.4	Fluorescence microscopy . . . . .	80
4.3.5	Atomic force microscopy in fluid . . . . .	81

---

DNA as a molecule has several advantages when compared with other molecules. It is simple enough to be relatively well understood (compared with proteins), complex enough to build technically advanced structures (compared with many natural and artificial polymers); it can be chemically synthesised (and nowadays ordered from companies over the Internet); and it is stable, reliable and predictable enough to be confidently handled by researchers with little in the way of chemistry background.

A major challenge in the field has been coping with exact stoichiometry requirements needed for high numbers of and/or physically large perfectly assembled structures. Typically several different short ( $\sim 5$ -100 bases) strands bind to each other, and if they are not at the correct absolute and relative concentrations then significant defects occur in the final assembled structures.

Three ideas have been introduced in recent years to overcome this problem. Structures have been assembled that require only one carefully designed sequence which takes advantage of sequence symmetry principles [43]. Examples of this include single-sequence DNA nanotubes shown in Figures 4 and 5. Two other techniques: error avoidance protocols and DNA origami that have been also introduced are left for another discussion [44–46].

To face the challenges of stoichiometry, one measures the absolute or relative concentrations of DNA very precisely. This is done in one of two ways. The absorption of DNA at a light wavelength of 260nm is dependent on its concentration, base sequence length and structure. If the DNA has a known base sequence and length, and does not have any structure (secondary structure), then its concentration can be related to its absorption [47].

If the DNA does have some structure, then the correct concentration ratio with its complementary strands can be chosen by mixing it at different ratios (titrating), and analysing these using titration gel electrophoresis [48].

Having determined the concentrations of the DNA strands, they can then be mixed in appropriate buffer conditions and slowly annealed over several days from 90-20°C to assemble the desired structures.

To visualise the structures several options may be used<sup>1</sup>. Fluorescent molecules that bind to DNA may be added and the structures viewed with a fluorescence microscope, which is relatively quick and easy. An advancement of this is to use a Total Internal Reflection Fluorescence Microscope, which assists in eliminating background fluorescence from above the surface. To optically image fluorophores attached to the DNA structures at resolutions below the diffraction limit, one uses recently developed 'super-resolution' techniques.

Significantly more challenging is the use of an Atomic Force Microscope and fluid cell, visualising the structures using a scanning probe, however this provides much higher resolution.

In this chapter we describe the theory and background of the equipment and techniques, followed by specific protocols with materials and steps. Additional details can be also found in Part III on Results and Discussion.

---

<sup>1</sup>There are other options such as Transmission Electron Microscopy that are not discussed here.

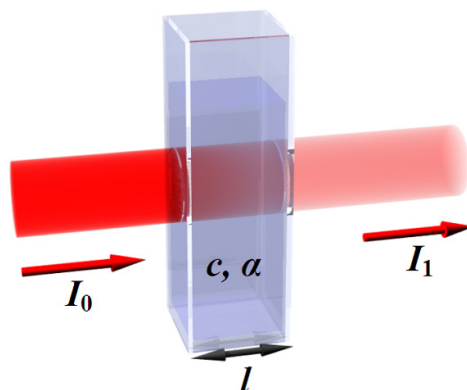


Figure 4.1: Concentration in solution can be determined by application of the Lambert-Beer law to measurements of the intensities of incident and transmitted light through the solution in a cuvette [49].

## 4.1 Equipment and techniques

### 4.1.1 Absorption spectroscopy

The purines and pyrimidines in DNA absorb strongly at UV-wavelengths. DNA has an absorption maximum at a wavelength of 260 nm, this results from in-plane transitions between  $\pi$  electrons of the bases ( $\pi - \pi^*$ ). Excitations of out-of-plane transitions are much weaker and can be neglected. Sugars and phosphates contribute to the absorption mostly below 190 nm [16,17]. As we will see, the concentration of DNA in solution can be determined from its absorption.

The Beer law states that there is a logarithmic dependence between the transmission  $I_1$ , of light through a substance and the product of the absorption coefficient of the substance,  $\alpha$ , and the path-length of the light through the material,  $l$  (in cm).

$$I_1 = I_0 \cdot 10^{-\alpha l} \quad (4.1)$$

The absorption coefficient can, in turn, be written as a product of a molar extinction coefficient,  $\epsilon$  (in  $\text{M}^{-1}\text{cm}^{-1}$ ), and the concentration  $c$  of absorbing species in the material (in  $\text{mol L}^{-1}$ ). The transmission can be expressed in terms of absorption

$$A = -\log \frac{I_1}{I_0} \quad (4.2)$$

$$= \epsilon l c \quad (4.3)$$

This implies that the absorbance becomes linear with the concentration of absorbers. This is known as the Lambert-Beer law. Both  $A$  and  $\epsilon$  are functions of wavelength  $\lambda$ .

If one knows the molecular mass  $M_W$  of single-stranded DNA in solution  $\text{g mol}^{-1}$ , then the approximate concentration can be calculated using

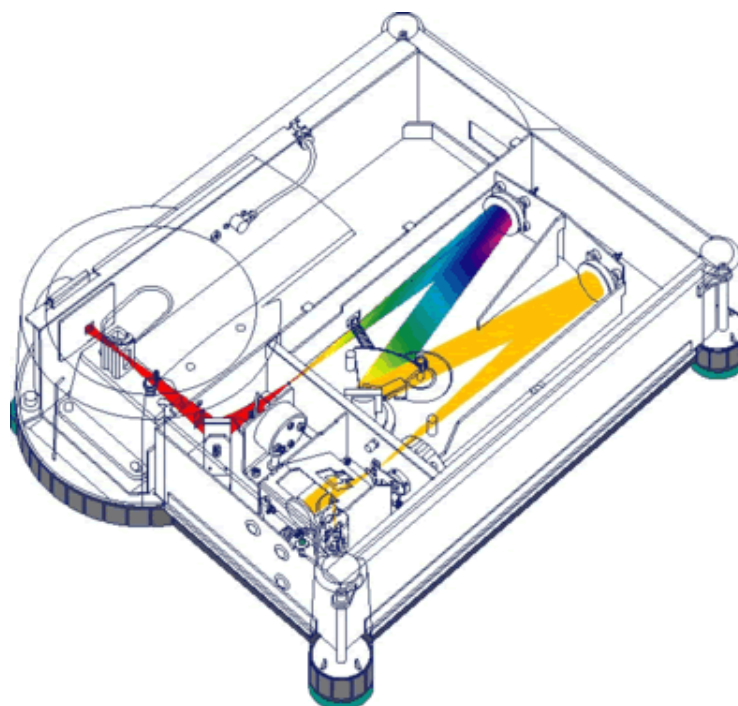


Figure 4.2: An overview of a typical UV-absorption spectrometer such as used in this work [50].

$$c = \frac{A_{meas} \cdot 33}{M_W} \times 10^3 \frac{mol}{l} \quad (4.4)$$

and for double-stranded DNA 50 is used instead of 33.

If one uses a cuvette of 1 cm in diameter and measures an absorption of 1 OD, then the concentration of double-stranded DNA would be approximately  $33 \mu\text{g mL}^{-1}$  or of single-stranded DNA would be  $33 \mu\text{g mL}^{-1}$  [51]. However, pH and ion concentration in the solution affect the measurements, and ideally one measures in a low concentration buffer with no salt. If necessary, low concentrations of monovalent ions such as  $\text{Na}^+$  can be taken into account, and to some extent those of divalent ions such as  $\text{Mg}^{2+}$ , but this is not optimal.

All measurements were performed on Jasco UV-Vis V-550 Spectrophotometer. A detailed protocol is found in section 4.3.1.

### 4.1.2 Gel electrophoresis

Electrophoresis allows one to separate DNA strands of different lengths and structures. The separation occurs under an electric field in a gel. Agarose gels are used to separate strands typically longer than  $\sim 500$  bases, and polyacrylamide gels are used to separate strands with less. The phosphate groups in the sugar-phosphate backbone of DNA are negatively charged, thus the DNA moves in the direction of the anode (which is positively

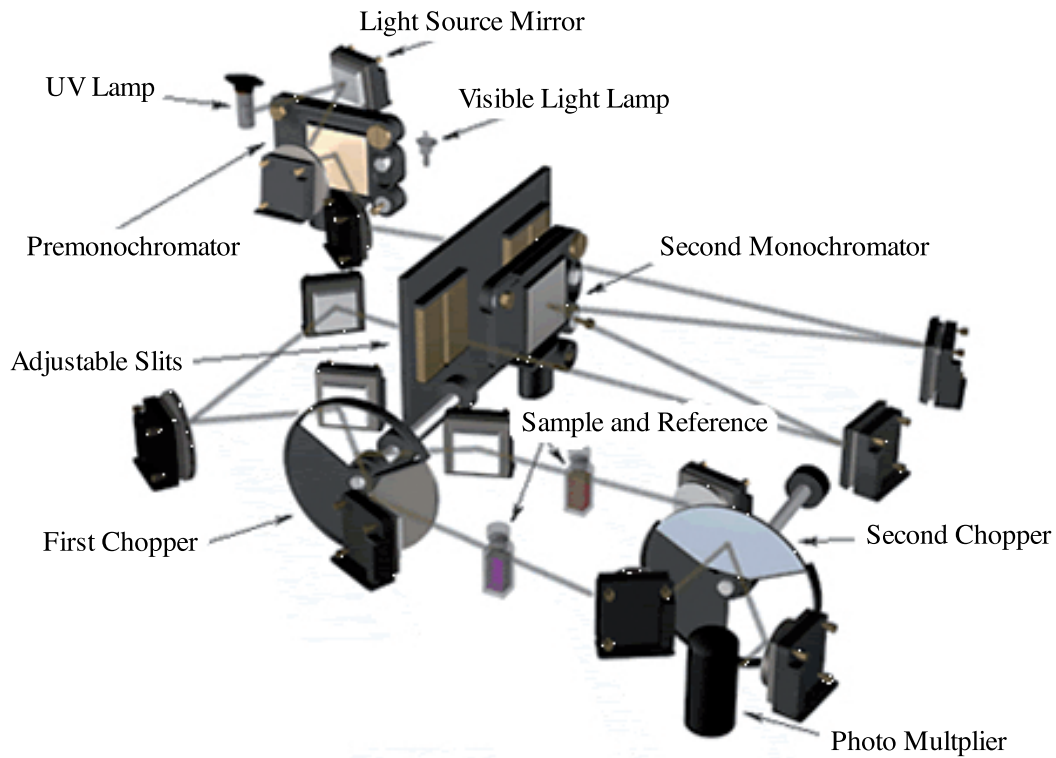


Figure 4.3: Detailed layout of the components inside such a spectrometer.

charged). DNA has a constant charge density, and so the ratio of molecular mass to charge is constant for different lengths.

A charged object disturbs the distribution of ions in a solution. This may be described as a cloud of counter-ions condensed around the charged object. The equilibrium distribution of the mobile ions can be determined with the help of the Poisson-Boltzmann-Equation. The Debye-Hueckel Theory is a linearised form of this equation and can be used as an approximation. It indicates that the external field is screened by the charged ions in the solution. The screening is described by a potential

$$V_s(x) = V_0 e^{-\frac{x}{l_D}} \quad (4.5)$$

where  $V_0$  is the maximum screening potential and  $l_D$  is the Debye screening length

$$l_D = \sqrt{\frac{\epsilon_r \epsilon_0 k_B T}{2 \cdot 10^3 e^2 N_A c}} \quad (4.6)$$

and  $c$  is the concentration of the monovalent ions in mol/l.

When an external electric field is applied, a force results not only on the charged object but also on the ions surrounding it. The ions outside of those within the screening cloud

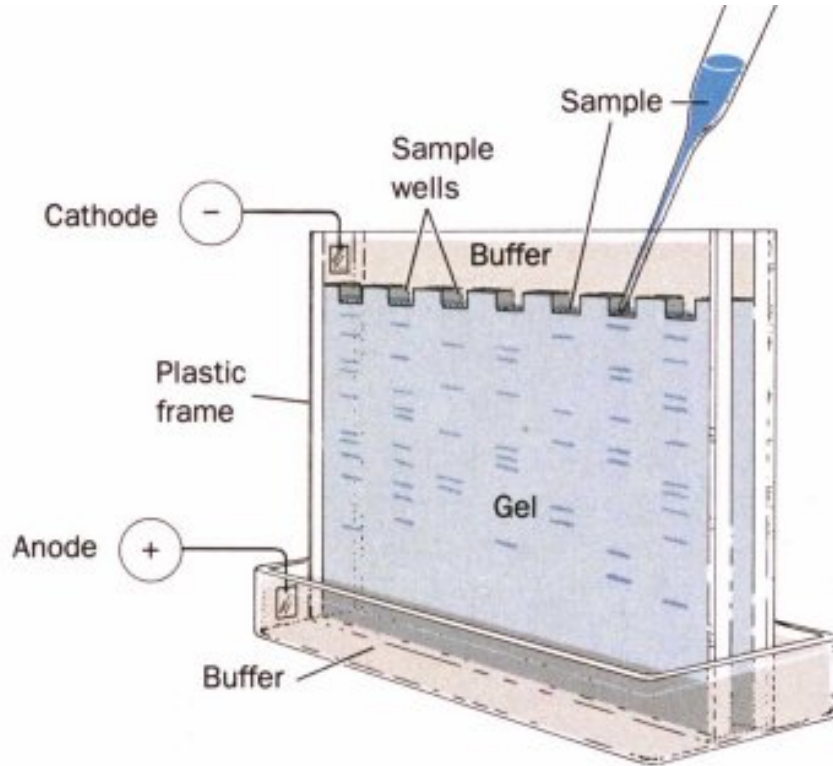


Figure 4.4: A typical polyacrylamide gel electrophoresis system [52].

to one Debye screening length will move in the opposite direction to the charged object and affects its motion hydrodynamically.

For the case that  $l_D$  is much smaller than the object, the Navier-Stokes equations have to be solved. Smoluchowski solved these and found that the velocity is independent of the size and form of the object and the electroosmotic mobility is

$$u = \frac{\epsilon_r \epsilon_0 \zeta}{\eta} \quad (4.7)$$

with Zeta-Potential  $\zeta$ , which is the potential at the edge of the screening cloud. The independence of mobility from size and form in the Smoluchowski theory has important consequences for separation. The Smoluchowski theory describes the relative motion of the charged surface of the object and the surrounding fluid taking into consideration the counter-ions. It is valid for the movement of ions in the vicinity of a motionless charged surface and the influence of an electric field, and the effect is known as the electroosmosis. Equation 4.7 describes the mobility of charged polymers in solution and this independence limits separation in free solution, make it unsuitable for separating DNA of different lengths.

In order to separate DNA of different lengths, one carries out the process in a gel rather than in free solution. This limits the motion of the charged polymer, and can be modelled

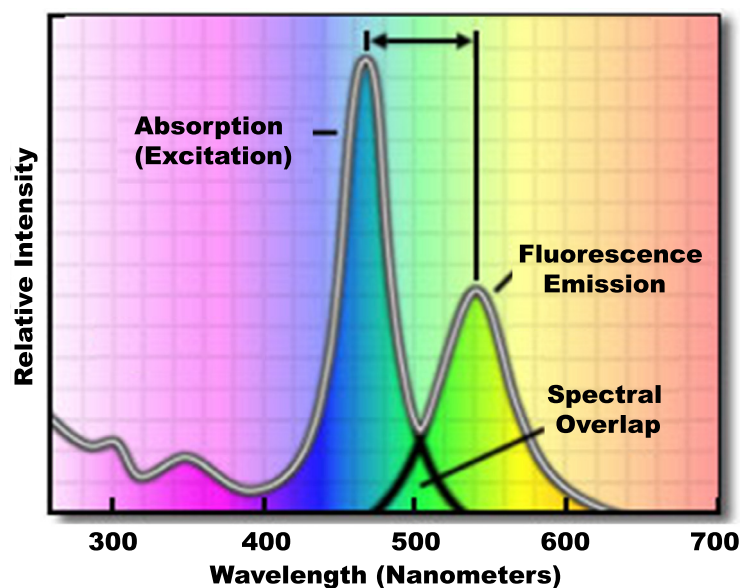


Figure 4.5: Stokes Shift - the difference in absorption and emission wavelengths [54].

with biased reptation to give

$$\frac{u}{u_0} \approx \frac{1}{3} \left( \frac{1}{N} + \frac{\epsilon^2}{3} \right) \quad (4.8)$$

in which  $u_0$  is the mobility in free solution,  $N$  is the polymer length of the backbone and  $\epsilon$  is a reduced electric field and is mainly dependant on the pore size of the gel used. For small  $N$  the first term in equation 4.8 dominates and the mobility is proportional to  $N^{-1}$ . The DNA sequences used in this work can be considered in the category small  $N$ , and thus can be separated using gel electrophoresis [53].

### 4.1.3 Fluorescence microscopy

Fluorescence is a form of photoluminescence - emission of light by an object that is excited by light. The difference in wavelengths (or energies) between absorption and emission is known as the Stokes-Shift (see Figure 4.5) and has its origins in the change in some of the excitation energy into molecular vibrations and rotations.

An overview of the processes at the molecular level are shown in the Jablonski diagram in Figure 4.6. A fluorescent molecule - fluorophore - is excited by a photon of suitable energy from its ground state  $S_0$  into an excited state  $S_2$  with a time scale of approximately  $10^{-15}$  s. Via internal conversion and vibrational relaxation, on time scales of order  $10^{-14}$  s -  $10^{-11}$  s and energy scales of less than 0.2 eV, followed by photon emission, on time scales of order  $10^{-9}$  s -  $10^{-7}$  s, the molecule can return to its ground state. In the diagram the spin quantum numbers in the ground state  $S_0$  and the excited states  $S_1$  and  $S_2$  are identical with a value of zero, these are known as Singlet states. Relaxation from an excited state to

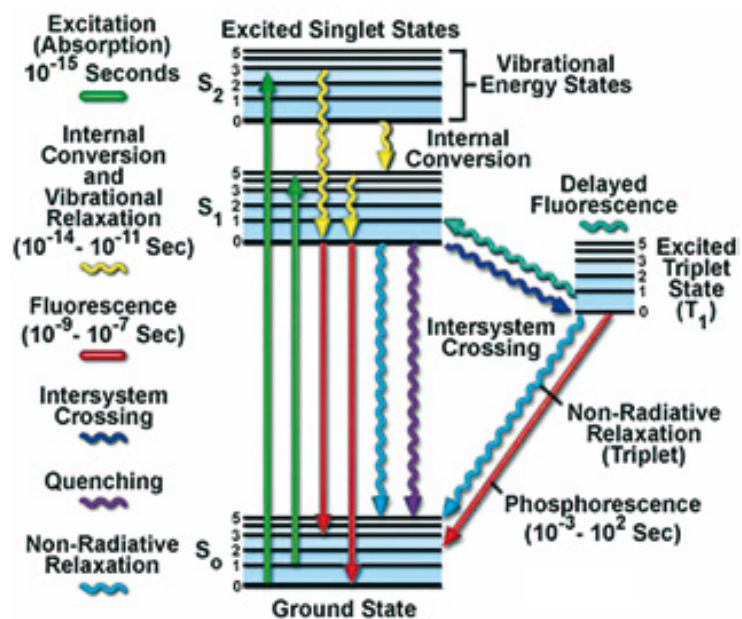


Figure 4.6: A Jablonski diagram showing the excitation and emission pathways of a molecule [55].



Figure 4.7: An Olympus IX71 fluorescence microscope as used in this work.

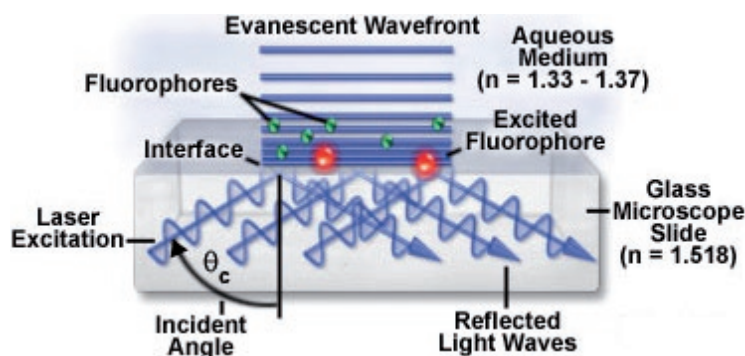


Figure 4.8: The principle of total internal reflection fluorescence microscopy (TIRF). Light meets the solid liquid interface, is reflected, and creates a rapidly spatially decaying evanescent wave that is used to image [58].

the ground state with the same quantum spin number is called fluorescence. Transitions to states with other spin quantum numbers are only possible through a spin flip of the excited electron. A triplet state  $T_1$  has a spin quantum number of value 1. A transition from a singlet to a triplet state requires additional processes (interaction with the nucleus via spin-orbit coupling) because of angular momentum conservation and is less probable. Once excited however such an excited state has a particularly long life time. Return to the ground state is only possible via a further spin flip of the electron and photon emission, this is known as phosphorescence.

One can make use of fluorophores that are excited by light of UV and visible wavelengths and that then fluoresce in the visible wavelength. These may be bound to DNA via covalent or other bond types in order to make visible the location of the DNA. Intercalating dyes that bind between base pairs in double-stranded DNA are particularly common and useful, an example is the YOYO-1 dye from the company Invitrogen.

The fluorescence microscope used in this work was an Olympus IX71, with  $40\times$  air and  $100\times$  oil objective lenses shown in Figure 4.7 on page 54 .

#### 4.1.4 Total internal reflection fluorescence microscopy

Total Internal Reflection Fluorescence (TIRF) employs the phenomenon of total internal reflection, which occurs at the interface between optically dense medium, such as glass, and optically less dense medium –water or aqueous solution. At large angle of incidence, the excitation beam reflects back into glass and generates at the interface with water so called evanescent wave. The evanescent wave has maximum of intensity at the surface and exponentially decays with the distance from the interface. Only molecules that are at the TIRF surface are excited and fluoresce, while molecules in the bulk of solution, at the distances larger than 100-200 nm are not excited and, respectively, do not fluoresce. TIRF efficiently rejects background signal from the bulk of solution and allows for sensitive detection - down to single molecules. [56,57].

The behaviour of a collimated light beam upon refraction or reflection from a plane

surface is fundamental to the understanding of TIRF. Light passing between two media of varying refractive index is either refracted as it enters the second medium or it is reflected at the interface, depending upon the incident angle and the difference in refractive index between the two media. In situations where the light beam is propagating through a medium having a high refractive index and encounters a boundary to a medium of lower refractive index, it is refracted according to Snell's Law

$$n_1 \sin(\theta_1) = n_2 \sin(\theta_2) \quad (4.9)$$

where  $n_1$  is the higher refractive index medium and  $n_2$  is the medium of lower refractive index. The incident wave is positioned at angle  $\theta_1$  from the normal, while  $\theta_2$  represents the angle of light refracted at the interface into the medium of lesser refractive index. As the incident angle slowly increases (relative to the normal), it reaches a point termed the critical angle where the refraction angle is  $90^\circ$ . At higher incident angles, light is completely reflected at the interface (total internal reflection), and no significant amount is refracted into the bulk phase of the medium having a lower refractive index - see Figure 4.8 on page 55.  $n_1$  represents the refractive index of the glass microscope slide or coverslip ( $n = 1.518$ ), while  $n_2$  is the refractive index of the buffer solution ( $n = 1.33$  to  $1.37$ ). Therefore,  $n_1$  is greater than  $n_2$ , and when  $\theta_1$  exceeds the critical angle  $\theta_c$ , total internal reflection occurs within the glass adjacent to the liquid medium. The critical angle is defined by the equation

$$n_1 \sin(\theta_c) = n_2 \quad (4.10)$$

$$\sin(\theta_c) = \frac{n_2}{n_1} \quad (4.11)$$

For angles less than  $\theta_c$ , a majority of the incident light propagates directly through the interface with a refraction angle measured from the normal as defined by Snell's Law. Even in this situation, some of the incident light is reflected back into the glass. However, for all angles greater than the critical angle, total internal reflection is achieved and a vast majority of the light is reflected. A small portion of the reflected light penetrates through the interface, and propagates parallel to the surface in the plane of incidence creating an electromagnetic field in the liquid adjacent to the interface. This field, as described above, is termed the evanescent field and is capable of exciting fluorophores residing in the immediate region near the interface.

The evanescent field intensity decays exponentially with increasing distance from the interface according to the equation

$$I_z = I_0 e^{-\frac{z}{d}} \quad (4.12)$$

where  $I_z$  represents the intensity at a perpendicular distance  $z$  from the interface and  $I_0$  is the intensity at the interface. The characteristic penetration depth ( $d$ ) at  $\lambda$ , the wavelength of incident light in a vacuum, is given by

$$d = \frac{\lambda}{4\pi\sqrt{n_1^2 \sin^2 \theta_1 - \sin^2 \theta_2}} \quad (4.13)$$

The penetration depth, which usually ranges between 30 and 300 nanometres, is independent of the incident light polarisation direction, and decreases as the reflection angle grows larger. This value is also dependent upon the refractive indices of the media present at the interface and the illumination wavelength. In general, the value of  $d$  is on the order of the incident wavelength, or perhaps somewhat smaller [59].

### 4.1.5 Super-resolution microscopy

Super-resolution microscopy is a collection of techniques to optically image with resolution below the diffraction limit using localisation of single fluorescent molecules with similar spectral characteristics. The techniques makes use of having fluorescent molecules which change from a dark state to a fluorescent state and vice versa over time. Different methods use different types of fluorescent molecules and different methods to change the molecule's state. All techniques make use of mathematical processing to generate high-resolution images. A range of these methods and others are depicted in Figure 4.9 on page 58.

The first example of this technique was developed by Stefan Hell from the Max Planck Institute for Biophysical Chemistry, publishing the theory in 1994 and the first truly nano-scale fluorescence images in 2000. His technique is known as STED - STimulated Emission Depletion and is based on fluorescently activating a spot and then shrinking the spot by depleting the emission in a doughnut-shaped area surrounding it.

Mats Fustafsson in 2000 developed SIM - Structured Illumination Microscopy - and is based on the illumination of the sample with a series of light patterns that can make an otherwise unresolvable fine structure visible in the form of low-resolution moiré fringes.

Samuel Hess in 2006 developed a technique based on photoactivatable proteins called PALM - Photoactivation Localisation Microscopy. Also in 2006, Xiaowei Zhuang developed STORM - STochastic Optical Reconstruction Microscopy - by using cyanine dyes that can be activated to a fluorescent state and deactivated to a dark state by using different colours of light.

Christian Steinhauer and Philip Tinnefeld developed an analogous approach called directSTORM that can use any synthetic, single-molecule compatible fluorophores by engineering dark states, e.g., by increasing the triplet state lifetime through oxygen removal or by inducing radical-ion states. The molecules thus 'blink' on and off. The key issue to using this blinking for super-resolution microscopy is to localise a sufficient number of fluorophores within a diffraction limited spot, see Figure 4.10 on page 59. This number is directly linked to the ratio of the off-times to the on-times of the fluorophores as well as to the data acquisition speed. To be able to resolve as many fluorophores as possible in a diffraction limited spot it is the aim to have very short but bright on-states and long off-states. On the other hand controlling the off-state duration with a balance of fast acquisition and high resolution is desired. To this end, the length of the off-state limits the achievable spatial resolution since due to technical limitations of the camera's acquisition

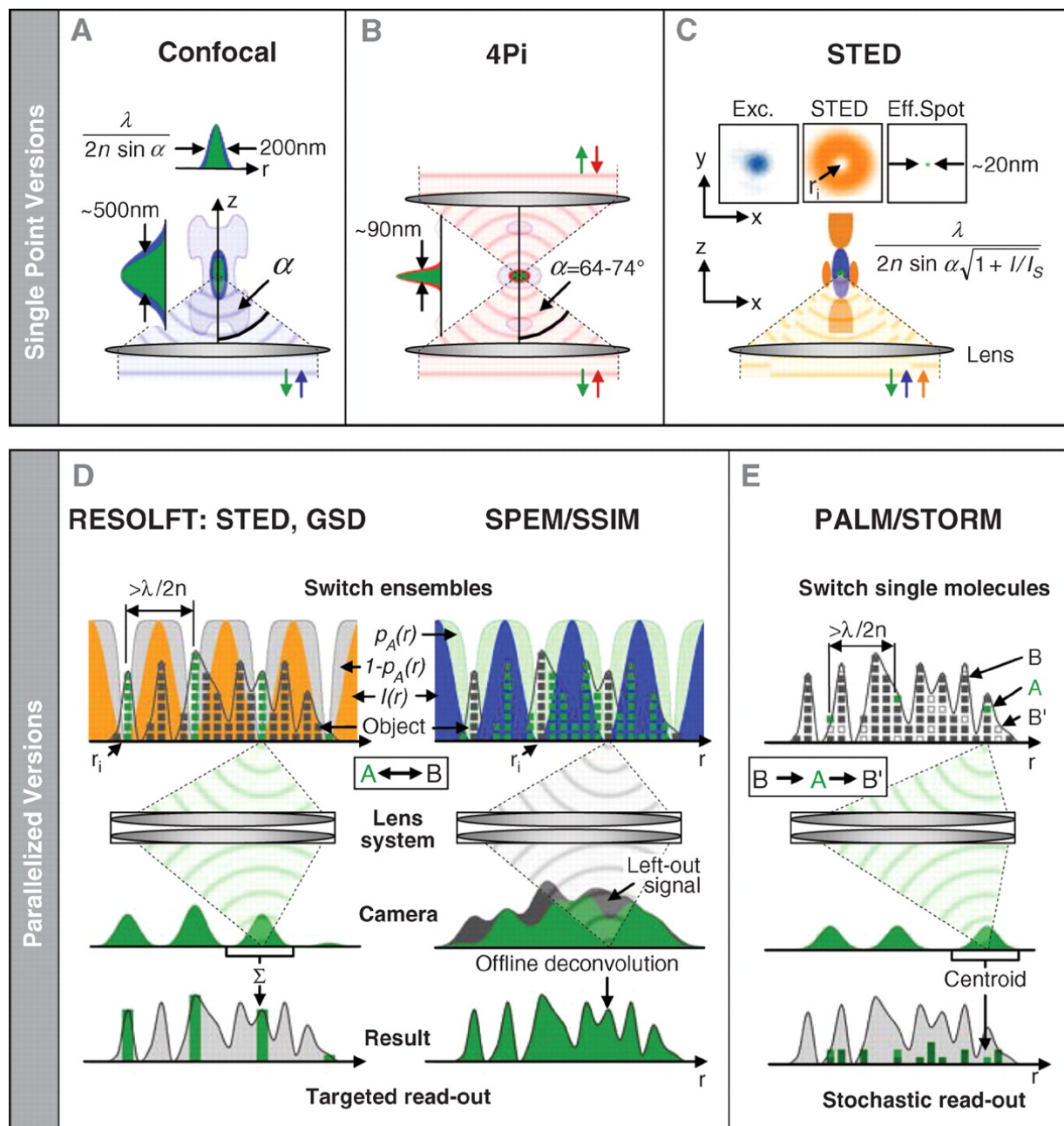


Figure 4.9: Fluorescence nanoscopy schemes: single-point scanning (upper row) and parallelized versions (lower row) [60].

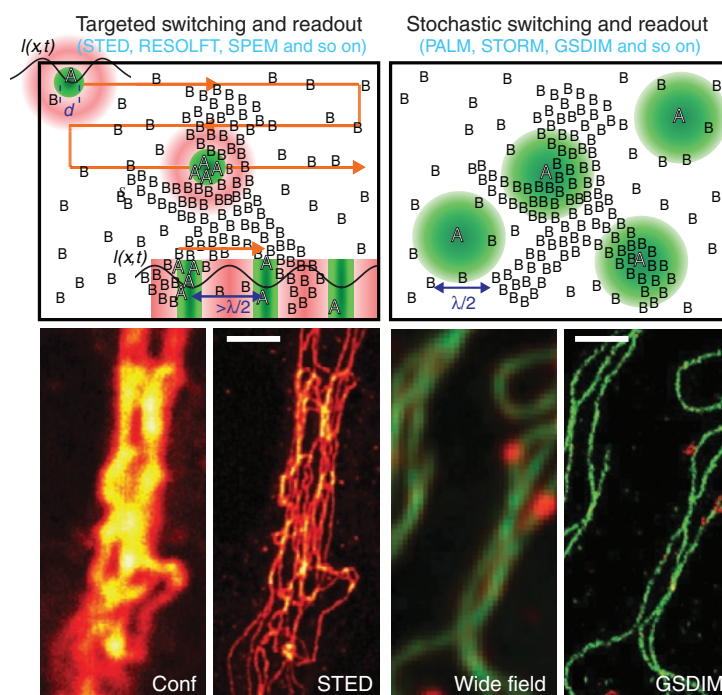


Figure 4.10: Fluorescence switching strategies for super-resolution image assembly. To resolve details that are closer than the diffraction limit  $\lambda/(2n \sin \alpha)$ , current far-field fluorescence nanoscopy schemes switch molecular fluorescence on and off so that adjacent features or molecules do not emit simultaneously. Switching means transferring the molecules from a fluorescent state (A) to a dark state (B), or vice versa [61].

speed the resolution cannot be improved infinitely by reducing on-state duration through high excitation intensities. The natural lifetime of the triplet state typically is in the lower millisecond range in the absence of oxygen and poses an upper limit of the dark state duration. They use electron transfer reactions to extend the range of achievable on- and off-times.

The methods above use experimental techniques to circumvent the diffraction barrier, but one can also use mathematical analysis to increase the ability to know where a nanoscale object is located. The image of a point source on a charge-coupled device camera is called a point-spread function (PSF), which is limited by diffraction to be no less than approximately half the wavelength of the light. But it is possible to simply fit that PSF with a Gaussian to locate the centre of the PSF — and thus the location of the fluorophore. The precision by which this technique can locate the centre depends on the number of photons collected (as well as the CCD pixel size and other factors). This concept has been used to achieve localisation of single fluorophores to a few nanometres. This, of course, requires careful measurements and collecting many photons. This is depicted in Figure 4.11 on page 60.

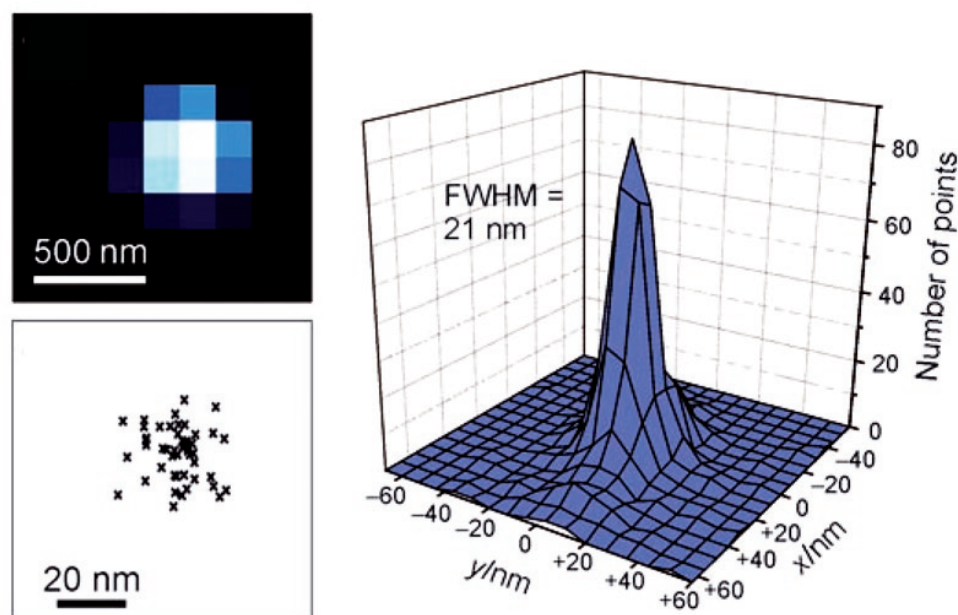


Figure 4.11: *Left upper)* Conventional fluorescence image showing the typical emission pattern of a single Cy5-labelled DNA molecule. The point spread function of activated fluorophores is analysed by a Gaussian function to determine its precise position. *Left lower)* Repetitive localisations of a single Cy5-labelled DNA molecule switching between its fluorescent and dark states are represented as crosses. *Right)* Aligned two-dimensional distribution of localisations from 50 Cy5-DNA molecules demonstrates a spatial resolution of  $21 \pm 1$  nm with conventional fluorescent probes [62].

#### 4.1.6 Atomic force microscopy

**Theory** The Atomic force microscope (AFM) belongs to a class of microscopes known as scanning probe microscopes. These provide non-destructive three dimensional high spatial resolution real space images of surfaces. Images are formed by detecting the local interactions between the specimen surface and a sharp probe.

**History and Definitions** The development of the AFM was preceded by the development of the Scanning Tunnelling Microscope (STM) in 1981 at IBM Zurich Research Laboratory by Binnig and Rohrer. Its ability to view the atomic lattice of a sample surface earned the inventors the Nobel Prize in physics in 1986. Although the STM provides sub-angstrom resolution in all three dimensions, it is limited to conductive and semiconductive samples. To image insulators as well as conductors, the AFM was developed in 1986, and the first commercial AFM's were produced in 1989 by Digital Instruments.

**Elements of the Microscope:** The major elements of an AFM are shown in Figure 4.12 and include a scanner to control tip movement over the surface, the tip itself, a tip

motion sensor, and control and data collection electronics, computers and software. These are discussed further below.

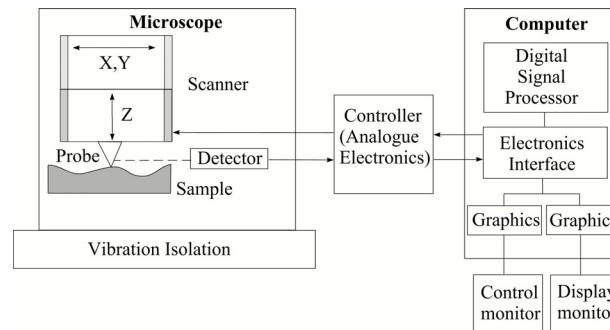


Figure 4.12: Schematic representation of an Atomic Force Microscope [63].

**Scanner** AFM involves scanning a sharp tip across a surface, or scanning surface across the tip. In order to image on the smallest scales possible, this is made possible using a piezoelectric tube scanner.

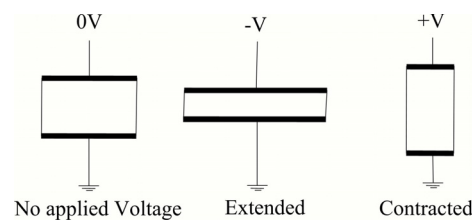


Figure 4.13: A piezoelectric crystal changes size depending on polarity and magnitude of an applied voltage. This is the basis of an AFM scanner [63].

These expand and contract proportionally to the magnitude and polarity of an applied voltage. The scanner is constructed by combining independently operated piezoelectrodes for X, Y, and Z axes into a single tube, forming a scanner which can manipulate samples and probes with extreme precision in 3 dimensions, as shown in Figure 4.14. A.C. voltages applied to the different electrodes of the scanner produce a scanning raster motion in X and Y. There are two segments of the piezoelectric crystal for X and Y.

#### Problems with piezoelectric scanners:

- The Sensitivity (how far the piezo extends or contracts per applied Volt) is not a linear relationship with respect to scan size. This can cause distortion of the image if it is not properly corrected during AFM calibration.
- Aging. The sensitivity of piezoelectric materials decreases exponentially with operation time. As the scanner ages, the sensitivity will change less with time and will

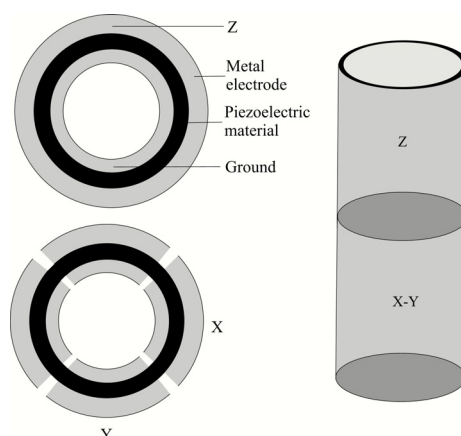


Figure 4.14: A schematic diagram of an AFM tube scanner. There are two elements, one controls horizontal X-Y motion and the other controls vertical Z motion [63].

eventually reach the point where it seldom needs recalibrating. The AFM is run continuously before leaving the factory until it reaches this point.

- Creep. This is the drift of the piezo displacement after a DC offset voltage is applied to the piezo. It results when large offsets are applied and it takes time (and several scan lines) to assume its correct position. This distorts the image. It can be minimised by ensuring small offsets.
- Bow. The scanner is fixed at one end, and moves the tip with the other end. This results in a curved motion, and in correcting for this a bowed shape can be induced in the image.

**Tapping Mode AFM** There are three main techniques used in AFM. The technique used by the inventors of the AFM (Binnig, Quate, and Gerber), and which is still used today, is ‘*contact mode*’. The probe tip is simply dragged across the surface. However under ambient air conditions, most surfaces are covered by a layer of adsorbed gases (water vapour and other contaminants) which is typically several nanometres thick. When the scanning tip touches this layer, capillary action causes a meniscus to form and surface tension pulls the cantilever down into the layer as drawn in Figure 4.15. This force and the lateral shear forces caused by the scanning motion can distort measurement data and cause damage to the tip and sample.

An attempt to avoid this problem resulted in a new technique: ‘*non-contact*’ mode. The probe is held a small distance above the sample and the Van der Waals acting between the sample and the tip are detected and used to form the topographic image. The Van der Waals forces are so small that there is a loss of resolution, and the tip must be kept so close to the surface that practical problems are encountered.

Thus a third technique has been used, and it is the technique I have used, which is known as ‘*tapping mode*’. The tip is placed alternatively in contact with the surface to provide

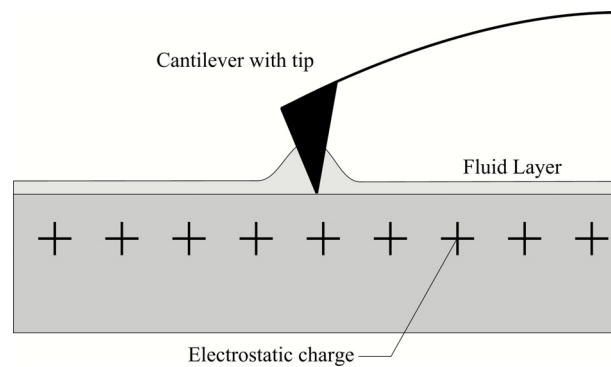


Figure 4.15: An AFM tip initially experiences electrostatic Coulomb forces but once close to the surface it feels capillary action due to adsorbed gases [63].

high resolution and then lifted off the surface to avoid dragging it to the new position. This is implemented by oscillating the cantilever (on which the tip is mounted) at or near the cantilever's resonant frequency.

The piezo motion causes the cantilever to oscillate with high amplitude (the 'free air' amplitude, typically greater than 20nm) when the tip is not in contact with the surface. The oscillating tip is then moved towards the surface until it begins to lightly 'tap' the surface. As the cantilever begins to intermittently contact the surface, the cantilever oscillation is necessarily reduced due to energy loss caused by the tip contacting the surface, as in Figure 4.16. The reduction in oscillation amplitude is used to identify and measure surface features.

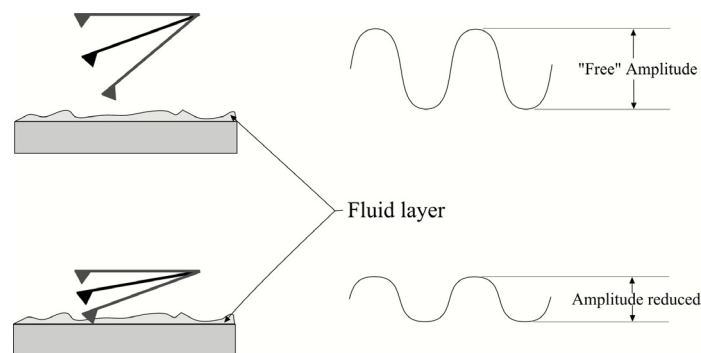


Figure 4.16: A Tapping Mode oscillating tip changes its oscillation amplitude as it contacts the surface [64].

The whole system is shown schematically in Figure 4.17 on page 64.

**Cantilevers and Tips** The cantilever and tip of an Atomic Force Microscope are extremely important, as it is these that interact with the sample in order to perform measurements. Some critical cantilever properties are listed below:

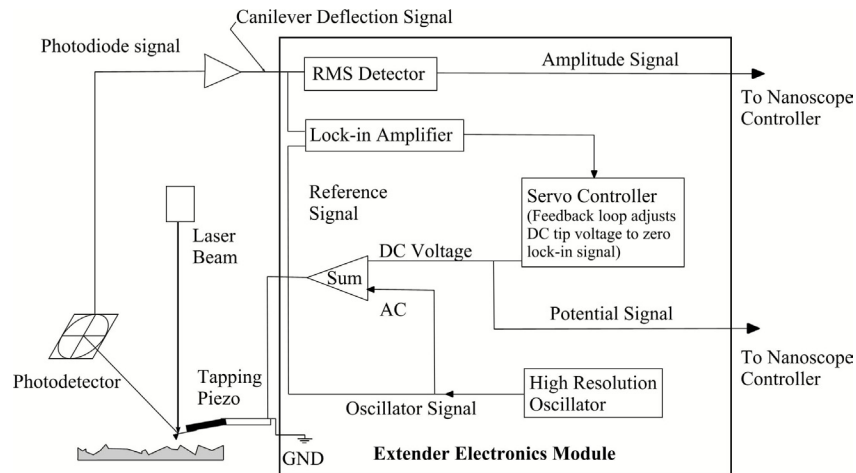


Figure 4.17: Tapping Mode Imaging [64] .

1. *Cantilever material* - affects the cantilever and tip through their inherent mechanical properties (elasticity modulus  $E$ , rigidity  $G$ ) and density to define the stiffness, resonant frequency and Q-factor (see below).
2. *Cantilever geometry* - for tapping mode imaging the geometry used is a thin rectangular bar.
3. *Cantilever stiffness* - the force constant  $k$  measures the stiffness of the cantilever. Rigid cantilevers with  $k > 1\text{Nm}^{-1}$  are used for tapping mode as they exhibit high resonant frequencies and small oscillation amplitudes of order 1nm. This provides a wide dynamic frequency range and substantially raises sensitivity. By shortening the length of the cantilever the resonant frequency can be increased. At the same time the cantilever can be made flexible by width or thickness adjustments compensating for the increase in force constant  $k$ . Cantilevers with high resonant frequencies  $f_0$  and low  $k$  are better choices for tapping mode since the tip very gently taps the surface at the same time oscillating at several hundred kilohertz.
4. *Q factor* - represents the energy lost from the vibrational system after a full cycle of oscillation. In other words it defines the minimal external vibrational force needed to maintain oscillation of the system. Ideally, no external force is needed since it contributes to noise and reduces sensitivity. The higher  $Q$  is, the greater the measurable sensitivity is.

Tip parameters include height, profile, angle at the tip apex (tip half angle) and apex curvature of radius. Tips are generally produced using (electro) chemical techniques from mono-crystalline Silicon. The resolution of Atomic Force Microscopy depends substantially on the sharpness of the imaging tip. This is demonstrated in Figure 4.18. The curvature of radius of a conventional tip is about 10-15nm. Ideally the tip apex must be round shaped

and terminate with a single atom. Deviations from this ideal situation cause ‘tip artifacts’ in the scanned images.

One of the technical issues users must abide by is the imperfect geometry and finite size of the tip. In general, a conventional tip is unable to penetrate high aspect ratio structures, touch every point on the sample surface, and profile complex geometries exactly. So the finite size of the tip and its imperfectness contributes significantly to the distortion of images.

Due to the long-range nature of Coulomb forces acting between the tip and sample, the resulting force is determined by the mean interaction of a number of atoms from both the tip and sample surfaces especially when the features are comparable in size to the tip apex. Therefore, features of the sample surface become diluted by this interaction of collective nature.

Thus, the image is actually a convolution of tip and surface shapes. This convolution is unavoidable but it is possible to reconstruct the true image using particular mathematical techniques.

These methods rely on knowledge of the tip geometry. Specially designed calibration gratings can serve as tip characterisers.

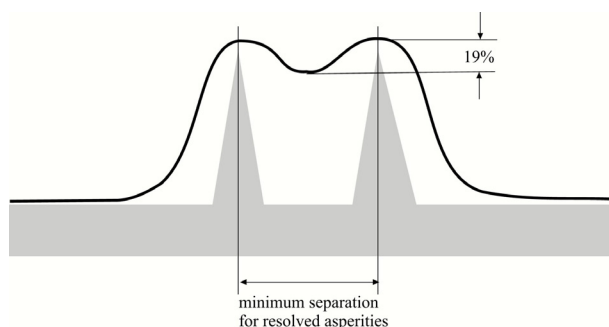


Figure 4.18: Definition of lateral resolution using Rayleigh’s criterion.

**Tip Motion Sensor** The tip-sample interaction is monitored by a position sensitive detector. Laser light from a solid state diode is reflected off the back of the cantilever (which is coated with metallic surface such as Gold) and onto two closely spaced photodiodes. The angular displacement of the cantilever results in one photodiode collecting more light than the other photodiode, producing an output signal. The output signal from each diode is sent to one input of a differential amplifier. The output signal from this is proportional to the deflection of the cantilever. This is shown schematically in Figure 4.19.

The long beam path (several cm) amplifies changes in beam angle and cantilever deflections of less than one Angstrom (1) are detected. This method produces the root-mean-square amplitude of the cantilever oscillation.

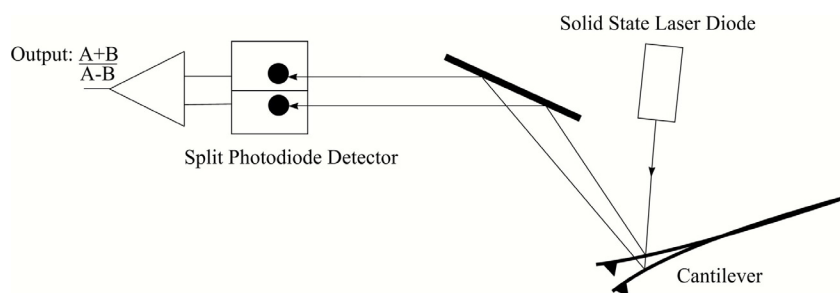


Figure 4.19: Schematic of a Tip Motion Detector. A laser beam is reflected differently onto a split Photodiode detector depending on oscillation amplitude. This difference is detected using a differential amplifier [64].

**Imaging in Fluids** Imaging samples under fluid eliminates attractive forces due to surface tension. This enables the sample surface to be imaged with a minimum of cantilever tip force—a decided advantage when imaging soft materials such as DNA. Essentially, the procedure for observing samples under fluid is the same as that for Tapping Mode AFM in air; however, special hardware is utilised to contain the fluid. In addition, minor adjustments must be made to correct for refractive effects as the laser beam transits air-fluid boundaries.

**Equipment** The atomic force microscope used in this work is a Veeco Multimode with Nanoscope V controller, shown in Figure 4.20 on page 67. The majority of imaging was done with a fluid cell and Tapping Mode using DNP-S Silicon Nitride cantilevers from Veeco Probes. Images of such cantilevers are in Figure 4.21 on page 67, tip parameter definitions are shown in Figure 4.22 and cantilever and tip parameters are in Table 4.1 on page 68.

## 4.2 Materials

Following is a list of materials needed for each of the techniques, and then the steps for the techniques.

The following lists of materials and equipment are suggested, along with recommended suppliers. There are often many other good suppliers for these, the following are suggestions only, in particular with regards to equipment. Note also that product numbers may change with time.

All water used should be 18 M $\Omega$  and of pH 7-8.



Figure 4.20: A Veeco Multimode atomic force microscope.

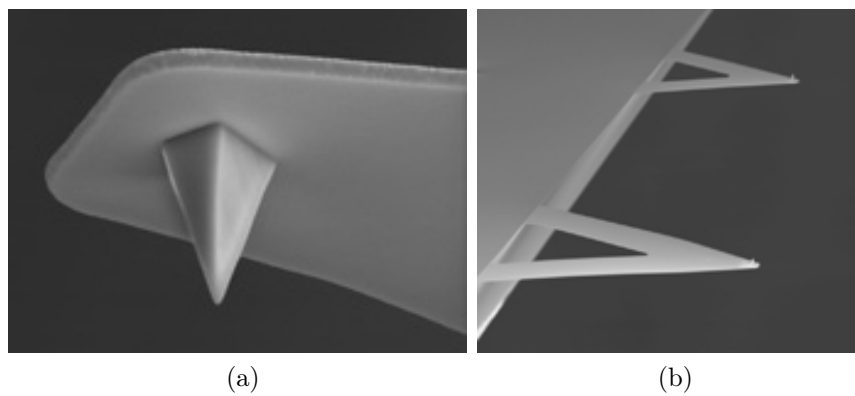


Figure 4.21: *a)* A scanning electron microscope image of a silicon-nitride tip of the type used in this work. *b)* Multiple cantilevers are mounted on the silicon chip, the smaller thinner cantilever is suitable for the soft DNA.

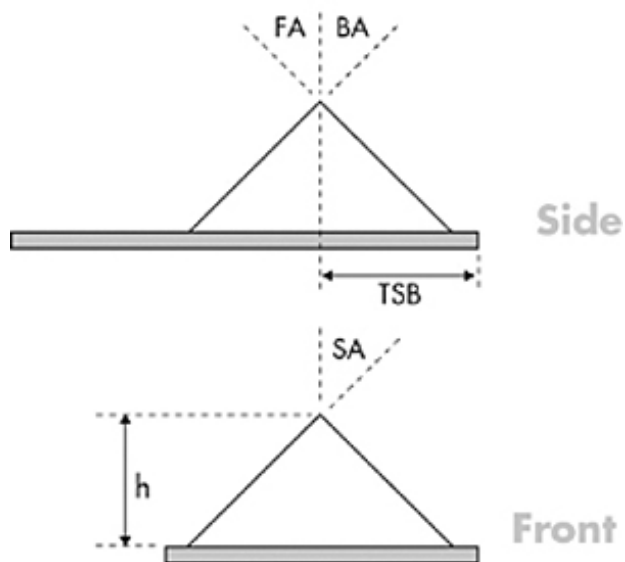


Figure 4.22: Atomic force microscope tip parameters, see also Table 4.1 on page 68.

Cantilever type	SiNi
Tip height ( $h$ )	2.5-8 $\mu\text{m}$
Front angle (FA)	$15 \pm 2.5^\circ$
Back angle (BA)	$25 \pm 2.5^\circ$
Side angle (SA)	$22.5 \pm 2.5^\circ$
Radius of Curvature	$\sim 10$ nm
Tip setback	5 $\mu\text{m}$
Thickness	0.6 $\mu\text{m}$
Length	120 $\mu\text{m}$
Width	20 $\mu\text{m}$
Force Constant	0.32 N/m
Resonant Frequency in fluid	$\sim 8$ (kHz)

Table 4.1: Cantilever and tip parameters

### 4.2.1 Absolute concentration by UV absorption

1. UV spectrometer<sup>2,3</sup> (V-630Bio, Jasco, Japan)
2. Cuvettes: 2 (105.202, Hellma, Germany)
3. Water: 18 M $\Omega$ , pH 7-8
4. Pipettes: 100  $\mu$ L, 2.5  $\mu$ L (3111 000.114, 3111 000.149, Eppendorf, Germany)
5. Centrifuge tubes: 0.5 mL (0030 108.035, Eppendorf, Germany)
6. Clean compressed air/nitrogen and/or lens cleaning tissue
7. DNA (Integrated DNA Technologies, USA)

### 4.2.2 Relative concentration by polyacrylamide gel electrophoresis

1. Gel electrophoresis system (PerfectBlue Dual Gel System, 45-2020, Peqlab Biotechnologie, Germany)
2. Electrophoresis Power supply (EPS301, GE Healthcare, USA)
3. Circulating cooling water<sup>4</sup> at 4 °C
4. Detergent (1104-1, Alconox, USA)
5. Ethanol in squirt dispenser (E7023, Sigma-Aldrich, Germany)
6. Acrylamide-bisacrylamide: (Rotiphorese Gel 40(37. 5:1), T802.1, Roth, Germany). This is a neurotoxin and should be handled with care in a fume cupboard.
7. Buffer (10x TAE (400 mM Tris-acetate, 10 mM EDTA) buffer, pH 8.3)
8. Water: 18 M $\Omega$ , pH 7-8
9. MgCl<sub>2</sub>: 1 M (M1028, Sigma-Aldrich, Germany)
10. TEMED (Tetramethylethylenediamine, T9281, Sigma-Aldrich, Germany)
11. APS (Ammonium persulfate, A1433, Sigma-Aldrich, Germany) prepare fresh solutions weekly at 10% w/v in water.

---

<sup>2</sup>There are now ultraviolet absorption spectrometer systems that are designed to quickly measure  $\mu$ L volumes in the  $\mu$ M range. These may not be accurate enough for the standards required here.

<sup>3</sup> For DNA concentration measurements, temperature control (via a programmable water bath or peltier element) of the sample while measuring absorption is not usually necessary, however this is useful for making DNA melting measurements, often used to assist in analysing these structures.

<sup>4</sup>The gels should be 'run' at 4°C, this can also be achieved by placing the system in a cool room or refrigerator.

12. Glass beakers: 2, 150 mL (2110629, Duran Group, Germany)
13. Pipettes: 100  $\mu$ L, 2.5  $\mu$ L (3111 000.114, 3111 000.149, Eppendorf, Germany)
14. Vacuum chamber and pump (2478257, Duran Group, Germany) (MVP 015-4, Pfeiffer Vacuum, USA)
15. Aspirating pipettes: 25 mL (357556, BD Falcon, USA)
16. Pipette Filler (612-1931, VWR International, USA)
17. Bulldog clips
18. Centrifuge tubes: 0.5 mL (0030 108.035, Eppendorf, Germany)
19. Syringe (Omnifix Luer 20 ml, 4616200V, B. Braun Melsungen, Germany)
20. Needle (Sterican G 14 0.60x30mm, 4657640, B. Braun Melsungen, Germany)
21. Gel loading buffer: 4 g sucrose, 25 mg bromophenol blue, 25 mg xylene cyanol, 25 mg Orange G (S0389, B8026, X4126, O3756, Sigma-Aldrich, Germany), H<sub>2</sub>O to 10 mL. Store in small aliquots at 4 °C.
22. DNA ladder (Low Molecular Weight, N3233, New England Biolabs, USA)
23. Sybrgold (S11494, Invitrogen, USA). This is toxic and should be handled carefully according to the manufacturer's instructions.
24. Stiff plastic/card sheet larger than the gel plates
25. Aluminium foil
26. Staining tray: opaque plastic box with lid slightly larger than the size of the gel.
27. Gel documentation system (Molecular Imager Gel Doc XR, Bio-Rad, USA)
28. DNA strands (Integrated DNA Technologies, USA)

### 4.2.3 Thermal annealing

1. Buffer (10x TAE ( 400 mM Tris-acetate, 10 mM EDTA) buffer, pH 8.3)
2. MgCl<sub>2</sub> 1 M (M1028, Sigma-Aldrich, Germany)
3. Water: 18 M $\Omega$ , pH 7-8
4. Membrane filter: 0.02  $\mu$ m (Anotop 25 Plus, Whatman, England)
5. Beaker: 2-4 L (2110668, Duran Group, Germany)

6. Styrofoam box to fit beaker<sup>5</sup>
7. Boiling water to fill beaker<sup>6</sup>
8. Screw-top microtubes: 0.5 mL (212-9588, VWR International, USA)
9. Zip-lock bag
10. Metal weights (nuts and bolts)
11. Glass thermometer 0-100 °C
12. Pipettes: 100  $\mu$ L, 2.5  $\mu$ L (3111000.114, 3111000.149, Eppendorf, Germany)
13. DNA strands (Integrated DNA Technologies, USA)

#### 4.2.4 Fluorescence microscopy

1. Fluorescence microscope<sup>7</sup> (Olympus IX71, Olympus, Japan)
2. Buffer (10x TAE ( 400 mM Tris-acetate, 10 mM EDTA) buffer, pH 8.3)
3. Water: 18 M $\Omega$ , pH 7-8
4. YOYO-1 (Y3601, Invitrogen, USA). This is toxic and should be handled carefully according to the manufacturer's instructions.
5. Microscope slides or cover slips, thickness 0 (BB024040A1, Menzel, Germany)
6. Fingernail varnish
7. Wavelength filter (U-MWIB2, Olympus, Japan)
8. Light source (X-Cite Series 120, EXFO Photonic Solutions, Canada)
9. Ascorbic acid<sup>8</sup> (255564, Sigma-Aldrich, Germany)
10. Pipettes: 100  $\mu$ L, 2.5  $\mu$ L (3111000.114, 3111000.149, Eppendorf, Germany)
11. DNA product

---

<sup>5</sup> Instead of annealing in hot water, a programmable PCR machine can be used with small temperature steps, ensuring that the lid is a few degrees warmer than the heating block.

<sup>6</sup>This can be normal tap water.

<sup>7</sup> A Total Internal Reflection Fluorescence (TIRF) microscope is advantageous to remove background fluorescent light from sources not in focus (at the surface), but imaging is certainly manageable without such a system.

<sup>8</sup>This helps to prevent photobleaching of the fluorescent molecules.

### 4.2.5 Atomic force microscopy in fluid

1. Atomic force microscope (Multimode V, Veeco Instruments, USA): operated in intermittent contact (tapping) mode.
2. Fluid cell (MTFML, Veeco Probes, USA)
3. Mica (50, Ted Pella, USA)
4. Metal puck (16218, Ted Pella, USA)
5. Cantilevers (DNP-S10, Veeco Probes, USA)
6. Buffer: (10x TAE ( 400 mM Tris-acetate, 10 mM EDTA) buffer, pH 8.3)
7. Water: 18M $\Omega$ , pH 7-8
8. Membrane filter: 0.02  $\mu\text{m}$  (Anotop 25 Plus, Whatman, England)
9. Optical microscope
10. Tweezers (5599, Ted Pella, USA)
11. Pipettes: 100  $\mu\text{L}$ , 2.5  $\mu\text{L}$  (3111000.114, 3111000.149, Eppendorf, Germany)
12. DNA product

## 4.3 Steps

### 4.3.1 Absolute concentration by UV absorption

1. Single-stranded DNA can have significant secondary structure (where bases in the same strand bind to each other). This alters the extinction coefficient and leads to incorrect concentration determination. With current models and technology there is no way around this (apart from using strands that are designed not to have secondary structure) and the best way to circumvent this is to use titration gel electrophoresis. However, titration gel electrophoresis requires much more time and effort, and thus is usually only conducted when it is found the lattice is not forming as desired from the concentrations determined by UV absorption measurements, see Figure 4.23 on page 74.
2. Turn on spectrometer-allow lamp and system to stabilise for one-to-two hours.
3. Appropriate DNA sequences can be dissolved in water to a concentration of 100  $\mu\text{M}$ , this can be determined from the information sheet accompanying the sequences. These should be briefly heated to 60  $^{\circ}\text{C}$  and well vortexed to ensure complete mixing.

4. Calculate a molar extinction coefficient for each DNA sequence using the nearest-neighbour model [65–67]- for example using Scitools on the Internet from Integrated DNA Technologies.<sup>9</sup>
5. Rinse cuvette under flowing water, shake water out by hand *hard*, repeat several times. Dry the outside surface with compressed air/nitrogen and lens cleaning tissue.
6. Load cuvettes with 100  $\mu\text{L}$  water, set parameters (depending on the model of spectrometer, these exact options may not be possible, but there should be similar possibilities):
  - Wavelength scan: 350 nm-220 nm
    - Scan rate: 400 nm/min
    - Bandpass: 1 nm
    - Response (integration) time: medium
1. Measure baseline, set baseline subtraction.
2. Add 2  $\mu\text{L}$  of DNA to measurement cuvette without removing it from the spectrometer, stir with pipette tip for 10-20 s.
3. Measure absorbance, ensure that the absorbance lies between 0.1 and 1 or add or dilute DNA until this is the case. Also ensure that absorbance between 320-350 nm is extremely close to zero or apply an offset if it isn't, read-off absorbance at 260 nm (note this may not be the peak maximum).<sup>10,11</sup> See Figure 4.23 on page 74 for an example.
4. Calculate the concentration of DNA using the Beer-Lambert law:

$$\text{absorbance} = \text{path length} \times \text{extinction coefficient} \times \text{concentration} \quad (4.14)$$

$$\text{concentration} = \frac{\text{absorbance}}{\text{path length} \times \text{extinction coefficient}} \quad (4.15)$$

5. For example with an absorbance of 0.5 and an extinction coefficient of 100 000 L/mol cm and a cuvette of width 1 cm:

$$\text{concentration} = \frac{0.5}{1 \text{ cm} \times 100000 \frac{\text{L}}{\text{mol cm}}} = 5 \mu\text{M} \quad (4.16)$$

<sup>9</sup> The extinction coefficient is calculated using a nearest-neighbour model. One can for example make use of the online calculator 'Scitools' provided by Integrated DNA Technologies at <http://www.idtdna.com/analyzer/Applications/OligoAnalyzer/>

<sup>10</sup>The absorption spectrum of DNA is sequence dependent, and thus the UV absorption peak of DNA may be found between approximately 260±15nm, however the absorption should be measured at the wavelength that the extinction coefficient is calculated for, which is generally 260nm.

<sup>11</sup> Depending on the cuvette, it may be necessary to stir the sample with a pipette tip to remove air bubbles and make a second measurement to ensure reproducibility.

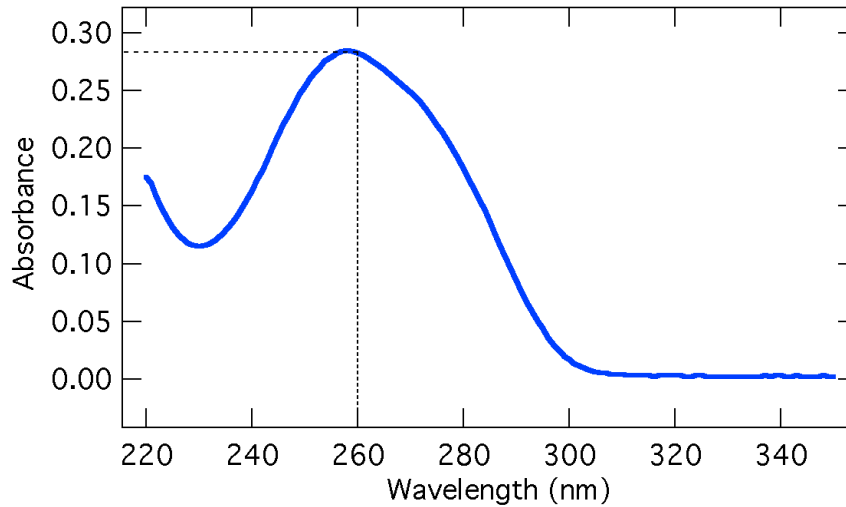


Figure 4.23: A representative ultraviolet absorbance curve of a single-stranded DNA sequence. Note that the maximum is not exactly at a wavelength of 260 nm (this is dependent on the sequence), however the absorbance is measured at 260 nm because this is the value that the extinction coefficient is normally calculated at. Note also that a baseline is measured directly before adding DNA, thus there is no vertical offset necessary, this can be seen by the 0 values at higher wavelengths (320-350 nm).

6. Calculate the amount of water needed to be added achieve a concentration of 1  $\mu\text{M}$  (the DNA nanostructures are generally assembled at a DNA concentration of 1  $\mu\text{L}$  or less). Continuing the example:

$$\text{concentration}_{\text{initial}} \times \text{volume}_{\text{initial}} = \text{concentration}_{\text{final}} \times \text{volume}_{\text{final}} \quad (4.17)$$

$$\text{volume}_{\text{final}} = \frac{\text{concentration}_{\text{initial}} \times \text{volume}_{\text{initial}}}{\text{concentration}_{\text{final}}} \quad (4.18)$$

$$\text{volume}_{\text{final}} = \frac{5 \mu\text{M} \times 102 \mu\text{L}}{1 \mu\text{M}} = 510 \mu\text{L} \quad (4.19)$$

$$\text{volume}_{\text{needed}} = 510 \mu\text{L} - 102 \mu\text{L} = 408 \mu\text{L} \quad (4.20)$$

Add this amount and mix with pipette tip.

7. Transfer solution to a centrifuge tube (loss of small amounts here is not critical, if well mixed, the concentration will not change)
8. Repeat steps from 3 onwards for all DNA strands.

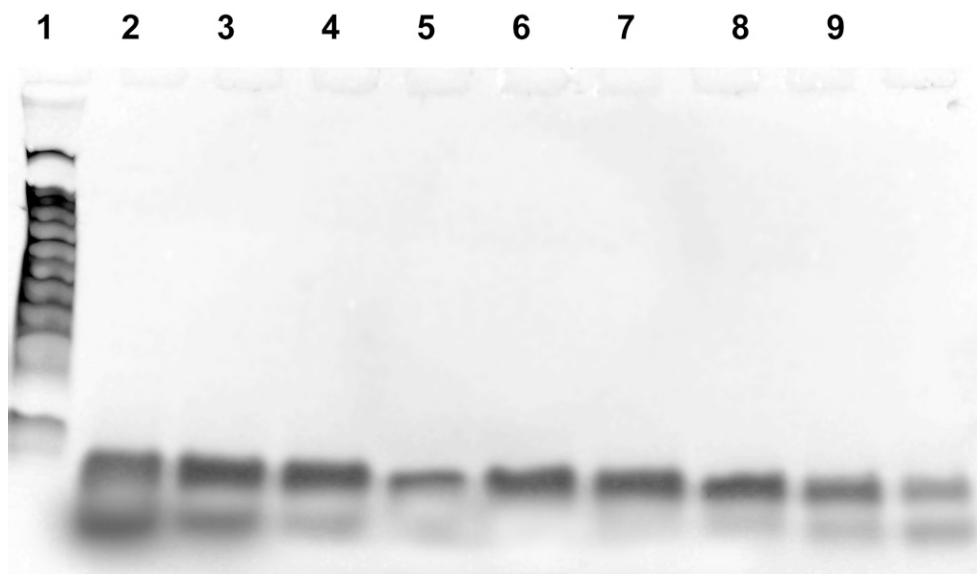


Figure 4.24: A native PAGE gel electrophoresis titration analysis of the concentration of two complementary DNA strands. Each strand is 8 bases long, the gel is 20% and was run at 10V /cm for 3 hours. Lane 1: low molecular weight DNA ladder (766-25bp); Lanes 2-9: relative concentration increments from factors of 2 to 0.25 as listed in the protocol. The upper band represents the hybridised DNA, the lower band excess single-stranded DNA: Lane 6 has the correct ratio of the two strands in this case, as there is no excess single-stranded DNA.

### 4.3.2 Relative concentration by polyacrylamide gel electrophoresis

1. Clean electrophoresis plates thoroughly with detergent and rinse thoroughly with water, wipe with ethanol then wipe dry.
2. Place plates with spacers together and set in the electrophoresis unit, with the gap for the comb upwards and inwards.
3. Squirt ethanol in between the plates until approximately 1/4 full and leave for several minutes to ensure there are no leaks.
4. Mix Acrylamide-bisacrylamide, TAE buffer,  $\text{MgCl}_2$  solution and water in the following ratio per 10 mL of resulting solution<sup>12</sup>:

Polyacrylamide Gel (%)	Acrylamide-bisacrylamide (37.5:1) (mL)	10x TAE (mL)	1 M $\text{MgCl}_2$ ( $\mu\text{L}$ )	$\text{H}_2\text{O}$ (mL)
20	5.00	1	120	3.88

<sup>12</sup>This gel concentration is suitable for DNA strands up to 100 bases long, for longer strands smaller gel concentrations are needed.

1. Place in vacuum chamber for 5 minutes to remove air from the solution (this speeds up polymerisation).
2. Check electrophoresis plates to see that there are no leaks, pour out ethanol. If there are leaks, pull the plates apart, put them back together again and recheck.
3. Remove solution from vacuum chamber. Divide solution gently into two (for two gels) without mixing in unnecessary air.
4. Prepare pipettes and tips for the APS and TEMED solutions.
5. Under the fume-hood, working without pause, add APS solution at 50  $\mu\text{L}$  per 10 mL of solution to the first flask, and swirl gently to mix. Add TEMED (closing TEMED lid immediately) at 10  $\mu\text{L}$  per 10 mL of solution to the second flask, and swirl gently to mix.
6. Immediately pipette (slowly to avoid bubbles) solution between the first set of gel electrophoresis plates, making sure no air bubbles get trapped. Fill until the level reaches the bottom of the gap for the comb.
7. Insert the comb, ensure that it traps no air bubbles, if this is the case take it out and reinsert it. It is useful to have the top of the comb slightly ( $\sim 1$  mm) above the upper edge of the glass plates.<sup>13</sup> Use bulldog clips to hold the comb securely into position (otherwise the expanding polymerising gel will displace it).
8. Repeat steps 9 to 11 for the second solution.
9. Optimally wait 90 minutes for the gel to polymerise (shorter times and the gel will not have polymerised completely with even and static pore sizes, longer than a couple of hours and the gel will swell and dry.)<sup>14</sup>
10. Fill buffer between the gels and into the reservoirs of the electrophoresis unit.
11. Remove one of the combs and immediately flush the wells completely with buffer using the syringe and needle to remove unpolymerised acrylamide.<sup>15</sup>
12. Repeat for second comb.
13. Set out 9x 0.5 mL centrifuge tubes in a holder.

---

<sup>13</sup>The gels can be stored for several days in their glass plates if wrapped with tensioned rubber bands to keep the comb pressed securely into the wells (with the upper edge of the comb above the glass taking some of the tension) and kept in buffer. Metal clips oxidise in buffer and should not be used.

<sup>14</sup>Gels may be stored for several days if wrapped securely with rubber bands – ensure that there is tension holding the comb correctly in place otherwise the wells will fill with unpolymerised Acrylamide – and stored in 1xTAE solution.

<sup>15</sup> A small battery head lamp can help to make the gel wells more visible (Petzl Tikka).

14. Calculate - from the concentrations (in  $\mu\text{M}$ ) determined by UV absorption - the volume of the first strand needed for 100 ng (shorter strands run relatively faster and spread relatively wider, thus may need to be relatively more concentrated when run with longer strands). Use the formula:

$$\text{volume } \mu\text{L} = \frac{100 \times 10^{-9} \text{ g}}{\text{molecular mass } \frac{\text{g}}{\text{mol}} \times \text{concentration } \frac{\text{mol}}{\mu\text{L}}} \quad (4.21)$$

Add this volume of the first strand to each tube.

15. Calculate the quantity in moles of the first DNA strand that this volume holds using:

$$\text{quantity} = \text{concentration} \times \text{volume} \quad (4.22)$$

16. Calculate the volume needed of the second strand for each these (suggested) factors of the first DNA strand: 0.25, 0.5, 0.75, 1, 1.25, 1.5, 1.75, 2.

$$\text{volume} = \frac{\text{quantity}}{\text{concentration}} \times \text{factor} \quad (4.23)$$

17. Add each volume to one of the tubes (there will be one tube left).
18. Calculate the amount of 1 M  $\text{MgCl}_2$  solution needed to be added to each tube to give a concentration of 12.5 mM. Add this amount to each respective tube.
19. Close the tubes, label them, and vortex briefly.
20. Using a Polymerase Chain Reaction(PCR) machine, heat tubes to 90 °C (lid temperature 92 °C) for 1 minute and cool evenly in small steps to room temperature over one hour. This should ensure hybridisation of the strands.
21. Add 0.4  $\mu\text{L}$  of low molecular weight DNA ladder to the remaining tube. Pipette 3  $\mu\text{L}$  of loading buffer into each tube and vortex.
22. Prepare running buffer and salt (1 L or more depending on the size of the electrophoresis unit): 20 mL 50x TAE buffer, 12.5 mL 1 M  $\text{MgCl}_2$ , and water to fill to one litre. Refrigerate until at 4 °C. The buffer stock should be the same as that used for the gel and at the same concentration (1x).
23. Flush wells again with buffer using the syringe and needle, immediately before loading wells with DNA.
24. Load the first well with prepared DNA ladder solution and the rest of the wells with the DNA strand solutions in order.
25. Connect the electrophoresis unit to the circulating cooling water. This ensures that the gels remain cool while running and do not thermally denature the hybridised DNA samples<sup>4</sup>.

26. Connect the electrophoresis unit to the power supply and run at a constant voltage of 10 V per cm gel length until the yellow loading dye runs to the bottom of the gel (typically one to three hours).
27. During this time, the staining solution can be prepared. An opaque plastic container with a flat bottom just larger than the gel is needed, and this is filled with buffer to a depth that would be the same as the thickness of the gel. Sybrgold is added at a ratio of 1  $\mu$ L per 10 mL, this is covered with an opaque lid or aluminium foil and allowed to mix on a rotator at a small angle to the horizontal at the lowest speed (1 Hz).
28. Prepare a sheet of aluminium foil about three times the size of the gel flat on the table.
29. When the gel is finished, turn off the power-supply, remove the gel from the unit. Use a thin blade or plastic scraper to carefully remove the top gel plate. A few droplets of water between the plate and the gel can help. Spread the aluminium foil over the top of the gel, then place a flat stiff piece of plastic over the aluminium foil. Use this to support the gel 'sandwich' as it is flipped up so that the bottom gel plate is now on top. This plate is also removed, and two opposite sides of the foil are trimmed to the gel width and the remaining two sides are used to lift and support the gel and the whole lot is placed in the staining container. The lid is placed on and the gel is left to stain on the rotator for 30-60 mins.
30. The rotator is then stopped, the staining solution is removed using the 25 mL pipette and disposed of as toxic waste.
31. The gel is lifted out using the aluminium foil support and onto the UV light box. The gel can then be slid off the aluminium foil onto the glass using a few drops of water as lubricant if necessary.
32. The aluminium foil is stored safely for next time or disposed of as toxic waste.
33. The gel is examined/photographed using the gel documentation system and an appropriate wavelength filter for Sybrgold making sure the focal distance of the camera is set to reach the gel and not to the inner UV bulbs.
34. The correct ratio of DNA strands is chosen by comparing the bands to see the one-to-one binding ratio. This ratio can be used with the excess (not used in the gel analysis) DNA to self-assemble the desired structure.

### 4.3.3 Thermal annealing

1. The DNA strands are mixed at the correct concentrations and thermally annealed in appropriate buffer conditions<sup>16</sup>.
2. All stock buffer and salt solutions should be filtered with a 0.02  $\mu\text{m}$  membrane filter before use, this is quite critical.
3. The final volume and concentration of required DNA product is decided. Typically volumes between 20 -2000  $\mu\text{L}$  are produced, at concentrations between 50-1000 nM. As an example 100  $\mu\text{L}$  of 5-stranded lattice at 500 nM total concentration is chosen.
4. The concentration needed of each strand is calculated, this depends on the stoichiometry of the strands in the final structure.

$$\text{concentration of strand} = \frac{\text{stoichiometry of strand}}{\text{total stoichiometry}} \times \text{total concentration} \quad (4.24)$$

5. For a strand mixed at a ratio of 1 with a total of 5 strands this is

$$\text{concentration of strand} = \frac{1}{5} \times 500 \text{ nM} = 100 \text{ nM} \quad (4.25)$$

6. The volume needed from each DNA strand solution is calculated using Equation 4.17. For example, if each strand solution has been diluted to 1000 nM, then for 100  $\mu\text{L}$  final volume:

$$1000 \text{ nM} \times \text{volume}_{\text{initial}} \mu\text{L} = 100 \text{ nM} \times 100 \mu\text{L} \quad (4.26)$$

$$\text{volume}_{\text{initial}} = \frac{100 \text{ nM} \times 100 \mu\text{L}}{1000 \text{ nM}} = 10 \mu\text{L} \quad (4.27)$$

7. The calculated volume of each strand is pipetted into a screw-top microcentrifuge tube.
8. The volume of 50x TAE buffer needed for a 1x solution of 100  $\mu\text{L}$  is calculated using the Equation 4. For example:

$$50 \times \text{volume}_{\text{initial}} \mu\text{L} = 1 \times 100 \mu\text{L} \quad (4.28)$$

$$\text{volume}_{\text{initial}} = \frac{1 \times 100 \mu\text{L}}{50} = 2 \mu\text{L} \quad (4.29)$$

This volume is pipetted into the screw-top microcentrifuge tube.

---

<sup>16</sup> We have also developed a technique that does not rely on thermal annealing but rather on the basis of dilution of DNA denaturing agents in the buffer (See Chapter 7).

9. The volume of 1000 mM (1 M) MgCl<sub>2</sub> solution needed for a 12.5 mM solution of 100 μL is

$$1000 \text{ mM} \times \text{volume}_{\text{initial}} \mu\text{L} = 12.5 \text{ mM} \times 100 \mu\text{L} \quad (4.30)$$

$$\text{volume}_{\text{initial}} = \frac{12.5 \text{ mM} \times 100 \mu\text{L}}{1000 \text{ mM}} = 1.25 \mu\text{L} \quad (4.31)$$

This is pipetted into the screw-top microcentrifuge tube.

10. Enough water is added (here 46.75 μL) to make up the total required volume (here 100 μL).
11. The lid is screwed *tightly* onto the tube, and it is briefly (10 s each) centrifuged, vortexed, then centrifuged again.
12. The tube is placed into the zip-lock plastic bag with enough weights (nuts and bolts) to make sure it sinks, the bag is rolled up and secured with a rubber band, and a few small holes are made in it to allow the air to escape.
13. Enough (tap) water is boiled to fill the large (2-4 L) beaker. The bag with weights and microcentrifuge tube is placed in the bottom of the beaker, along with the thermometer. The beaker is filled with water just below boiling point.
14. The beaker is placed inside the Styrofoam box which is closed, and this is placed in a safe place and left for 48 hours or until the water has cooled to room temperature (~20 °C).
15. The microcentrifuge tube is then taken out and dried, to ensure that no water droplets on the outside enter upon opening the lid of the microcentrifuge tube.

#### 4.3.4 Fluorescence microscopy

1. If the chosen DNA structure has dimensions on the order of several micrometres or greater (for example a large two-dimensional lattice), then it may be viewed with a fluorescence microscope if it is 'dyed' using an intercalating fluorescent molecule such as YOYO-1 (Invitrogen). This binds between base pairs of double-stranded DNA, optimally at a ratio of 1 dye molecule per 5 base pairs.<sup>17</sup>
2. Thus if the total number of bases of the 5 strands is 100, then the number of base pairs is 50. The YOYO-1 stock solution is 1000 000 nM (1 mM) and typically one dyes a DNA structure solution of 10 μL. The volume of YOYO-1 needed is

$$1000000 \text{ nM} \times \text{volume}_{\text{initial}} \mu\text{L} = \frac{50 \text{ base pairs}}{5} \times 500 \text{ nM} \times 10 \mu\text{L} \quad (4.32)$$

$$\text{volume}_{\text{initial}} = \frac{50 \text{ base pairs}}{5} \times 500 \text{ nM} \times 10 \frac{\mu\text{L}}{1000000 \text{ nM}} \mu\text{L} = 0.05 \mu\text{L} \quad (4.33)$$

---

<sup>17</sup> A YOYO-1 molecule every five base pairs gives the best ratio of minimal structural deformation of the DNA helix to maximal fluorescence intensity, giving an optimal signal to noise ratio [68].

3. This volume is not realistic to pipette, so the YOYO-1 is diluted in 1x TAE buffer, for example (100x dilution): 0.5  $\mu\text{L}$  YOYO-1 stock solution, 2  $\mu\text{L}$  50x TAE buffer, 97.5  $\mu\text{L}$  water in a plastic (YOYO-1 binds to glass containers) microcentrifuge tube.
4. With 100x dilution, 5  $\mu\text{L}$  of this is pipetted into a microcentrifuge tube.
5. Using a cut-off tip 10  $\mu\text{L}$  of DNA structure solution is added.<sup>18</sup>
6. Ascorbic acid is used to minimise photobleaching of the fluorescent molecules. It is prepared at 100 mM in a volume of, for example, 10 mL. With a molecular mass of 176.12 g/mol this is:

$$\text{mass} = \text{molecular mass} \times \text{concentration} \times \text{volume} \quad (4.34)$$

$$\text{mass} = 176.12 \frac{\text{g}}{\text{mol}} \times 100 \times 10^{-3} \frac{\text{mol}}{\text{L}} \times 10 \times 10^{-3} \text{L} = 176 \text{ mg} \quad (4.35)$$

This mass is dissolved in 10 mL of water and stored in a light proof jar. New solutions should be made every week.

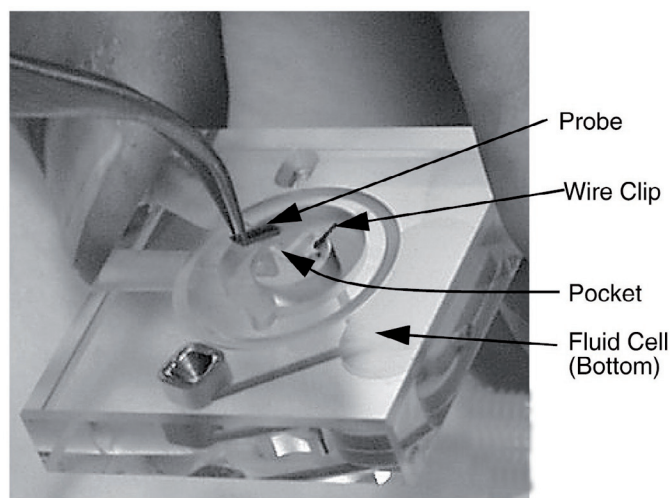
7. This is added to a final concentration of 10 mM, so with 5  $\mu\text{L}$  of YOYO-1 solution and 10  $\mu\text{L}$  of DNA solution, one adds approximately 1.5  $\mu\text{L}$ .
8. The fluorescence microscope is prepared, the light source is switched on, the correct filter is loaded, and an appropriate objective (40x air) is chosen.
9. For a very quick look, 1  $\mu\text{L}$  of dyed-DNA solutions can be pipetted using a cut-off tip onto a Number 0 cover slip and placed on the microscope. There will be large amounts of background fluorescence, but normally the structures themselves can also be seen.
10. For a better image, this process is repeated but the droplet is covered with a second cover-slip and the edges of the cover slip are sealed with fingernail varnish. There is much less fluorescence background using this technique.

### 4.3.5 Atomic force microscopy in fluid

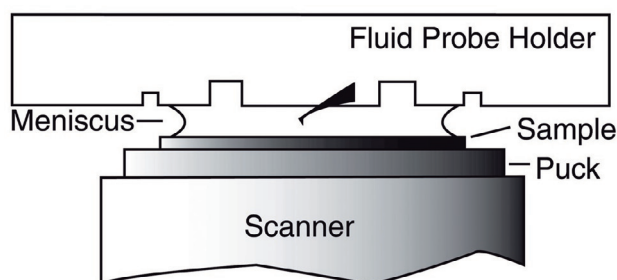
1. The DNA structures will bind in solution to a mica surface given the correct conditions, and the topography of the structure can then be measured/'visualised' using an atomic force microscope. The precise details of this protocol will vary greatly depending on the model of atomic force microscope used.
2. The microscope and control computer are switched on, and the software loaded.

---

<sup>18</sup> The DNA structures can be so large that the normal hole diameter of the pipette tip will damage them as they pass through.



(a)



(b)

Figure 4.25: a) Loading the probe into the fluid cell. b) A depiction of the fluid cell above the sample [69].

3. It is generally much easier to set the correct engage height of the cantilever above the mica surface in air, as the surface of the mica is difficult to see with an optical microscope when submerged in buffer.
4. The cantilever holder is set to a distance far enough from the surface to ensure that upon loading the cantilever the tip of the cantilever will not contact the surface.
5. Using a small optical microscope and tweezers, the tip is loaded correctly in the fluid cell.
6. The mica is loaded into the microscope (initially without any sample).
7. The fluid cell/holder is loaded into the microscope.
8. With the aid of the optical microscope that comes with the atomic force microscope, the laser spot is aligned onto the very end and centre of the cantilever. This is important!

9. If there is a reflecting mirror, its angle is adjusted so the laser shines close to the centre of the photodiode window.
10. The photodiode position is adjusted so that the laser is reflected directly at its centre.
11. The steps 8-11 are repeated to fine-tune the system to ensure that the detected signal is high (with the laser reflecting very close to the end of the tip) and deflection error signals (relating to the laser reflecting onto the centre of the photodiode) are minimal.
12. The surface of the mica is brought into focus of the optical microscope. The surface can be difficult to observe (being semi-transparent), it can help to move around looking for cracks on the surface. The cantilever is brought to a level just before it comes into perfect focus, indicating it is very close to, but not in contact with the surface.<sup>19</sup> As a guide, as the cantilever moves closer to the focal height a double image of the cantilever is seen, and this merges into one at the focal height.
13. The mica is then removed (this probably entails removing the fluid cell/holder also) and a fresh surface is prepared using (opaque) masking tape.<sup>20</sup> This is best done by pressing firmly a strip of tape flat onto the mica on a table, lifting the far edge of the mica up so that it stands perpendicular to the table on its bottom edge, and peeling the tape slowly and evenly downwards. A thin, complete, *shiny* layer of mica should have adhered to the tape. Quality of results may depend on the orientation of the tape relative to the mica, there is an optimal direction found by experimenting.
14. 5  $\mu\text{L}$  of DNA structure solution is carefully pipetted onto the centre of the mica using a cut-off pipette.
15. 1x TAE 12.5 mM  $\text{MgCl}_2$  (filtered through a 0.02  $\mu\text{m}$  membrane filter before use) buffer solution is added to the mica, and/or the surface of the fluid cell/holder and/or through a tube into the fluid cell, dependent on the system. Care should be taken that no air bubbles are trapped on the cantilever.
16. The mica is carefully reloaded into the microscope.
17. The buffer has a different refractive index so that the laser beam travels a slightly different path, steps 8-11 may need to be repeated with small changes to optimise the measured laser signal.
18. The cantilever is tuned (generally using a function in the software) to  $\sim 5\%$  below its resonant vibration frequency.<sup>21,22</sup> The amplitudes used are much smaller than

---

<sup>19</sup> It is important to come into focus on the surface from a starting point far away from the surface, otherwise one may focus on the reflection and not on the real surface.

<sup>20</sup> One can see the thin peeled layers of mica with better contrast if the tape is opaque.

<sup>21</sup> The feedback loop in the electronics of the microscope works optimally at values just below the resonance frequency of the cantilever.

<sup>22</sup> In the 10kHz range with small buffer volumes there may be a resonance in the buffer itself which can be heard as a high-pitched tone. This is normal.

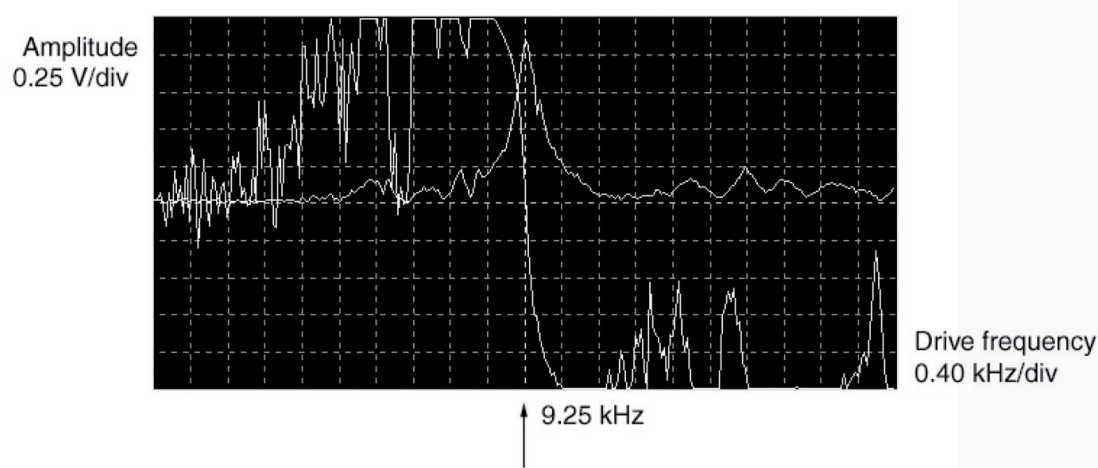


Figure 4.26: A sample frequency tune of the cantilever in fluid. Both amplitude and phase are shown [69].

those in air, and should be adjusted to be above the level at which the tip sticks to the surface when imaging, but not so large that the sample is damaged by the tip's vibrations. This is best determined through trial and error.

19. The amplitude setpoint (ratio of the free amplitude of vibration to the amplitude while imaging) is generally set just below 1, for example 0.98 (or 98%). However this can vary greatly dependent on the system.
20. The imaging parameters are then set. Initial scan sizes and speeds are set small ( $1\mu\text{M}$ ) and slow (0.5 Hz) to prevent damage to the tip as it first 'contacts' the surface.
21. The most important two other parameters are the integral and proportional gains, these should be initially set extremely small (exact values are system dependent).
22. The number of measurements per scan line (pixels) can be set to 256.
23. The 'engage surface' function of the microscope is actuated. Several errors may occur during this process.<sup>23</sup>
24. When correctly engaged on the surface, the imaging parameters are optimised. It is generally helpful to first withdraw the cantilever from the surface slightly (several hundred nanometers), retune the cantilever to the correct frequency and drive amplitude, before reengaging the surface.

<sup>23</sup> Several errors often occur whilst engaging, if these occur, the engage should be aborted. The amplitude may change significantly (more than ten percent), thus the cantilever should be retuned with the correct amplitude. The deflection errors may increase significantly, particularly if the buffer was initially at a different temperature to the fluid cell/holder and/or mica, thus the errors should be brought to a minimum. Once corrected, the engage can be restarted.

25. There are generally at least two 'views' in the software, an 'image' view and an 'oscilloscope' view of the trace and retrace of the current line scan profile. The amplitude setpoint is slowly increased until the tip just no longer contacts the surface, the is best seen in the oscilloscope mode when the trace and retrace scan profiles significantly depart vertically from each other. It is then decreased to just below the value when they come back vertically on top of each other for optimal imaging.
26. The integral gain is gradually increased so that the trace and retrace scan profiles correlate optimally with one another without excessive noise being introduced into the signals.
27. The proportional gain is then adjusted similarly.
28. The scan size and speed can then be increased and suitable DNA structures for imaging are found.
29. The desired scan size is set, and the scan speed is slowed to 1-3 Hz, and the number of measurements per line is increased to 512 or 1024. An image is then captured.
30. Care should be taken that no imaging artifacts like double tip images (coming from broken tips with two or more points) or material sticking to the tip occur, if so the cantilever should be changed and the whole process repeated.
31. When a new sample is required, the process can be simplified if care is taken. The tip is withdrawn approximately 100 $\mu$ m from the surface. If the cantilever is not moved within its holder, and a thin layer of mica is removed from the same mica sample, and the mica is returned afterwards to the same position in the Microscope, then the cantilever should be relatively close to the surface and should not need long for the engage procedure.

---

We now have an understanding of the experimental techniques such as concentration determination by UV absorption or gel electrophoresis, assembly by thermal heating and cooling (annealing), and imaging assembled structures using fluorescence, total internal reflection, super-resolution, and atomic force microscopy techniques.

With this understanding we can go on to look at real examples and applications.



Part III

Results & Discussion



# Chapter 5

## DNA nanodevices [2]

Before we look at examples created in the laboratory here, I would like to sidestep and examine some active DNA nanostructures, that is, DNA nanodevices. There are a host of such devices in development, and a relevant overview is given here.

There is a diverse range of research on molecular devices and machines [70]. The nanomechanical principles of operation of many of the natural machine-like macromolecular structures in living cells are perhaps the most thoroughly investigated. Examples of these include molecular motors in the myosin family and kinesin, and proteins that display an intimate coupling of nanomechanical switching and enzymatic function [71–73]. Synthesis of machine-like devices ‘from scratch’ by organic chemists can be relatively complex, but recent progress in supramolecular chemistry is of significant use.

Fitting in between the biological and synthetic world, DNA nanodevices are a comparatively new ‘class’ of molecular devices [74]. At the heart of DNA’s biological role is information storage via the highly specific base pairing. The base pairing is also used in assembling and controlling the DNA nanodevices. However, the DNA in these is ‘designed’ and synthesised chemically.

These artificially assembled DNA nanodevices generally have no biological counterpart. A short survey is given in the following of the basic principles of such devices and the experimental methods of their characterisation, and then discussion of two major research directions: progress towards realisation of artificial molecular motors based on DNA; and the use of DNA nanodevices as novel biosensors and their coupling to biological phenomena.

### 5.1 Using DNA as an intermediary between information processing and mechanical action

Molecular ‘addresses’ can be created in DNA sequences using combinations of the four DNA bases – the number of distinct sequences of length  $N$  is  $4^N$  and becomes very large for large  $N$ . Alongside this feature, stiffness of arms and junctions can be controlled by making use of single-stranded DNA, double-stranded DNA, and multiple interlinked double strands. Thus specific sequences addressed for particular locations can induce changes in structure.

Or a specific device can be targeted in a pool of several species of DNA nanodevices. It also allows interfacing between multiple devices, or to naturally occurring nucleic acids in cells.

## 5.2 Characterising DNA nanodevices experimentally

Many of the techniques discussed in Chapter 4 are used to measure the properties of DNA nanodevices. For example, gel electrophoresis can be used to study conformational changes in such devices. However, it cannot be used in real-time, only before and after the change. Förster resonance energy transfer (FRET) experiments can be used for this purpose [75]. They make use of non-radiative energy transfer between two fluorophores with overlapping emission and excitation wavelengths. This occurs via dipole-dipole coupling of the fluorophore dipoles, and is predictably dependent on distances between fluorophores of less than  $\sim 10$  nm. Given that one helical turn of (B form) DNA is 10.5 base pairs and 3.4 nm in length, FRET experiments are useful for devices with arm lengths of 10-30 base pairs. Displacements outside of this range may be investigated with other energy transfer systems such as quenching of fluorescence by metal surfaces, or coupling between surface plasmons in metal nanoparticles [76–78]. Advanced techniques such as super-resolution change measurement techniques from bulk ensembles to single devices [79, 80].

Atomic force microscopy of devices attached to smooth surfaces can also identify before and after conformation states at the nanometer level [81, 82]. Recently developed high-speed scanning atomic force microscopy techniques allow the tip to move much more rapidly while still imaging accurately, and provide access to near real-time changes in conformation [83]. Atomic force measurements can also gather data using DNA-induced bending of micro-cantilevers [84]. Such measurements present experimental proof that DNA nanodevices can do work and eventually act as molecular motors.

## 5.3 Towards molecular motors based on DNA

Since the first examples were reported in 1998, the variety and complexity of DNA nanodevices that can move or change their structure has rapidly advanced [85]. Still, to this point in time, there are not really any examples that have been demonstrated which are of practical use, and thus ‘towards’ is to be emphasised in the section title. Devices that have been demonstrated may be driven by DNA hybridisation and branch migration, use Hoogsteen bonding (rather than Watson-Crick base pairing) to form multiplex (rather than double helix) DNA structures, walk and rotate, and respond to environmental conditions. However, at least some of these concepts will need to be extended, combined, and/or new ones developed, before such devices will be of practical use.

Watson-Crick base pairing has been made use of in at least different methods: with single-stranded extensions (‘toeholds’) to initiate strand binding, with strand displacement (‘branch migration’ see Section 3.2.1.4) to displace strands from a helix, and with set-

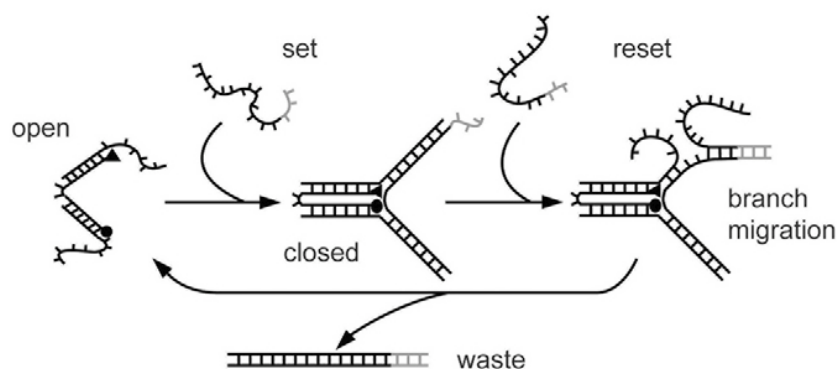


Figure 5.1: In the open state DNA tweezers are composed of three strands of DNA forming two double-stranded arms connected by a short single-stranded hinge. Hybridisation with a ‘set’ strand closes the two arms. The set strand can be removed via branch migration using the fully complementary ‘reset’ strand, thus restoring the open state under formation of a ‘waste’ product [2].

ting structural integrity by converting between single-stranded and double-stranded DNA forms.

These three methods been combined to assemble DNA ‘tweezers’ in which two DNA double strands are joined by a short single strand acting as a flexible hinge (Figure 5.1 on page 91). The open ends of the double strands are labelled with two fluorophores which can undergo FRET [86]. Additionally protruding from the open ends of the double strands are single-stranded extensions. By adding a single ‘set’ strand with a sequence which allows it to bind to both of these single-stranded extensions, the two double strands can be closed like arms of tweezers. This motion can be observed with FRET measurements. A single ‘reset’ strand then binds to a single-stranded extension that protrudes from the set strand, and through branch migration displaces the set strand from the device, freeing it to open again. The cycle may then be repeated.

Several different types of devices have been assembled using similar principles. These include a nano-actuator that switches from a relaxed, circular form to a stretched confirmation; and scissor-like devices comprised of two sets of tweezer-structures that are joined at their hinges with short carbon linkers [87]. The motion of one set of tweezers is transduced to the other set, resulting in a scissor-like motion.

Single-molecule analysis of tweezer devices has shown that bonding of multiple set strands to one device can occur, without the device actually closing [80]. Such unwanted interactions might be removed by optimised sequence design. To drive devices autonomously, the use of DNazymes (DNA molecules with enzymatic activity) have been introduced [88]. Further, fully addressable tweezers bound to a DNA ‘track’ have allowed the actuating of coupling reactions in a programmable fashion [89].

Devices have also been assembled that rotate arms around a helical axis [82, 90]. These are based on a ‘paranemic-crossover’ structure, in which multiple double helices are inter-

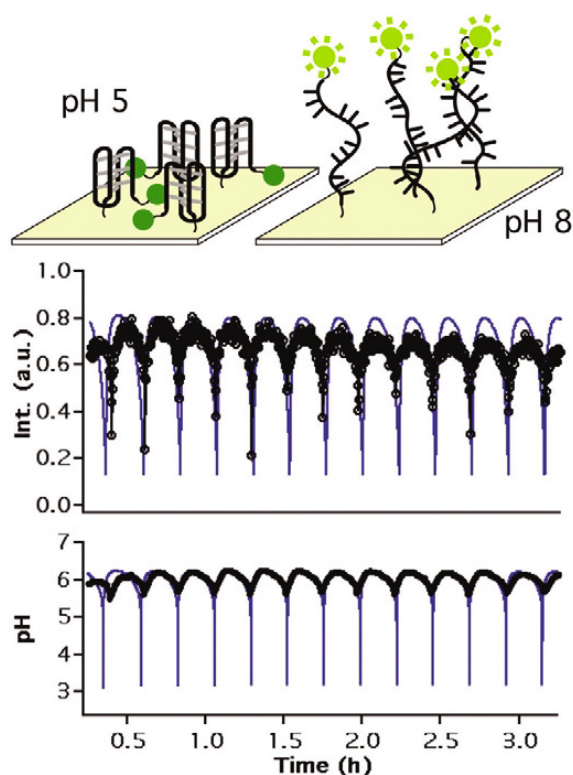


Figure 5.2: At high pH values, the surface-tethered i-motif adopts its open conformation and there is significant fluorescence. At low pH values, it adopts its closed conformation, which brings the fluorophore close to the surface, quenching fluorescence. The intensity and pH correlation can be seen in the middle and lower plots [2].

linked with strands which cross between helices at each possible adjacent position. When some of these crossover strands are replaced through branch migration leaving sections without crossovers, the helices rotate around the helical axis  $180^\circ$  into a ‘juxtaposed’ position.

Under certain buffer conditions and with certain sequences, DNA can form ‘quadruplexes’. One example is the association of four guanine bases in a cyclic hydrogen bonding arrangement (known as Hoogsteen bonding), each guanine makes hydrogen bonds with its two neighbouring guanines. This is known as a G-Quartet. A shape changing device based on such has been optimised using and added strand and branch migration to switch to a double helix [91,92].

A number of other structures are also possible, and are often switched by changing environmental conditions. Addition and removal to the buffer of intercalating molecules (molecules that bind in between the strands of the double helix), proteins, salts, and ion species, have all been used to activate devices. Changes in temperature and pH have also been used.

One example was assembled from a cruciform-shaped double strand [85]. By adding intercalating ethidium molecules that bind in the helix, torque is applied to the cruciform

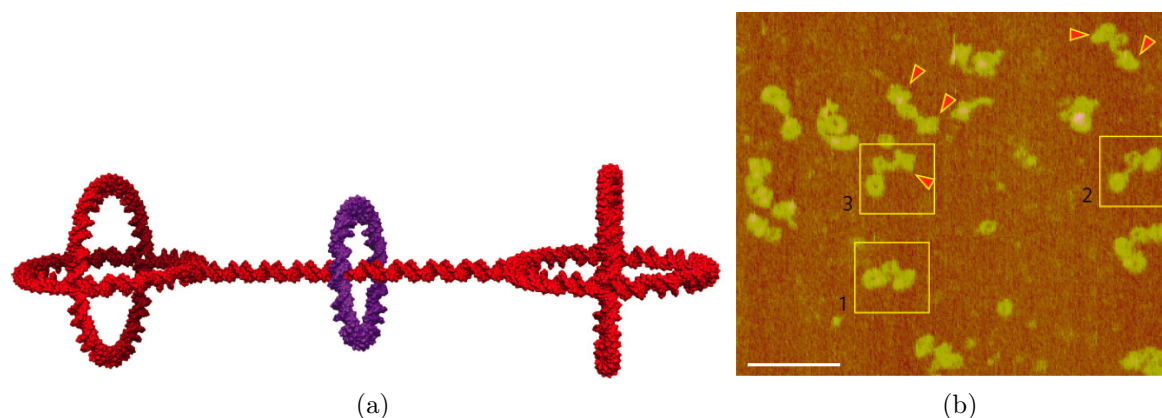


Figure 5.3: *a)* Mechanically interlocked molecules such as rotaxanes have potential as components of molecular machinery. Rotaxanes consist of a dumb-bell-shaped molecule encircled by a macrocycle that can move unhindered along the axle, trapped by bulky stoppers. *b)* Atomic force microscopy images of the rotaxane structure. Arrows indicate the crossover structure of the stopper rings. Scale bar: 130 nm [93].

branch point and it changes its location along the helix. A similar further example is the changing between two states of super-helical DNA (DNA in which the helix is itself coiled into a helix) [94].

DNA can also form triplexes. A third DNA strand binds along the major groove of a normal double helix with Hoogsteen bonding. Such bonding can be activated and deactivated by changing pH, and creates mechanical motion [95,96].

One further structure is the ‘i-motif’ in which four single strands are bound together by an unconventional base pairing between protonated and deprotonated cytosine bases [78,84,97]. This structure also responds to pH changes and has been continuously switched by proton concentration changes driven by a chemical oscillator Figure 5.2 on page 92 . The system can be further improved by attaching the DNA to a solid substrate in a continuous-flow stirred-tank reactor, thus in principle allowing an infinite number of autonomous conformational switching events [77,98]. Assembly of gold nanoparticles using the i-motif has also been achieved, and a solution containing these components changes colour from red to blue within a narrow pH range and is reversible [99].

Using a straightforward, reliable and modular threading method has allowed the assembly of a class of double-stranded interlocked DNA nano-objects of circular geometry (Figure 5.3 on page 93). These are known as rotaxanes and have the potential to be applied as versatile components in nano-mechanics [93].

The incorporation of double-stranded DNA into a novel molecular valve has been demonstrated (Figure 5.3 on page 93). The valve can be opened and closed by changing the surrounding buffer temperature, and many valves are used to cover a porous silica nanoparticle [100]. The nanoparticles can be filled with guest molecules, effectively acting as containers. Upon changing the temperature appropriately, the valves open releasing the

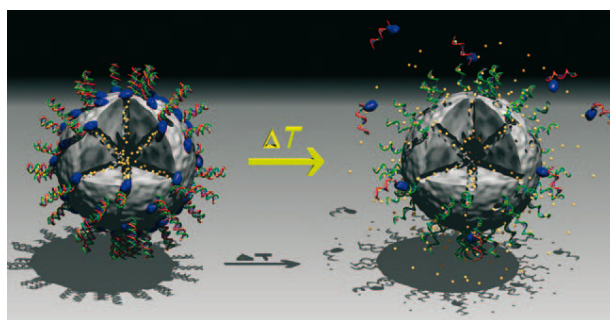


Figure 5.4: Concept of the programmable molecular valve system. The avidin caps are opened by melting the DNA linkers at specifically encoded temperatures [100].

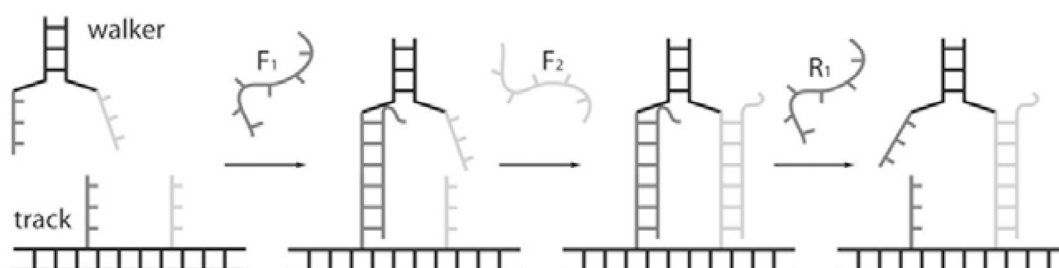


Figure 5.5: A simple molecular walker based on DNA. The walker can be connected to single-stranded extensions of a double-stranded DNA ‘track’ using ‘fuel’ strands. The ‘feet’ can be selectively unlinked from the track using a ‘removal’ strand and reconnected to the next free extension along the track using a fuel strand [2].

guest molecules. The general concept might be of use for targeted drug release.

## 5.4 DNA walkers

There has been a significant effort to demonstrate ‘walking devices’ that bind to ‘track’ stands, as inspired by naturally occurring biological molecular motors such as kinesin.

Initial efforts involved a double strand with two single-stranded extensions at one end acting as ‘legs’ (Figure 5.5 on page 94). Additional ‘fuel’ strands bind the legs to single-stranded extensions at periodic locations along a double-stranded track [101, 102]. Specific ‘removal’ strands added in a particular order unbind the the appropriate leg successively by strand displacement. Motion comes from Brownian motion, and the order of adding fuel and removal strands dictates directionality. Molecular ‘gears’ have been demonstrated using similar principles [103].

To generate walkers that move autonomously – rather than requiring different fuel strands to be added sequentially over time – enzymatic functions have been made use of [104, 105]. Both using (restriction) enzymes themselves, and using DNAzymes. The DNAzymes have allowed the assembly of molecular ‘spiders’ – walkers with several legs that

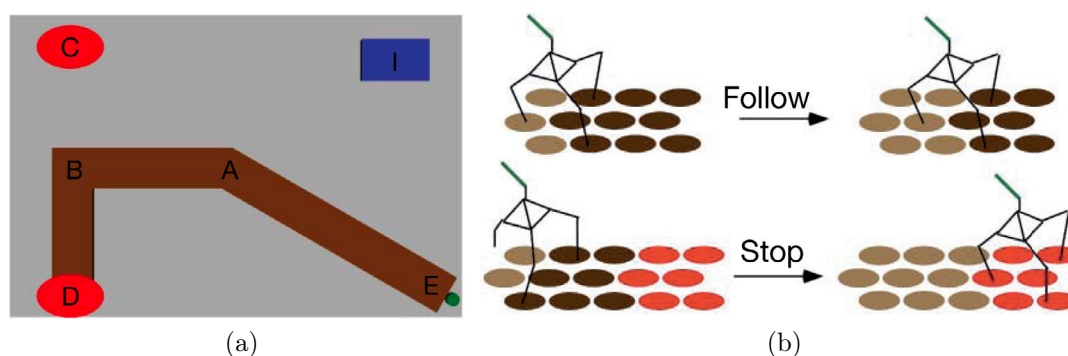


Figure 5.6: *a)* A DNAzyme spider and origami track. The spider follows the substrate track, turns and continues to a Stop site. *b)* A representative origami structure showing the Start position (green), the substrate track (brown), Stop position and Control sites (red), and a topographical imaging marker (blue) [107].

diffuse across a ‘breadboard’ of single-stranded footholds extending from the surface [106]. By creating pathways of footholds on DNA origami, these spiders can be directed around a surface (Figure 5.6 on page 95) [107].

Spiders have also been assembled that make use of fuel strands rather than DNAzymes, and move across origami tracks ‘picking up’ (binding) ‘cargo’ (gold nanoparticles) as they go, a type of ‘molecular assembly line’ [108].

These recent examples give exciting hints of what may be possible in the future at the molecular level.

## 5.5 Novel DNA biosensors

DNA is useful for sensing tasks at the molecular level in a biological environment. DNA naturally interacts with a variety of proteins, e.g. during transcription of DNA into RNA and the creation/repair of single- or double-stranded breaks. However, DNA can also be synthetically linked to proteins using covalent bonds.

One approach is to make use of DNA strands that fold into structures that bind to proteins - known as aptamers. Aptamer sequences have been successfully identified using a process known as Systematic Evolution of Ligands by EXponential enrichment (SELEX). Aptamers have been selected for a large variety of proteins and small ligands such as ATP and cocaine [109–113].

Aptamers may bind to either their aptamer target or to their complementary DNA strand. Competition between these two binding possibilities can be used to create switches and sensors. This has been used to cyclically bind and release the human blood-clotting factor  $\alpha$ -thrombin [114]. The thrombin aptamer consists of three loops bound by two G-Quartets. A single-stranded extension on one end allow the binding of a partly complementary strand. This displaces thrombin from the aptamer. When an extra strand,

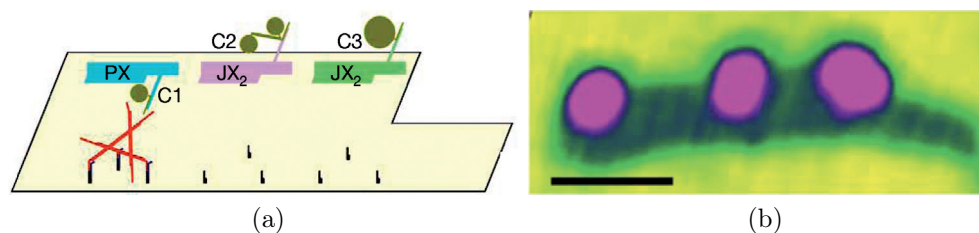


Figure 5.7: The molecular assembly line and its operation. *a)* The basic components of the system are the origami tile (shown as a tan outline), programmable two-state DNA machines inserted in series into the file (shown in blue, purple and green) and the walker (shown as a triangular arrangement of DNA double helices in red). The machines have cargoes consisting respectively of a 5-nm gold particle (C1), a coupled pair of 5-nm particles (C2) and a 10-nm particle (C3) (indicated by green–brown dots), and their state can be PX (meaning ON or ‘donate’ cargo) or JX2 (meaning OFF or ‘do not donate’ cargo). In the example shown, the walker collects cargo from each machine. *b)* Atomic force microscopy image of the system in its initial state [108].

that is completely complementary to the strand just added, is itself added, it displaces this strand and allows the thrombin to once again bind to the aptamer. Such aptamers have been incorporated into two dimensional lattices, and allow the detection of thrombin in nanomolar concentration using fluorescence microscopy [115,116].

A unique design involving a double aptamer has been developed that uses one aptamer to detect a particular molecular species (analyte) and the other aptamer to bind and activate a fluorescent molecule [117]. Importantly, the latter aptamer can only (for structural reasons) bind once the initial aptamer has bound the analyte. The fluorescent molecule is ‘malachite green’, and upon binding, it increases its fluorescence intensity significantly, signalling the presence of the analyte.

Using the DNA restriction enzyme FokI (which cuts DNA at a specific recognition base sequence), an arbitrary DNA sequence has been translated into a DNA strand that triggers the release of thrombin from an aptamer [118].

DNAzymes have also been made use of. A catalytic DNAzyme has been used to discriminate between short strands with single base pair resolution [119]. And single-stranded viral DNA has been detected at very low concentrations (10 femtomolar) using autocatalysis by a DNAzyme (a DNAzyme that catalyses its own production) [120].

These differing examples demonstrate the high-potential of DNA nanodevices for sensing in biological environments.

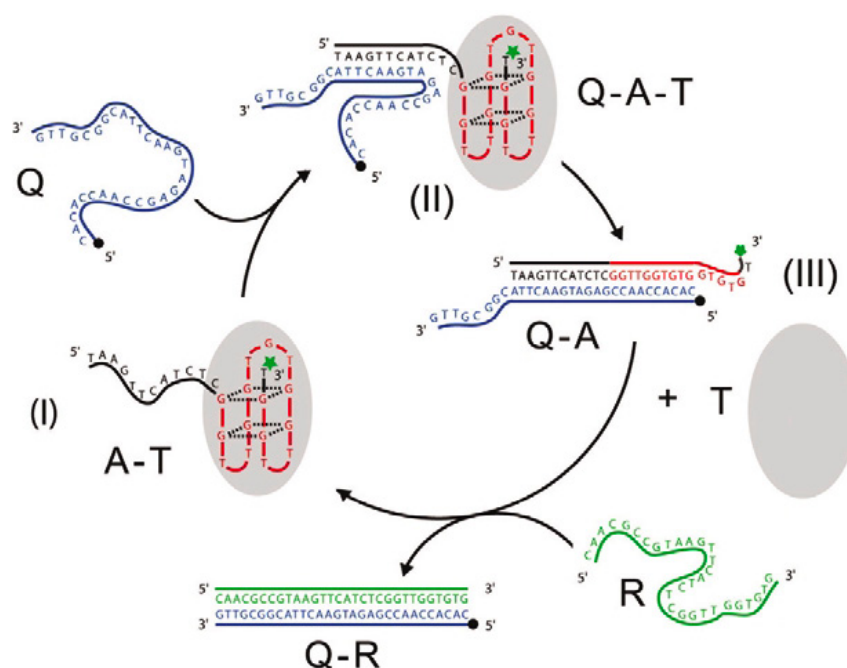


Figure 5.8: Cyclical release and binding of human  $\alpha$ -thrombin (T). The thrombin aptamer-thrombin complex (A-T) dissociates after the addition of an oligonucleotide (Q), that replaces thrombin (I-III) via strand displacement. A removal strand R forms a full double-strand (Q-R) with the strand (R), thus setting the aptamer strand (A) free, which can then bind the thrombin again [2].

## 5.6 DNA nanodevices controlled using genetic mechanisms

The complex genetic processes that occur within the cell on DNA include activation, inhibition, transcription, and translation [121]. By making use of such processes with DNA nanodevices we can engineer novel-molecular machinery in synthetic environments, and possibly within the cell itself. Further, this can help us to understand natural biochemical networks. Initial work demonstrated principles of cell-free genetic circuit assembly, in which DNA sequences are ‘circuit elements’ [122, 123].

Such work includes a simple gene regulatory switch to actuate DNA tweezers using short ribonucleic acid (RNA) strands transcribed from an artificial DNA template Figure 5.10 on page 99. RNA is ‘transcribed’ from DNA by enzymes and is generally further processed by other enzymes. RNA is central to protein synthesis in processes known as translation. A double-stranded DNA template contains a promoter sequence for an RNA polymerase (from phage T7). A promoter sequence is a DNA sequence that provides a binding site for the RNA polymerase. Following the promoter sequence is a binding sequence for a ‘LacI’ protein [124]. RNA polymerase binds to the promoter sequence and then transcribes the DNA into RNA, and the RNA is released and can bind to the DNA tweezer device, closing

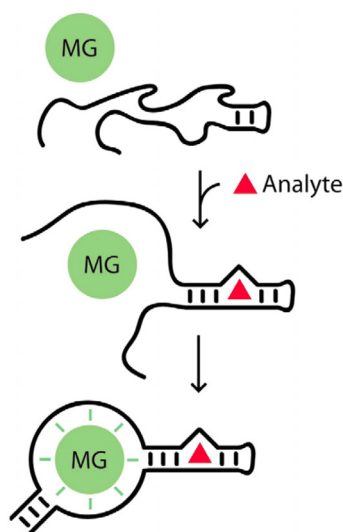


Figure 5.9: The malachite green aptamer as a reporter system for analyte binding. The strand comprises of an aptamer sequence for an analyte in its middle section and aptamer sequences for the malachite green molecule at its two end regions. In the absence of the analyte, neither the analyte aptamer – nor as a consequence – the malachite green aptamer can bind. Upon introduction and binding of the analyte, the malachite green aptamer can form and bind the reporter molecule malachite green, which is accompanied by a strong fluorescence increase [2].

it. However, in the presence of Lac1 bound to its binding sequence on the DNA, the RNA polymerase is blocked from transcribing the DNA into RNA, and the tweezer device remains open. The Lac1 can in turn be blocked by addition of the small molecule isopropyl  $\beta$ -D- thiogalactoside. Thus, the circuit provides several methods for controlling the closing of the tweezer device, and might be introduced into cells.

Further work has demonstrated a synthetic biochemical oscillator [25]. This uses DNA, RNA, and enzymes to control the coupling to, and timing of, a DNA tweezer opening and closing, and is a significant step forward in being able to control DNA nanodevices.

During the last decade there have been a significant development in the field of DNA nanodevices. The complexity, sensitivity, and level of control of such devices now allows directed motion in two dimensions with cargo across a surface, autonomous repetitive actuation and increasing and decreasing actuation with time, processing of multiple inputs to change outputs and processes, and coupling of devices to genetic processes. Extending the concepts discussed here may well see practical devices in use within the next several years.

---

One might now have an overview in mind of these dynamic DNA structures that can perform various actions. These thoughts can be held as we now look at some examples of structures demonstrated in the laboratory here and their potential uses and applications.

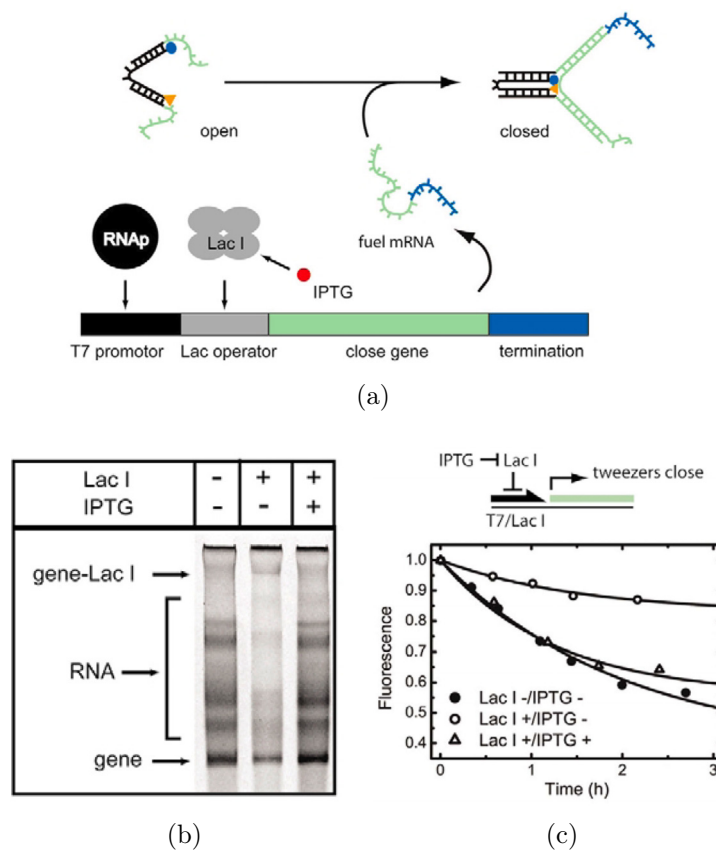


Figure 5.10: a) Working principle of a regulated gene encoding the closing sequence for DNA tweezers (see text for explanation). b) Gel electrophoresis and c) FRET experiments prove the regulatory behaviour and functionality of the network [2].



# Chapter 6

## Examples of DNA self-assembly demonstrated

### Contents

---

<b>6.1</b>	<b>DNA lattices . . . . .</b>	<b>101</b>
<b>6.2</b>	<b>DNA nanotubes . . . . .</b>	<b>103</b>
<b>6.3</b>	<b>Stretched and aligned DNA . . . . .</b>	<b>105</b>
<b>6.4</b>	<b>DNA-wrapped carbon nanotubes with quantum dots . . . . .</b>	<b>108</b>
<b>6.5</b>	<b>DNA-wrapped carbon nanotubes with origami rectangles . . . . .</b>	<b>109</b>

---

In this chapter five examples of DNA self-assembly that I have demonstrated in the laboratory are presented<sup>1</sup>:

1. A lattice assembled from two sequences.
2. DNA nanotubes assembled from a single sequence.
3. DNA stretched (molecular combing) on a mica surface (not strictly self-assembly).
4. Wrapping of single-walled carbon nanotubes with DNA, followed by biotin-streptavidin binding of commercial quantum dots to the DNA.
5. Wrapping of single-walled carbon nanotubes with DNA, followed by hybridisation of these to DNA origami (introduced in Chapter 7) structures.

### 6.1 DNA lattices

The major challenge to assembling DNA lattices is that of experimentally achieving correct stoichiometry of the DNA component strands. The larger the number of component strands, the more difficult is this task. The experimental problems arise in two

---

<sup>1</sup>This work has not yet been published.

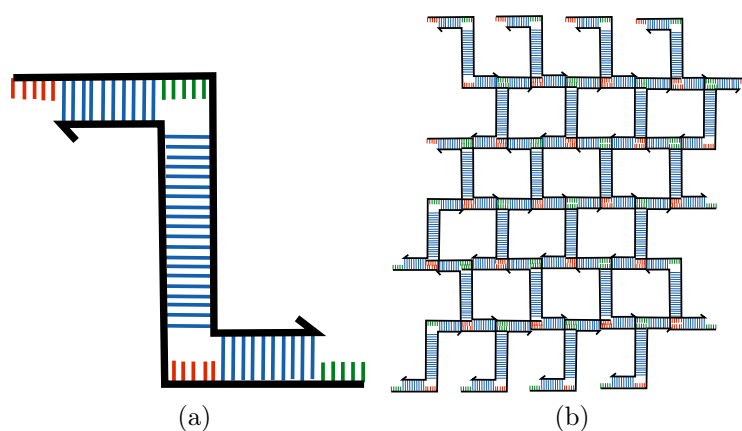


Figure 6.1: A depiction of the structure for the assembled lattice from the design of Murata and colleagues. *a)* Two strands bind to form a ‘Z’ structure with multiple regions of single bases. *b)* These bind together to form a lattice.

forms. Firstly, accurately measuring concentrations via ultraviolet absorption is hindered by secondary structure formed in the DNA strands, and our inability to account for this. Secondly, pipetting and dilution inaccuracies (which to some extent are unavoidable).

Thus, designs that minimise the number of component strands are of great benefit to the ease of assembly. One such design from Murata and colleagues [125] that I assembled is described here. Two strands bind to form a ‘Z’ structure, and such structures correspondingly to form a lattice. Details of assembly methods are given in detail in Section 4.3.3, however for convenience are also briefly described here.

The two sequences are mixed at dilute equimolar concentrations in  $1 \times \text{TAE}$  buffer with 12.5 mM  $\text{MgAc}_2$ . This buffer *must* be filtered, preferably through a  $0.02 \mu\text{m}$ , otherwise  $0.2 \mu\text{m}$ , filter. This is important for successful assembly. The solution is then cooled in a securely fastened tube from  $90^\circ\text{C}$  to  $20^\circ\text{C}$  over several days, either in a large water bath or with a polymerase chain reaction machine. A  $5 \mu\text{l}$  droplet of this solution is then pipetted (with a wide cut-off pipette tip) onto a freshly cleaved mica surface and imaged with the same  $\text{TAE}/\text{Mg}^{2+}$  using an atomic force microscope and a fluid cell. Better images may occur by pre-treating the mica surface with 10 mM  $\text{NiCl}_2$  solution beforehand. As can be seen in Figure 6.2 on page 103, lattices are formed, and ‘domains’ of constant orientation can be seen. To improve the size of the domains, one may place a small piece of freshly cleaved mica in the DNA solution before cooling, and then complete one standard cool, followed by repeated cooling from  $40^\circ\text{C}$ . The lattices form on the mica surface, and repeated cooling allows growth of the domain size. The surface should be imaged without being allowed to dry out. To achieve this one slides the mica (without touching it) onto a metal puck coated with 5-minute epoxy glue and then gently covers it with the  $\text{TAE}/\text{Mg}^{2+}$  buffer.

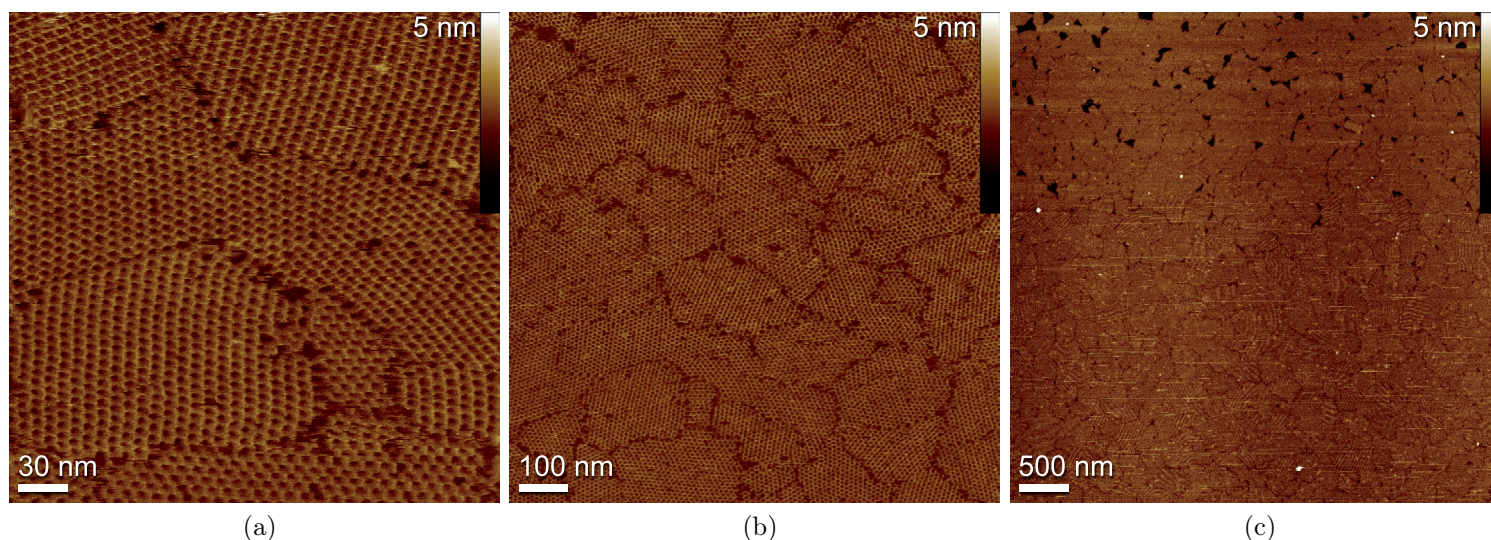


Figure 6.2: Atomic force microscopy images of the lattice assembled from two different sequences shown in Figure 6.1. Domains of constant orientation are observed, the size of these are controlled by the cooling conditions.

## 6.2 DNA nanotubes

As discussed in the previous section, stoichiometry is a challenge for assembling periodic DNA structures. Mao and colleagues developed a strand with multiple palindromic sequences that bind to copies of itself and assemble into DNA nanotubes. This is beautiful because it does away with stoichiometry all together. The structure is discussed thoroughly in Chapter 9, here I present some examples that I have assembled.

The assembly protocol is similar to that discussed in the previous section. The DNA nanotubes tend to clump together, probably due to single strands extending from defects on the nanotubes hybridising and binding multiple nanotubes together. This can be seen in Figure 6.3a on page 104. They can have lengths up to approximately  $50 \mu\text{m}$ , depending on the time that they were left to cool. They have measured diameters of approximately 8 nm. On one occasion a nanotube was observed with both ends joined forming a loop, and was of significantly greater diameter than the rest of the nanotubes. One can verify that they are indeed tubes by increasing the force of the atomic force microscope tip while imaging so that they break open. An example shown in three dimensions is given in Figure 6.3c.

To alleviate the previously mentioned clumping, one can filter the nanotubes after the cooling stage through a  $0.45 \mu\text{m}$  pore centrifuge filter at  $2000\times g$ . Examples of such filtered nanotubes that have been labelled with the fluorescent intercalating dye YOYO-1 (see 4.3.4) and imaged with a fluorescence microscope and  $100\times$  objective are given in Figure 6.4 on page 105.

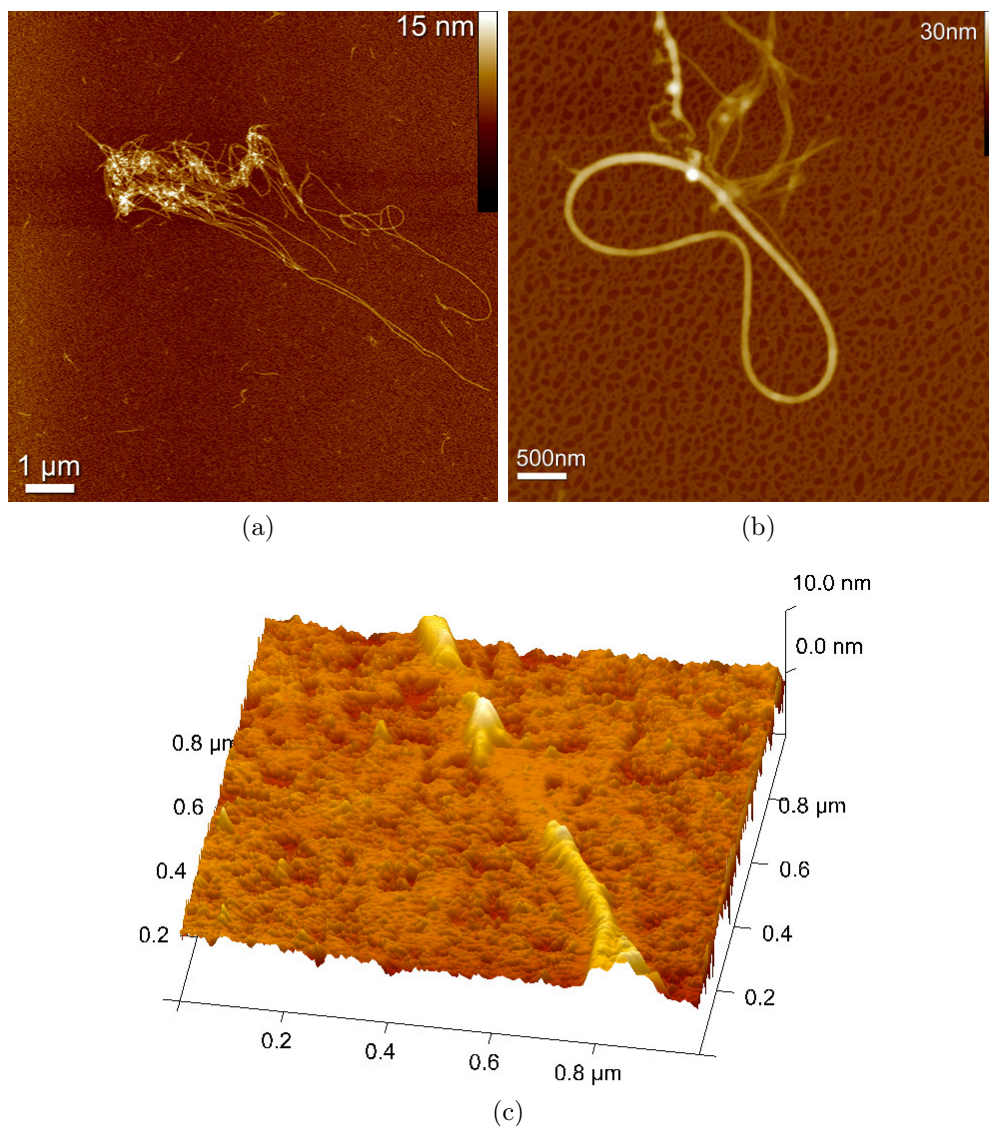


Figure 6.3: Atomic force microscopy images of DNA nanotubes assembled from a single sequence. *a)* A clump of nanotubes, held together by electrostatic interactions. *b)* Observation of a nanotube that has joined at its ends, and has a much greater diameter than the surrounding nanotubes. *c)* A three-dimensional plot of part of a nanotube that has been broken in places by the force from the scanning microscope tip.

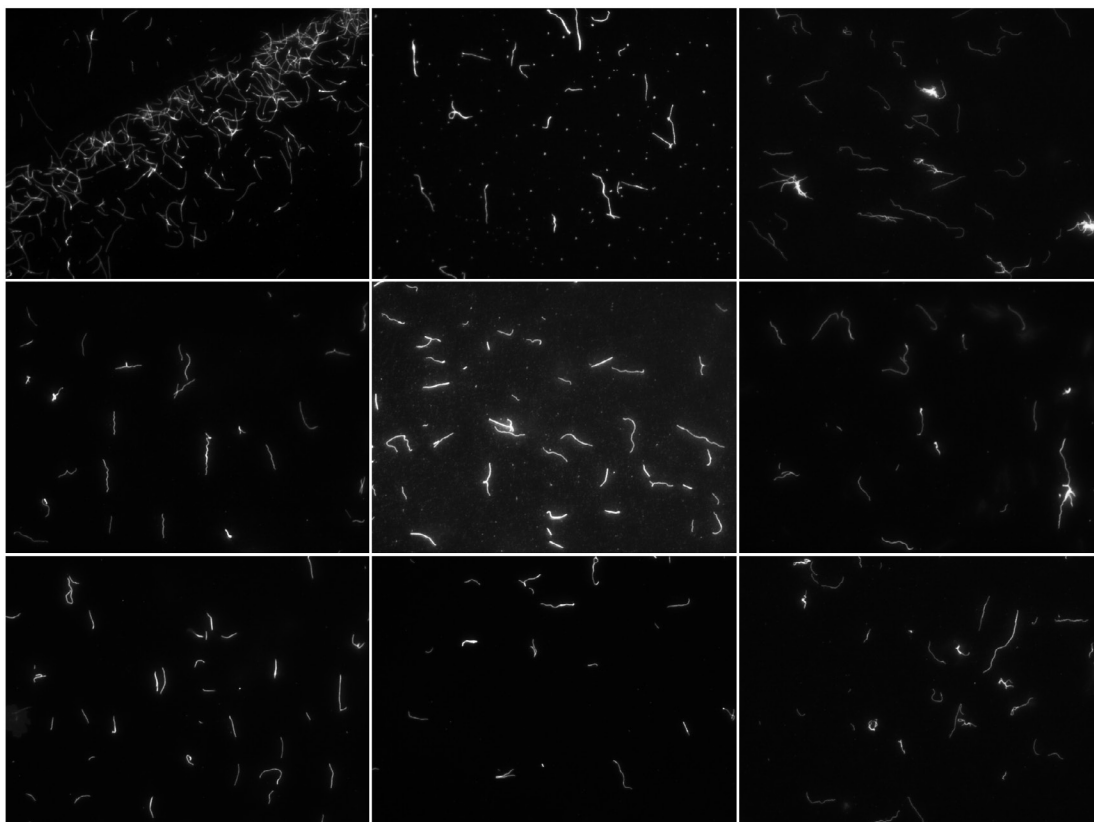


Figure 6.4: A montage of fluorescence microscopy images of DNA nanotubes labelled with a intercalating fluorescence dye YOYO-1. Images are of width  $1.5 \mu\text{m}$ . These have been ‘declumped’ by filtration through a centrifuge filter.

### 6.3 Stretched and aligned DNA

Researchers would often like to have long (many thousands of base pairs) sequences of DNA stretched out straight on a flat surface. There are several uses: one can observe enzymes interacting with the DNA using single molecule techniques (transcription processes for example), one can observe fluorescent in-situ hybridisation of the DNA (FISH), or one can coat it with metal (such as platinum) to create molecular wires.

The stretching and straightening of DNA molecules is achieved through different methods collectively known as molecular combing. The most popular method is to use deprotonated DNA that attaches to hydrophobic surfaces at its ends. A hydrophobic surface is generally created by coating glass or silicon with a silane layer. This layer has a surface roughness of several nanometers which results in very poor imaging using atomic force microscopy, given that the stretched DNA has a diameter of 2 nm (or less) when dehydrated. Thus, most experiments are observed using fluorescence microscopy, which has significantly lower resolution than atomic force microscopy.

I have developed a simple method that achieves high quality combing on a flat mica

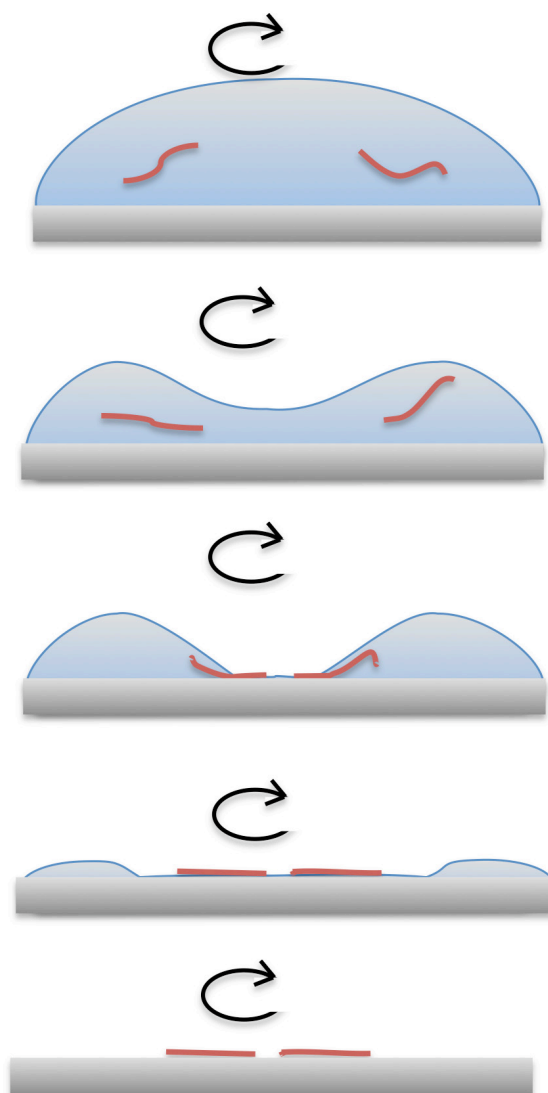


Figure 6.5: Stretching and aligning (molecular combing) of DNA by meniscus recession with a spin coater. A droplet of DNA diluted in sodium phosphate buffer completely covers a round mica sheet (in grey). This sits centred on a spin coater. Upon gradual increase of rotation the droplet deforms as shown. Eventually the centre of the droplet touches the mica, and a ring shape forms. The inner surface of the ring retreats rapidly outwards, and at this water/air/mica boundary the DNA is stretched. Eventually the droplet dries completely away, leaving just the DNA on the surface. Results are shown in Figure 6.6.

surface, ideal for observation with atomic force microscopy. The DNA – for example Lambda DNA – is diluted by a factor of one thousand in sodium phosphate buffer of pH 6 from 500  $\mu\text{g}/\text{ml}$ . A 9 mm round mica sheet is glued to a metal puck. This puck is

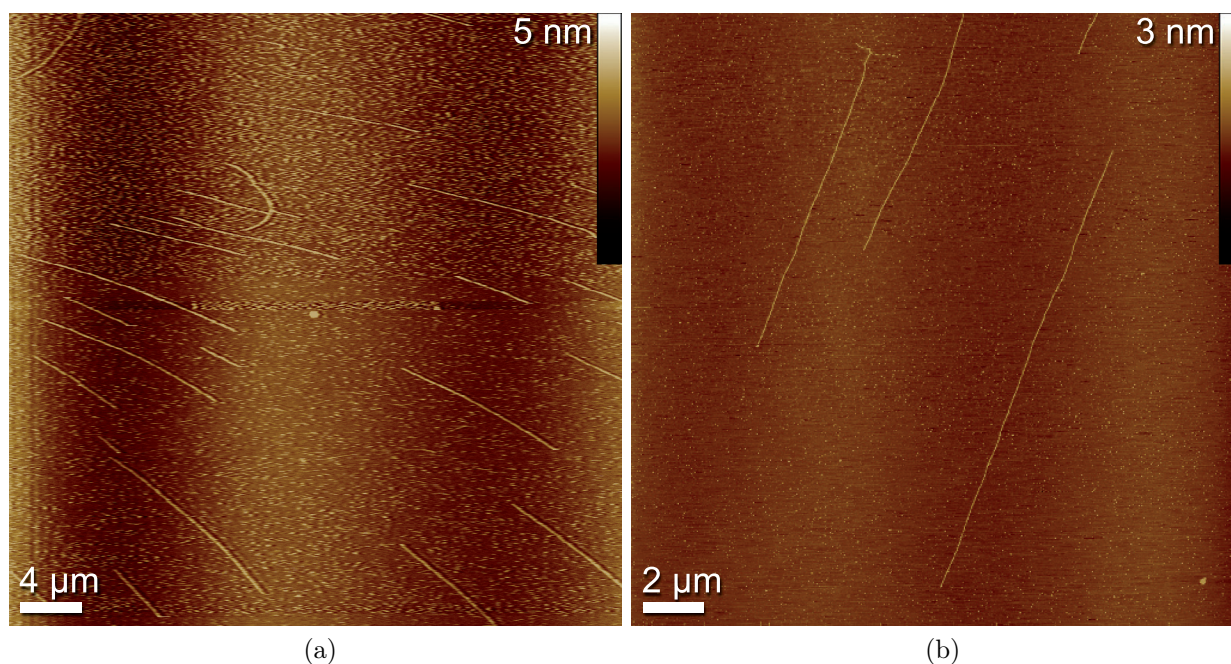


Figure 6.6: Stretched and aligned (molecular combed) Lambda DNA on a mica surface, created using a spin-coating technique, as shown in Figure 6.5 on page 106. Previously, DNA has been stretched on hydrophobic surfaces such as silane which are quite rough and do not allow adequate atomic force imaging of the DNA, fluorescence imaging was used instead providing much lower resolution than is shown here. This may be a useful technique for high-resolution studies of interactions of enzymes with genomic DNA.

mounted in a spin-coater.  $10 \mu\text{l}$  of DNA solution is pipetted onto the mica, followed by  $20 \mu\text{l}$  of deionised water. The volumes are important with respect to the area of the mica sheet, they create an optimal size droplet that spreads out to the edges of the mica. This is depicted in Figure 6.5 on page 106. The spin-coater is then slowly accelerated towards 500 rpm.

The centrifugal effect causes the droplet to deform. At some point, the centre of the droplet becomes thin enough for the droplet to change into a ring shape. This is critical. Within 1-2 s, this ring shape thins, and the inner surface of the ring moves rapidly towards the outer surface of the ring. The spin coater is held at constant velocity when this is observed to occur, and then accelerated to 1500 rpm for 90 s to dry the surface.

It is assumed that the meniscus of the ring inner surface moving outwards combs the DNA. Why this works on an unmodified hydrophilic flat surface such as mica is not understood. However, the end result is nicely combed DNA that can be observed in ambient conditions using an atomic force microscope, as shown in Figure 6.6.

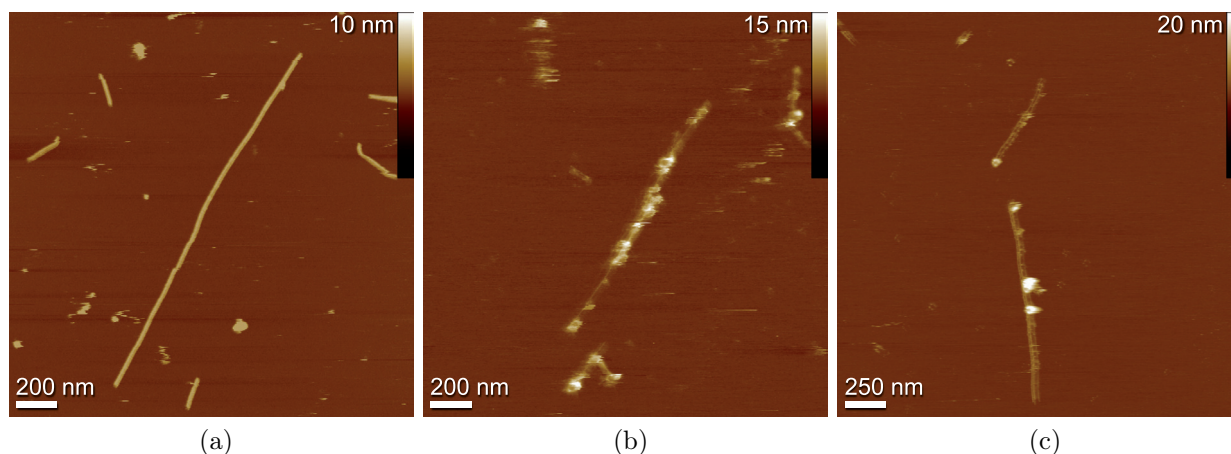


Figure 6.7: Atomic force microscope images of DNA-wrapped carbon nanotubes. *a)* A DNA-wrapped carbon nanotube on a mica surface. The DNA itself cannot be resolved, however the diameter of the structure (as measured from its height) is too wide for just a carbon nanotube, and carbon nanotubes by themselves clump together; good indications that this is wrapped with DNA. *b, c)* Such DNA-wrapped carbon nanotubes with extra hybridised DNA modified with biotin-streptavidin bound quantum dots. Tip-sample interactions caused the slightly blurry images.

## 6.4 DNA-wrapped carbon nanotubes with quantum dots

In 2003 Zheng and colleagues from the company DuPont demonstrated that it is possible to disperse hydrophobic single-walled carbon nanotubes in aqueous solutions using high concentrations of short single-stranded DNA sequences that are combinations of guanine and thymine bases [126]. Several strands bind to any one carbon nanotube, however the coverage density is not known.

Carbon nanotubes are an exciting nano-material because of their novel properties. They have very high tensile strength, elastic moduli and thermal conduction. Different chiralities exhibit metallic or semiconducting behaviours, and superconduction has also been observed.

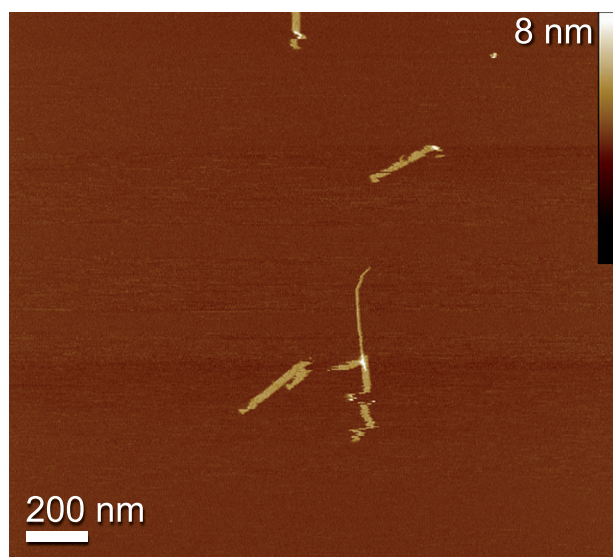
By adding a known random sequence of all four bases to the guanine-thymine binding sequence, one creates a ‘tail’ that does not bind effectively to the carbon nanotube. This single-stranded tail can hybridise to a complementary sequence.

Following the protocol of Zheng, I assembled DNA-wrapped single-walled carbon nanotubes and imaged them using atomic force microscopy in ambient conditions. An example is shown in Figure 6.7a on page 108. One cannot resolve the DNA around the nanotube, however without the DNA only large clumps and no single nanotubes are observed.

I then hybridised a biotinylated complementary strand to the tail of the single strand wrapping the carbon nanotubes, and followed this by adding high stoichiometric concentrations of commercially available streptavidin-labelled quantum dots (Invitrogen 565 nm). A



(a)



(b)

Figure 6.8: Atomic force microscopy images of DNA-wrapped carbon nanotubes hybridised to DNA origami structures, imaged on a mica surface. The DNA origami are  $300 \times 20$  nm and appear as rectangles (some deformed by imaging with the microscope tip), the tubes appear as long thin rods. In the top image a red arrow indicates an example, in the lower image an example is in the middle.

droplet of the solution was placed on a freshly cleaved mica surface, rinsed with deionised water to remove unbound quantum dots, dried with nitrogen gas and imaged in ambient conditions. Examples are shown in Figures 6.7b and 6.7c.

This method provides a simple way of combining three exciting nano-materials: DNA, carbon-nanotubes, and quantum dots.

## 6.5 DNA-wrapped carbon nanotubes with origami rectangles

The ability to orient carbon nanotubes on a surface with respect to each other via deposition from solution is a challenge. One might want to do this in order to create nanoscale transistor elements for example. Rothmund and colleagues recently achieved this by

hybridising DNA-wrapped carbon nanotubes to a relatively new type of self-assembled DNA nanostructure known as DNA origami. DNA origami is introduced in Chapter 7, it is useful for assembling structures of arbitrary form with size scales of the order of hundreds of nanometers. To do so, they used a special modified synthetic DNA known as locked DNA: LNA (the ribose structure is modified by a methylene bridge connecting the 2'-O atom with the 4'C atom). LNA provides stronger binding, however it is only available from a small number of suppliers and is expensive. It is thus perhaps not the optimal solution.

Using the tail and hybridisation technique presented in the previous section (Section 6.4), I successfully hybridised DNA-wrapped carbon nanotubes to DNA origami using standard DNA (without locked DNA). The origami structure is a rectangle of dimensions  $300 \times 20$  nm. I modified ten short strands aligned in a row along the length of the structure in the middle, such that they had a complementary sequence to the tail sequence of the DNA wrapping the carbon nanotubes. Because there are several such tails extending from each nanotube, and ten complementary sequences extending from the origami, the nanotubes should be able to bind in an aligned fashion along the origami structure.

This is indeed the case, two such examples are shown in Figure 6.8 on page 109.

---

Several examples of the DNA nanostructures self-assembled in the laboratory here have been presented. In the following, a technique known as DNA-origami is introduced (it has already been mentioned several times), moreover it is shown that one can assemble such structures without heating and cooling but using a chemical dilution method instead.

## Chapter 7

# Isothermal assembly of DNA origami structures using denaturing agents [3]

One of the challenges of assembling structures such as lattices composed of multiple different DNA sequences is that of correct stoichiometry. In order for such a structure to assemble correctly, each molecule has to find a suitable position in the structure during assembly. This requires time and reversible binding of the molecules, so that the molecules can ‘explore’ the structure, binding and unbinding until they find such a position. However, if one species of the molecule is present in the wrong concentration ratio in comparison to the other molecular species needed, then this has significant effects on the assembly of the structure. If the species is present in too high a concentration, then it will tend to be overly present in false positions on the structure as it ‘explores’ for correct positions. This slows the assembly of the structure, and/or creates defects. If the species is present in too low a concentration, then the other molecular species present will tend to explore the positions that it should occupy, slowing the rate at which it can fill the correct positions and/or creating defects. Thus correct stoichiometry is extremely important for correct and fast assembly of such structures.

However, a ‘beautiful’ technique has been developed that bypasses this challenge to a significant extent. Rather than using a design based on several short sequences that bind into a periodic structure and this structure increases its size with assembly time, one can use another possibility. One can provide a long single strand that ‘templates’ the position of the short strands, and becomes part of the structure itself [45, 46]. One might see some analogies with top-down versus bottom-up approaches (see Introduction on page vi).

Of importance is that each particular short strand has only one position that it can correctly occupy in the final structure. This requires the long strand to have a sequence that is non-repetitive – otherwise multiple positions would be present.

Secondly, the concentration of the long strand should be relatively low, so that interactions between long strands are very infrequent. Given this situation, one can provide short strands in higher stoichiometry than necessary, as they will only ever interact with one long strand at any point in time (as a result of the low concentration of the long strand). Further, strand displacement, high stoichiometry and the ability for short strands to find

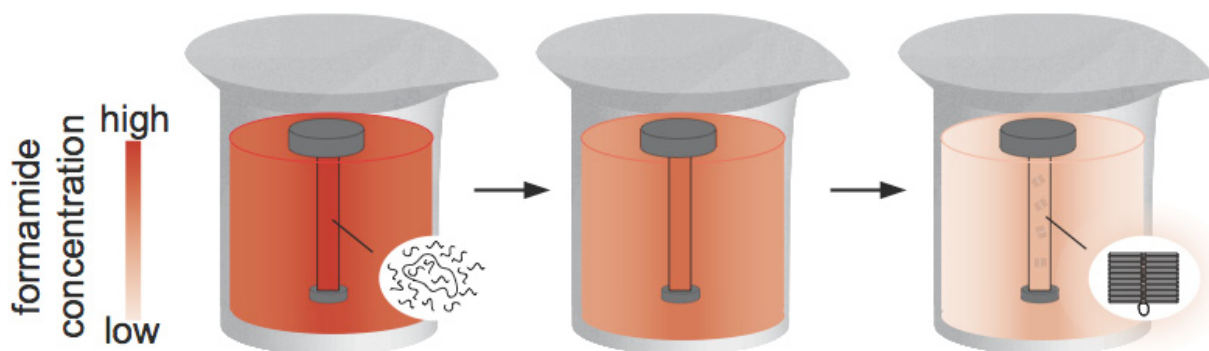


Figure 7.1: Isothermal formation of DNA origami by dialysis over several stages against buffer solutions with successively decreasing formamide (denaturant) concentrations [3].

there correct positions simultaneously (rather than waiting for the structure to grow in size, as in the previous method) increase the rate at which each position on the long strand is correctly filled, thus the rate of assembly is very fast, and the yield very high.

Effectively, the short strands ‘fold’ the long strand into the final structure. For this reason, the process is known as DNA origami, the short strands are known as ‘staples’ and the long strand is known as the backbone. Reversible binding is important so that short strands that initially bind in the wrong position can unbind and leave the position free for the correct strand. To create an environment suitable for this, one normally decreases the temperature from a high temperature (at which all bonds are broken and all strands are separate), to a lower temperature (at which bonds are formed and strands are bound together). This decrease in temperature must occur over some minimum time, so that the strands have ‘time’ to ‘explore’ as previously mentioned and find their correct positions.

This effect of changing from single strands and broken bonds to an assembled structure and formed bonds can be generated using another effect other than temperature.

Denaturing agents such as formamide are small molecules that form hydrogen bonds with DNA bases. If present in high enough concentrations, they can disrupt already formed bonds between DNA molecules and separate strands from one another. This effect is similar to changing temperature. Empirical measurements have shown a  $0.6^{\circ}\text{C}$  decrease in melting temperature per percent of formamide in the assembly solution (melting temperature is the temperature at which 50% of the bonds are intact) [127,128]. Thus by starting at high denaturant concentrations and decreasing the concentration with time, one achieves the same effect as decreasing temperature with time.

Experiments were performed with previously designed DNA origami structures including a rectangular form  $100 \times 70$  nm and a tube form of length 470 nm [45, 46, 129]. The backbone is a 7249 base sequence (the genome of bacteriophage M13mp18) and approximately 200 staple strands of 32 bases in length are used.

The backbone is added at a concentration of 1 nM and the staple strands are in 100 fold excess at 100 nM. These are mixed in hybridisation buffer and placed in a dialysis membrane (which is effectively a cage, allowing buffer and formamide molecules to diffuse

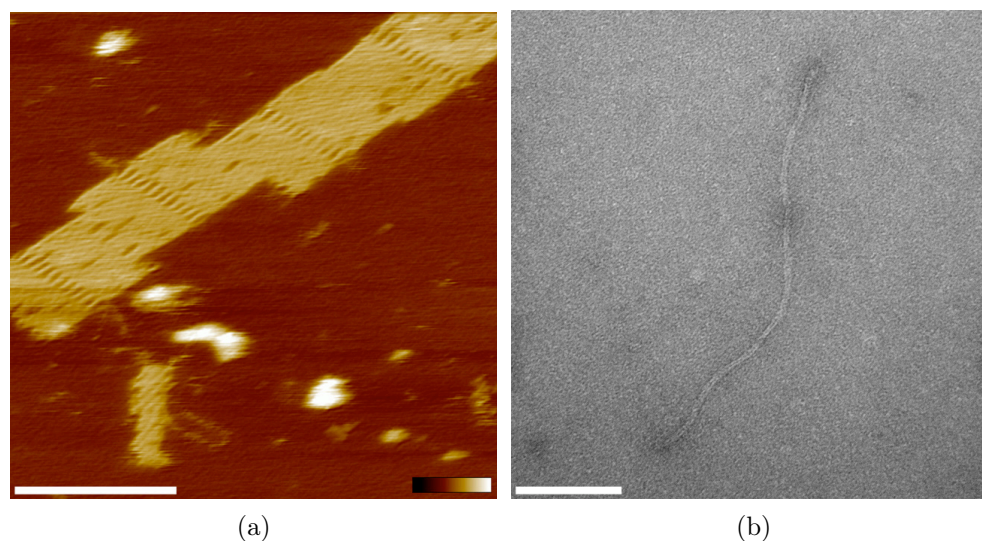


Figure 7.2: *a)* Atomic force microscopy image of DNA origami rectangles (four connected together) assembled using the isothermal, denaturant dialysis-based technique. Scale bar: 100 nm, height scale 5 nm . *b)* Transmission electron microscopy image of a DNA tube of length 410 nm assembled using the isothermal, denaturant dialysis-based technique. Scale bare: 100 nm [3].

in and out, but holding the larger DNA molecules captive). Two different protocols were used: firstly, a gradual decrease in denaturant concentration by slowly pumping buffer into the solution; and secondly, a stepwise decrease in denaturant concentration by changing the buffer solution with sequentially decreasing concentrations of denaturant (Figure 7.1 on page 112). These processes were carried out over 12-24 hours.

The protocols work quite well, appear relatively insensitive and need little optimisation. The continuous reduction occurred between levels of 85-1% denaturant with TAE (tris-acetate-EDTA) buffer. Tris (base) buffer is a typical buffer used for DNA hybridisation, acetic acid is used to lower its pH to 8.0 suitable for DNA, and EDTA is used to sequester divalent ions such as  $Mg^{2+}$  during storage of DNA, as these ions are required by enzymes that may occur in solution and undesirably modify the DNA. However, in order for the DNA to fold the DNA into a relatively closely packed structure, increased concentrations of divalent ions (12 mM) are needed as counterions to shield the strongly negatively charged phosphate DNA backbone in close proximity. The stepwise dilutions with 85%, 44%, 22%, and 11% concentrations of denaturant. This corresponds to melting temperatures of 2, 26.5, 39.7, and 46.3°C for the staple strands by thermodynamic analysis [130]. Two different denaturants were used and found to give similar results: formamide and urea [131].

Resulting origami structures were imaged using atomic force microscopy and a fluid cell (Figure 7.2a on page 113) while the tube origami structures were imaged using transmission electron microscopy (Figure 7.2b on page 113).

The DNA solutions were also left for 12 hours without denaturant and no resulting

structures were formed, verifying that the denaturing agent is indeed necessary for correct assembly of the structures. The technique was also used to attempt to assemble DNA nanotubes based on a single sequence (Chapter 6) [132]. However, no successfully assembled structures were observed. It is suggested that templating with the long single strand and the high stoichiometry ratio of the short strands in the origami method provide for a significantly enhanced assembly process that provides the successful results.

This isothermal (constant temperature) technique for assembly may be useful for temperature sensitive components often used with assembly such as thiol molecules (for binding metallic nanoparticles) or sensitive ribonucleic acids. And larger, more complex origami structures which are currently in development may require longer times to assembly and this requirement, along with high temperatures, may damage even DNA, so that denaturant dilution may become the preferred technique in the future for these as well.

---

One can take such DNA-origami structures and use them as templates for nanoscale objects such as fluorescent molecules which are visible optically. However, the distances between such objects on an origami template are too small to be resolved using standard methods. In the following, some advanced methods are presented that overcome this limit.

## Chapter 8

# DNA origami as a nanoscopic ruler for super-resolution microscopy [4]

Atomic force microscopy and transmission electron microscopy are often used to image DNA nanostructures [3]. Optical fluorescence microscopy has been of little use because diffraction limits resolution at the nanometer scale. Diffraction is the apparent bending and/or spreading out of wavefronts as light encounters an object or aperture. The diffraction of a plane wave entering a circular aperture (e.g. a microscope lens) is a central spot with a series of concentric rings decreasing in intensity (known as an Airy disk). Two point sources will each produce their own Airy disk. If the point sources are moved together, the patterns will begin to overlap, and ultimately they will merge to form a single spot, in which case the two point sources cannot be resolved in the image.

Recent advances in far-field fluorescence microscopy below the diffraction limit have led to so-called super-resolution microscopy techniques (Section 4.1.5). These allow structures in the sub-200 nm regime to be analysed [133].

Using defined samples and these technique, one can calibrate distance measurements with nanometer precision. For example, short double-stranded DNA with defined numbers of bases can be used [134–137]. However, these have significant flexibility and are difficult to immobilise on a surface in a fixed orientation under relevant environmental conditions [138]. A better substrate would be a stiffer structure that can be fixed flat to a surface. Such a standard could be used to demonstrate and quantify resolution, verify optical magnification, correct for microscope aberrations, and study and calibrate the photochemical and photophysical properties of the fluorescent probes under defined conditions [62, 139].

Such a system can made using DNA origami. A rectangular DNA origami structure can be assembled (Figure 8.1 on page 116). Two staple strands that bind at diagonally opposite corners have fluorescent molecules (fluorophores) attached. Such a structure can have a size of  $100 \times 70$  nm, resulting in distances between the fluorophores being well below the diffraction limit of approximately 200 nm.

Having assembled the origami structures, there are many excess single strands in solution. These are filtered from the solution using an appropriate (molecular weight cut-off) filter. The structures are then imaged with atomic force microscopy using a fluid cell to

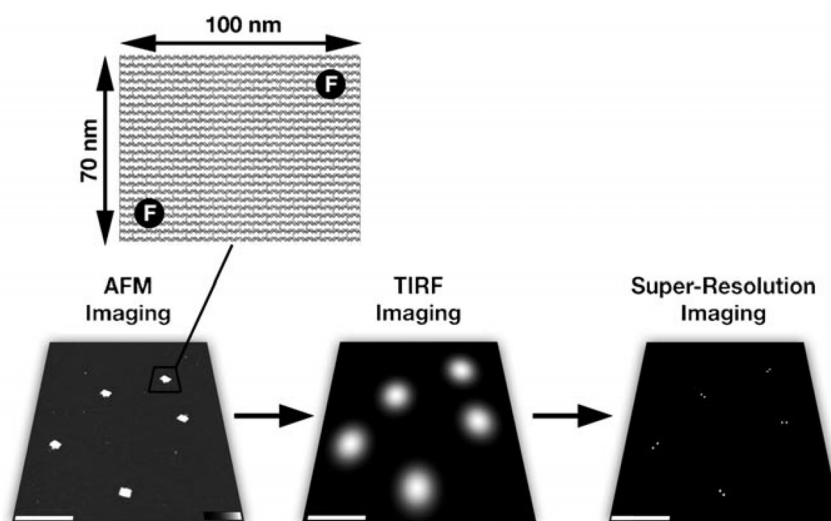


Figure 8.1: The rectangular DNA origami structure with two fluorescently labelled staple strands (F in black circle) at a specific distance from each other. After preparation, origami samples are imaged using atomic force microscopy with a fluid cell (bottom left) to check that the structures had formed correctly. They are then imaged using total internal fluorescence microscopy (bottom middle). Single fluorophores on the origami samples are identified using different super-resolution methods (bottom right). Scale bars: 500 nm, height scale 6 nm [4].

check that they have assembled correctly. They are then placed on a glass microscope slide in buffer with extra divalent salt ( $\text{Mg}^{2+}$ ) to bind them electrostatically to the surface. These can then be imaged using total internal reflection microscopy (Section as a single spot, which is actually the diffraction-limited image of the two fluorophores on diagonally opposite corners.

As a model system one can use the fluorophore ATTO 655. At opposite corners the distance between is 89.5 nm (assuming 10.67 bases per helical turn and a 3 nm displacement between parallel helices [46]). Figure 8.2a on page 117 shows an image of several such structures. Diffraction limited spots are observed.

The individual fluorophores can be located mathematically using Gaussian fitting of the spot intensities. However, in order to do so for each fluorophore, one needs images of each fluorophore emitting with the other fluorophore off. Thus, we need to be able to turn fluorophores off and on. This can be done by controlled using ‘reduction’ and ‘oxidation’ reactions in the buffer [139–142]. To do this one uses 50  $\mu\text{M}$  ascorbic acid and 50  $\mu\text{M}$  methylviologen. The individual fluorophores then turn on and off at random short intervals. Figure 8.3a on page 118 shows spikes in fluorescent intensity over time as this happens, measured from a single origami structure, captured by taking many images in rapid succession.

Using Gaussian fitting - in images when one fluorophores on and the other is off - each of the fluorophores can then be localised. This results in a sharper image as in Figure 8.2b

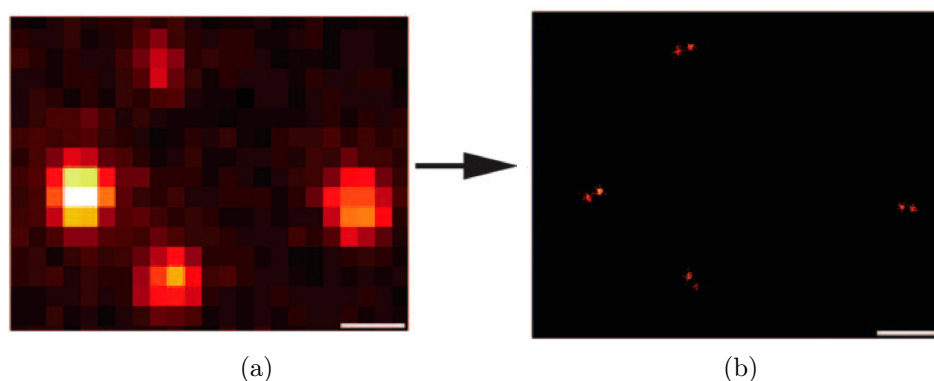


Figure 8.2: *a)* Total internal reflection microscopy image of several DNA origami structures - with two ATTO 655 fluorophores on diagonally opposite corners - bound on a glass surface. The individual fluorophores cannot be identified, only diffraction limited spots are seen. *b)* Super-resolution identification of the fluorophores clearly resolves their positions. Scale bar: 500 nm [4].

on page 117. By analysis of many such origami structures, one can calculate a distance distribution between fluorophore pairs as in Figure 8.3b on page 118, giving  $88.2 \pm 9.5$  nm (from 84 spots measured), in good agreement with the designed distance of 89.5 nm. Single molecules can be localised with a precision of  $\pm 5.9$  nm [143]. Hence the precision of localisation almost completely accounts for the width of the distribution obtained. Thus, one can use origami structures as robust reproducible nanoscopic calibration standards.

However, the yield of such structures in which both fluorophores can be resolved is about 50%. This may be because of interactions between the fluorophores and the glass surface. To increase the distance between the glass and the fluorophores and thus reduce such interactions, one can use three biotin modified staples that bind in positions in a diagonal line between the fluorophores and on the under side of the origami - the side that binds to the surface. Coating the surface with streptavidin provides binding opportunities via streptavidin-biotin interactions.

Doing so increases the resolvable yield from 50% to 71%. What explains the other remaining structures? During assembly only 79% of origami structures form with the two fluorophores correctly bound (measured by bleaching origami structures), thus indicating that approximately 90% of the correctly formed structures could be resolved.

Rather than analysing images to find instances where one, but not the other, fluorophore is on - and this for both fluorophores - one can use another technique. One can alter the reduction and oxidation conditions such that typically both fluorophores are on initially, and then one of the pair turns off [134, 136].

This gives an intensity profile of a spot with time as shown in Figure 8.3c on page 118. Initially both molecules are on, then one turns off and the intensity decreases, and then the second turns off and the intensity decreases again. By averaging the images when only one molecule is on and fitting a Gaussian profile, one localises this profile. One can

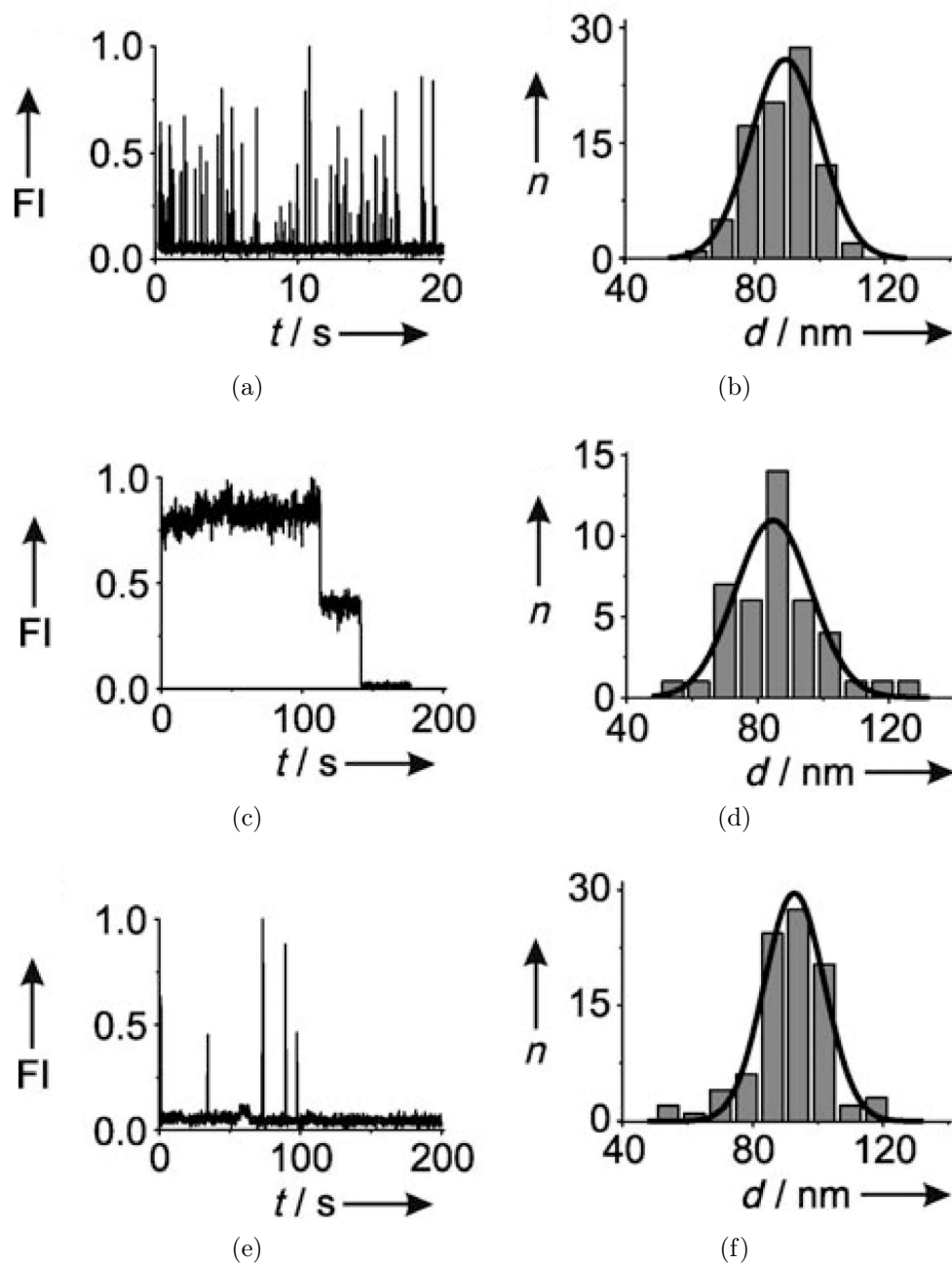


Figure 8.3: Super-resolution microscopy of doubly labelled DNA origami. *a, c, e*) Fluorescence intensity versus time profiles of an origami structure. *b, d, f*) Statistical distributions of measured distances between fluorophore pairs [4]. See text for the different measurement methods.

subtract the average image from the average image calculated when both fluorophores were initially on. This results in the average image of the other fluorophore, and it can likewise be localised with a Gaussian fit. The distance between the fluorophores can then be calculated. Statistical analysis of 42 spots gives a distance between fluorophore pairs of  $85.2 \pm 14.2$  nm (Figure 8.3d on page 118).

A further technique is to make use of particular fluorophores that can be switched on and off using different laser light wavelengths (known as direct Stochastic Optical Reconstruction Microscopy, Section 4.1.5 on page 57) [62]. Cy5 is one such fluorophore which, in the presence of thiol molecules ( $\beta$ -mercaptoethylamine) can be switched using blue and red laser excitation [144]. When both lasers are simultaneously on, the fluorophores continually turn on and off (Figure 8.3e on page 118). Making use of the first analysis technique with separate images with each of the two fluorophores are on by themselves, a distance between fluorophores of  $91.6 \pm 12.2$  nm is measured (90 spots analysed, Figure 8.3f on page 118).

Further experimental details can be found in [4].

The three methods discussed thus allow relatively precise optical determination of distances at the nanometer level. Recent advances in the origami technique will allow extension of this principle to three dimensions [39, 145]. Photo-switchable proteins that can be ‘expressed’ in cells could allow the technique to be used in cells themselves [146]. Single molecule methods thus can now finally cover the full critical length scale from a few nanometers using Förster resonance energy transfer up to that of hundreds of nanometers using conventional optical microscopy.

---

We have seen that we can use DNA nanostructures to organise nanoscale objects. What about the structural integrity of DNA nanostructures? Are they stable? Some answers to these questions are examined in the following chapter.



## Chapter 9

# Assembly and melting of DNA nanotubes from single-sequence tiles [5]

DNA hybridisation and melting studies are very useful for examining the kinetics and thermodynamics of molecular interactions between DNA strands. These are important not only in a biological context, but also for DNA nanotechnology which aims at the construction of molecular materials and devices via self-assembly. Here we experimentally examine the assembly and melting of a DNA nanotube structure composed of many copies of a DNA structure containing four palindromic sequences. Temperature-controlled ultraviolet absorption, atomic force microscopy, fluorescence microscopy and transmission electron microscopy measurements are correlated to investigate important factors such as hierarchy of assembly, DNA strand concentration, and annealing protocols. Assembly and melting are shown to proceed via different pathways: assembly occurs in several hierarchical steps including the formation of tiles, lattices and tubes, whereas melting occurs in a single step.

Accurate theoretical calculation of how two or more DNA strands will hybridise and of the three dimensional structure they will form has only become possible in the last couple of years [147–151]. However, these calculations are still limited to particular cases. Hybridised DNA structures can be represented by what are known as ‘polymer graphs’, with the strands represented as sequences on the circumference of a circle and the base pairs depicted as straight lines joining complementary bases (section 3.2.2.4 on page 33). Lines that cross indicate the presence of ‘pseudoknots’ in the structure. Pseudoknots represent more complex geometric structures and tertiary interactions; and are presently excluded from calculations as they are difficult (‘NP-hard’) to solve.

Rather than calculating kinetic and thermodynamic data using models of the end structure (which as mentioned cannot always be generated), an alternative approach is to extract this data from experimental measurements. In order to do so one needs to know how the reaction proceeds: that is, how many ‘states’ occur [152]. These states are artificial classifications of the reaction processes, often a single or two state reaction is assumed, however in reality even two perfectly complementary strands may hybridise via several intermediate states, and multiple strands hybridising into ‘pseudoknot’ structures can have many more states [151]. This means that the data extracted from such measurements is questionable

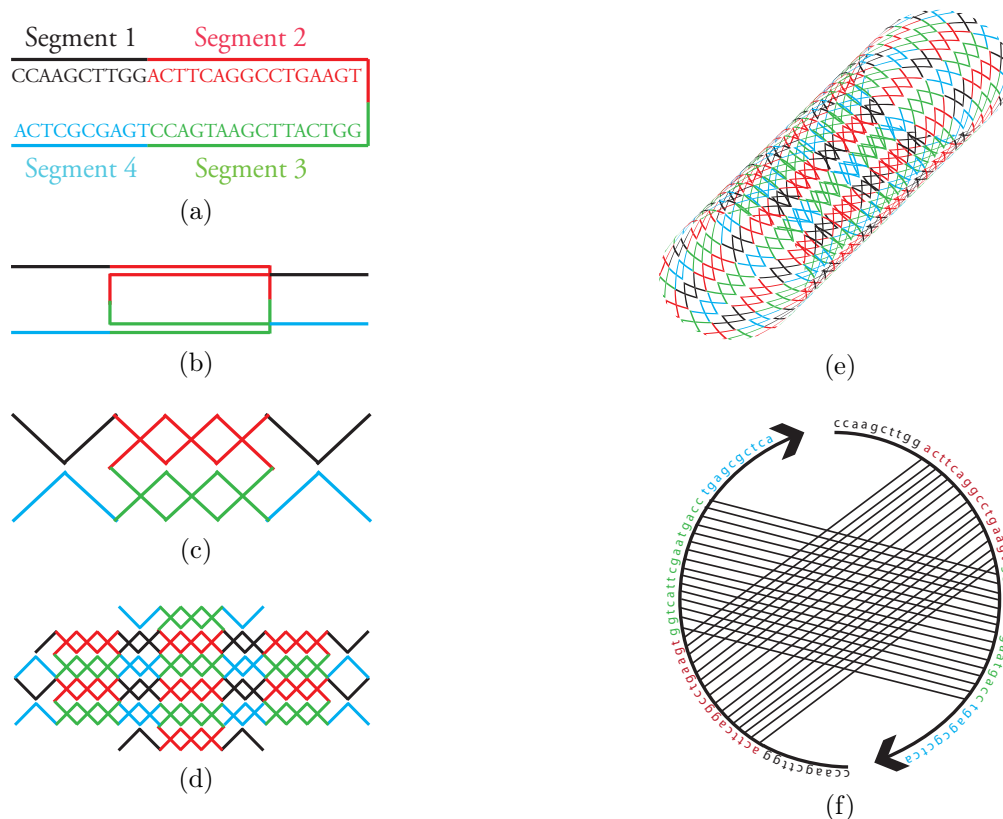


Figure 9.1: Assembly of a DNA nanotube from many copies of a single sequence developed by Mao and colleagues [132]. *a*) The sequence consists of four palindromic segments (segments that are self-complementary). These are called segments 1, 2, 3 and 4 in this study. *b,c*) Two copies of the sequence bind at segments 2 and 3 to create two double helices that cross over in two positions. This leaves four single-stranded ends from this ‘tile’. The double helices are 16 base-pairs in length. *d*) The single-stranded ends are 10 bases in length and can bind (at lower temperatures because they are shorter than the 16 base-pair helices above) to others in the solution. Segment 4 will bind to other segment 4s because these are designed to be self-complementary, likewise with the segment 1s. Thus a ‘lattice’ forms. *e*) These lattices can bind into DNA nanotubes in an intra-complex process. *f*) A polymer graph of the double crossover tile structure represented in *b*) and *c*). The crossing lines representing the base pairing indicate that this structure is a pseudoknot [5].

or invalid, because the assumptions are incorrect.

The assembly and melting that we study here is of many copies of a single sequence. This sequence was introduced by Mao and colleagues and is based on an elegant idea they had [132]. The sequence is 52 bases in length and consists of four palindromic segments (Figure 9.1a on page 122). These segments are called 1, 2, 3, and 4 in this study. A sequence is palindromic if it has the property of being self-complementary – that is, it can

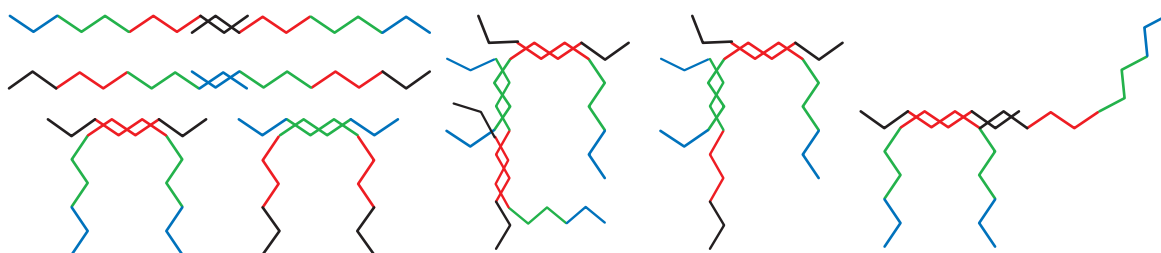


Figure 9.2: Many other complexes are possible apart from the double-stranded crossover tiles and regular lattices. Some of these complexes are depicted here. However, these result in either more single-stranded segments or structures with larger stress and are not favoured in equilibrium [5].

hybridise perfectly to another copy of itself when both are anti-parallel aligned. The entire strand is designed so that it hybridises into a double cross-over with another copy of itself (Figure 9.1b). This structure has two double helices of length 16 base pairs (the length of segments 2 and 3). This is approximately 1.5 helical turns, or an odd number of half-turns. The structure is called a ‘tile’. This is drawn as a polymer graph in Figure 9.1f. It can be seen that the lines representing base-pairs cross, indicating a pseudoknot, thus presenting calculation difficulties.

In this study we take an alternative approach to those techniques mentioned above. We study formation and melting of the structure formed by this sequence by making detailed ultraviolet absorption measurements of temperature-controlled DNA solutions and correlate these with atomic force microscopy and fluorescence microscopy observations. This provides new insights into the formation and melting that demonstrate the hierarchy of the dynamic assembly process.

The tile described is not the final structure however. It has four single-stranded DNA ends— two each of segments 1 and 4. These ends bind to the complementary ends of other tiles, and under slow cooling conditions ordered lattices of tiles will form.

Many configurations of this strand are possible. Some – other than the tile described – are depicted in Figure 9.2 on page 123. However, these structures always result in unbound single-stranded DNA, or in structures that are not at the minimum free energy. Thus with slow cooling (attempting to stay within dynamic equilibrium conditions), the ordered tile lattice will preferentially form.

This lattice is flexible, particularly as there are nicks in double-stranded DNA where tiles join one another. As the lattices form, free tile and lattice concentrations decrease (larger lattices resulting in fewer numbers of lattices) and intra-lattice interaction becomes more likely than inter-lattice interaction and tubes (helical or non-helical) are able to form.

An atomic force microscopy image of aggregated DNA nanotubes on a mica surface is shown in Figure 9.3a on page 124. These were annealed over 48 h. The individual tubes have diameters of approximately  $7 \pm 2$  nm (as measured by topographic height, which minimised the influence of atomic force microscope tip convolution) and lengths of 20  $\mu\text{m}$ ,

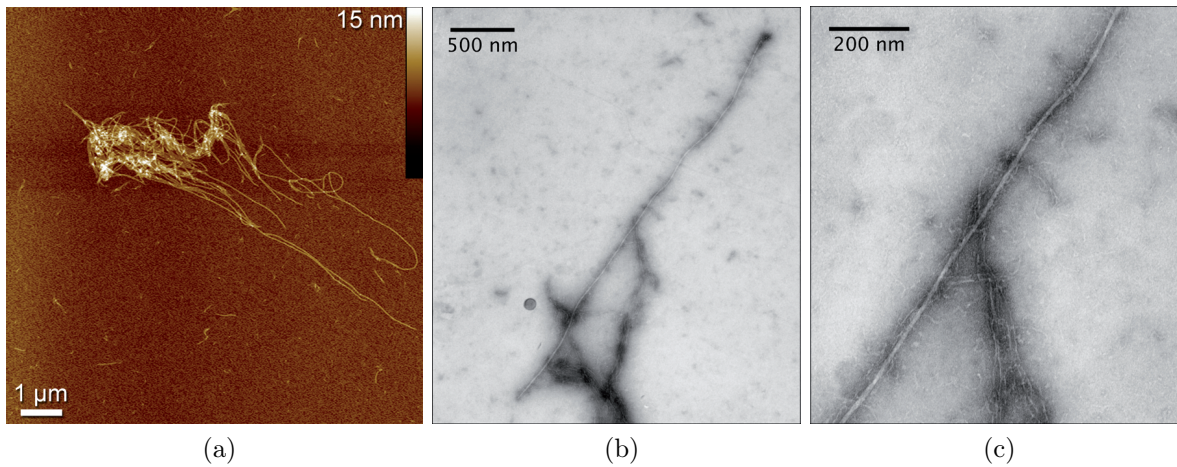


Figure 9.3: Images of the DNA nanotubes. *a)* An atomic force microscopy image of aggregated DNA nanotubes. Individual nanotubes have a diameter of approximately  $7\pm 2$  nm, as measured by topographic height. Scale bar:  $1\ \mu\text{m}$ , height scale: 15 nm. *b)* A negative stain transmission electron image of a DNA nanotube. The irregular dark area in the lower part of the image is thought to be DNA lattice that have not formed into nanotubes. Scale bar: 500 nm. *c)* Magnified image of the middle section of the previous image. The measured width of the nanotube is  $8\pm 3$  nm and measured length is  $3.5\pm 0.2\ \mu\text{m}$ . Observed fine (white) structure thinner than the nanotube is thought to be chains of tiles. Scale bar: 200 nm [5].

although this is dependent primarily on cooling times and is discussed in the results section. In Figure 9.3b and Figure 9.3c, transmission electron microscopy images of a single nanotube are shown from a solution annealed over 12 h. In *b)*, the whole nanotube of measured length  $3.48\pm 0.2\ \mu\text{m}$  is imaged, while in *c)* at higher magnification a section of it is imaged. Its measured width is  $8\pm 3$  nm, agreeing within error with that measured with atomic force microscopy.

Many different versions of DNA nanotubes requiring differing numbers of DNA strands and differing DNA sequences have been experimentally realised [153–158]. We choose to study this particular sequence because of its inherent simplicity based on symmetry, resulting in only one sequence being required. This removes problems of stoichiometry. However, despite its simplicity, a rich variety of thermodynamic behaviour was observed.

The nanotubes studied here have already been demonstrated as a useful link between bottom-up self-assembly and top-down nanolithography approaches. Yan and colleagues [159] have used biotin–streptavidin binding to organise quantum dots along the nanotubes, and followed this with PDMS (polydimethylsiloxane) stamping to create large-area (at least tens of microns squared) ordered arrays of these structures.

Increasing our understanding of the formation and assembly dynamics should lead to better control of yields and optimised formation times. Furthermore, it is expected to result in better control of the nanotube lengths and their variability.

The 260 nm absorption peak of DNA was measured using a ultraviolet spectrophotometer and heating was provided by a Peltier element stabilised by contact with a temperature-controlled water bath (See Sections 3.1.6 on page 21, 4.1.1 on page 49). The water bath was programmed at a constant 25°C. The sample solution was loaded into a screw-top cuvette, making certain that the cuvette was completely full (2700  $\mu\text{l}$ ) and the screw-top was closed firmly(!). This ensured that upon heating no gas bubbles formed in the solution. A 5 nm bandwidth excitation was used. Typically, a sample was cooled from 95 to 85°C at a rate of 30°C h<sup>-1</sup> (in order to minimise damage to the DNA), and then at a slower rate of 6°C h<sup>-1</sup> to 20°C. Measurements were median smoothed over 100 data points and typical measurements had tens of thousands to hundreds of thousands of data points. Curves were fitted with high order polynomials to allow numerical differentiation without interference from noise.

A 3  $\mu\text{l}$  drop of a sample solution was placed on a carbon-coated transmission electron microscopy grid. The drop was dabbed off with filter paper after 20 s followed by rinsing with deionised water. A drop 3  $\mu\text{l}$  of 1% uranyl acetate negative staining solution was then placed on the grid for 20 s, dabbed off and left to dry for one hour. Imaging was performed with a transmission electron microscope working at an accelerating voltage of 100 kV.

Further experimental details can be found in Reference [5].

Several sets of results are discussed. We show formation and melting curves of the nanotube solutions at different concentrations. Measurements of the individual segments are also presented for comparison, along with a modified strand that has the same number of nucleotides, but ends (segments 1 and 4) that are designed not to be complementary. The absorption curves of the nanotube solution are then compared with atomic force microscopy and fluorescent microscopy results, and the significance of these results is discussed.

Ultraviolet absorption measurements can follow the assembly and melting of DNA structures because double-stranded DNA has a lower absorbance at 260 nm than single-stranded DNA (hyperchromicity), so changes in absorbance are proportional to changes in the amount of unpaired DNA and slightly dependent on temperature [15]. Figure 9.4a on page 126 shows the formation and melting curves at 1  $\mu\text{M}$  strand concentration. The lower graph is a differential of absorption with temperature (numerically differentiated to a high order ( $n = 100$ ) polynomial fit of the data). The hysteretic cycle indicates kinetic barriers to nucleation. The formation process is not a two-state transition but has multiple intermediate states as indicated by the multiple peaks in the differential curve. The noise in the data at lower temperatures most likely arises from light scattering as the lattices form lattices of the order of the wavelength of light.

In comparison, a measurement of the DNA strand that is designed not to have complementary ends (segments 1 and 4) is plotted in Figure 9.4d. The formation and melting processes are reversible without hysteresis. This suggests that tiles are forming as expected – the inner segments 2 and 3 are each still self-complementary—and then no further assembly takes place because the tiles are unable to bind together. At 2.5- and 5-times higher concentrations, as shown in Figures 9.4b and 9.4c, an increasingly sharper second transition is observed in the formation process. The reason for this may be that at higher concentrations the tiles interact increasingly frequently and thus lattices form faster.

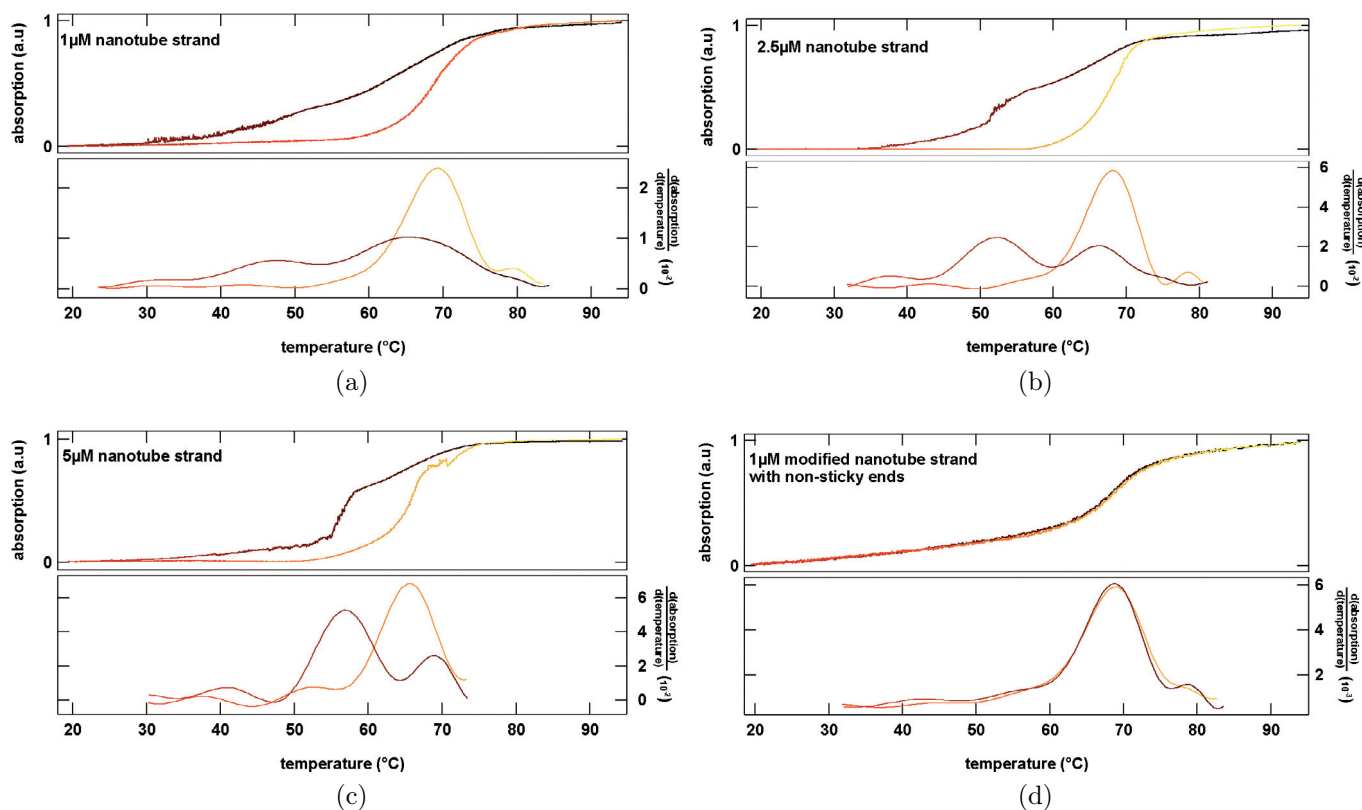


Figure 9.4: Assembly (darker line) and melting (lighter line) of DNA nanotubes in solution as measured by absorption at a wavelength of 260 nm. The lower graphs are differential absorption with respect to temperature (from fits to the data) illustrating assembly/melting transitions. The assembly process is clearly different to the melting process. *a)* 1  $\mu\text{M}$  concentration. *b)* 2.5  $\mu\text{M}$  concentration. *c)* 5  $\mu\text{M}$  concentration. *d)* A modified DNA sequence at 1  $\mu\text{M}$  concentration with an identical number of bases but with end segments (1 and 4) which are not complementary, so that the end segments should not hybridise. Thus it is expected that tiles form but no further development into lattices or nanotubes takes place. There appears to only one transition at a temperature similar to the higher transition in *a)*, confirming this hypothesis [5].

The melting processes all appear to exhibit two-state transitions of similar nature. They exhibit a single major peak in the differential curve. It has to be noted that such a behaviour is only observed reproducibly when the DNA strands have been carefully assembled in a previous cooling step. In an untreated sample, the whole spectrum of partially assembled DNA strands is present (as indicated in Figure 9.2), resulting in non-reproducible melting behaviour. Thus, initial cooling also serves to set a defined starting state for the melting experiments.

The hybridisation and melting curves of the individual segments 1, 2, 3 and 4 at 1  $\mu\text{M}$  concentration are shown in Figure 9.5. These all appear to be reversible and with little or

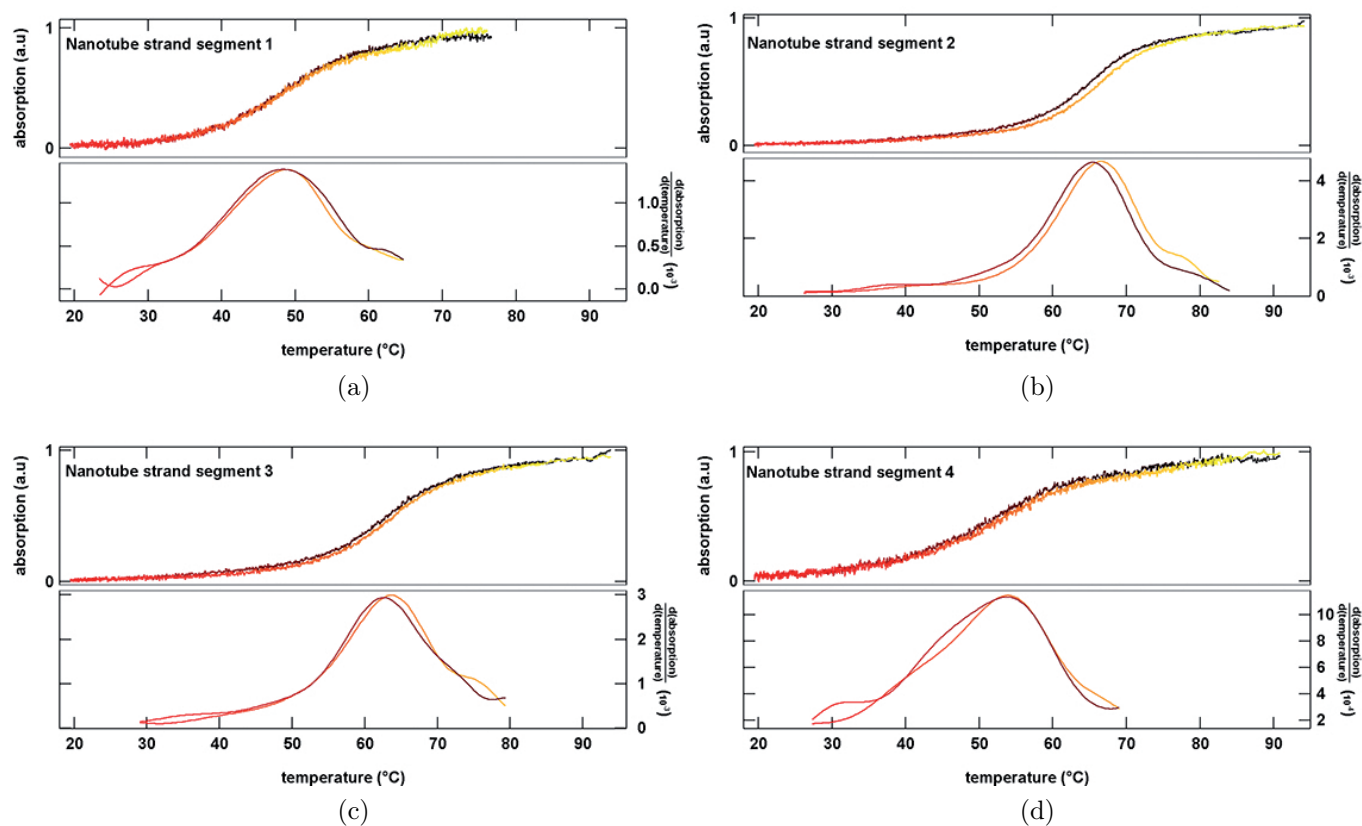


Figure 9.5: Hybridisation (darker line) and melting (lighter line) of the individual palindromic segments that together compose the sequence used for the DNA nanotubes. Segments 2 and 3 – the inner longer segments – which in the original sequence form the tile, have melting points close the highest temperature peak observed in the differential of the assembly of the tubes (Figure 9.4a), which indicates this is the peak of tile formation. Segments 1 and 4 have higher melting points than the next highest temperature peak observed in the differential of the assembly of the tubes (9.4a), indicating that co-operative effects are necessary for the lattice to form [5].

no hysteresis. The longer inner segments 2 and 3 have higher melting temperatures than the shorter ends. These are both close to the first transition observed in the formation of the  $1 \mu\text{M}$  DNA nanotube strand sample and indicate that this is likely to be the inner segments hybridising to form the double crossover tile as depicted in Figure 9.1b. The outer segments 1 and 4 are shorter and have a lower transition temperature. Hybridisation of these shorter segments are responsible for lattice and nanotube formation which occur at lower temperatures.

Experiments were performed to directly observe the structures as formation and melting took place. A DNA nanotube solution was sampled at certain temperatures. The sample volumes were immediately put on ice to stop continued structure formation. The sample

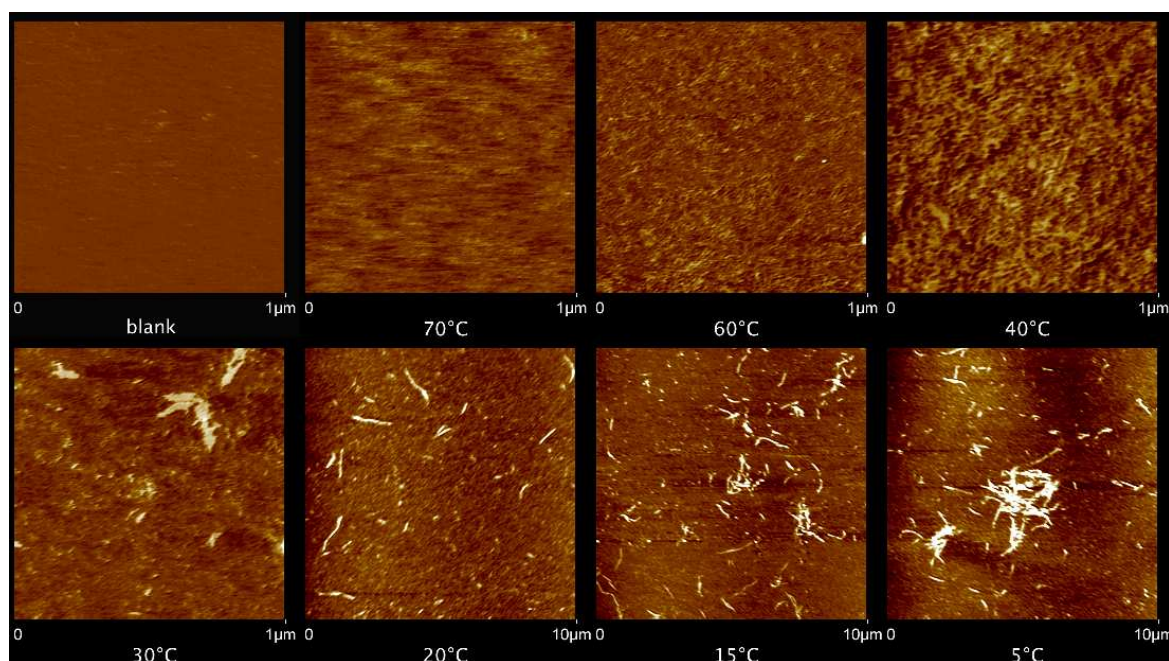


Figure 9.6: Atomic force microscopy images of a sequentially sampled DNA nanotube solution as it is cooled down from 95°C over 12 h. The first image is of a blank mica surface, following images are of samples taken at the indicated temperature. Height scale is 5 nm with lighter areas being higher. Several stages can be observed, initial binding of DNA (probably tile formation, resolution makes it difficult to clearly determine this) between 70 and 60°C, lattice formation between ~40 and ~30°C, and tube formation below ~30°C. This correlates well with the ultraviolet absorption measurement of assembly with the three peaks discernible in the assembly differential in Figure 9.4a [5].

was then imaged within a few minutes in buffer with atomic force microscopy.

The formation results are shown in Figure 9.7 on page 129. The first image is of the mica surface without DNA solution. The following images were sampled at the labelled temperature. At 70°C very little can be identified: presumably most of the DNA is still single-stranded at this high temperature. Between 70 and 60°C some structure forms: this is probably tiles as this corresponds to the temperature regime just after the first peak of the differential curve in Figure 9.4a. Between approximately 40 and 30°C lattices begin to appear: this correlates with being just after the second peak in the differential curve. Below approximately 30°C short nanotubes appear: this correlates with being just after the third peak in the differential curve. The tubes are relatively short compared to those in Figure 9.3a because the annealing protocol was 12 h as opposed to 48 h. The correlation between the atomic force microscopy images and the ultraviolet absorption measurements thus provides evidence for a hierarchy in the nature of the nanotube assembly.

The reverse process of nanotube melting by heating the solution was also observed and the results are shown in Figure 9.7 on page 129. The solution was heated over 12 h from 20 to over 75°C. The nanotubes are stable until at least 60°C and at 70°C there is little

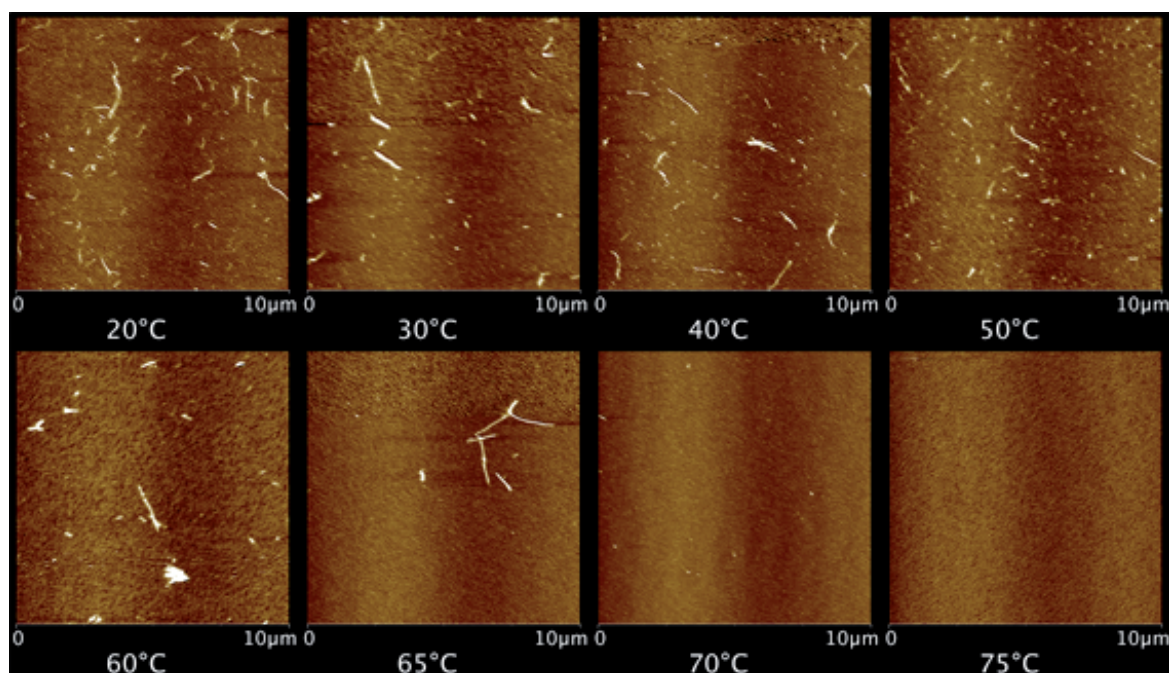


Figure 9.7: Atomic force microscopy images of a sequentially sampled DNA nanotube solution as it is heated from 20°C over 12 h. Height scale is 5 nm with lighter areas being higher. The tubes appear to be stable to approximately 70°C, and then melt rapidly above this temperature, no trace of them can be seen at 75°C. This correlates well with the ultraviolet absorptions measurement of of melting with the single peak discernible in the melting differential in Figure 9.4a [5].

sign of any remaining structure, while at 75°C no structure is seen. This again correlates with the ultraviolet absorption results in Figure 9.4a, where in the melting process a single transition is seen between 60 and 75°C. This is in agreement with Mao and colleagues who also measured ultraviolet absorption of a melting nanotube solution and saw no change until 60°C [20].

Observations with fluorescent microscopy also support these measurements. DNA nanotube solution was pipetted into a chamber between glass slides and stored at 4°C over night to allow the nanotubes to bind to the glass. This was then mounted on the microscope stage and heated while observing. The nanotubes in this case contained some (estimated 25%) DNA strands labelled with fluorescein. Fluorescein is pH dependent and the TAE buffer does change pH with temperature, but it is sufficient for qualitative visual observation. The results are shown in Figure 9.8 on page 130. Surface interactions with the glass may influence the stability of the nanotubes. However, it can be seen that the nanotubes appear to melt between 70 and 73°C, supporting the results from ultraviolet absorption measurements and atomic force microscopy images.

The significant difference in formation and melting processes is important. It is not observed in recent experiments on two-dimensional assemblies demonstrated by Winfree

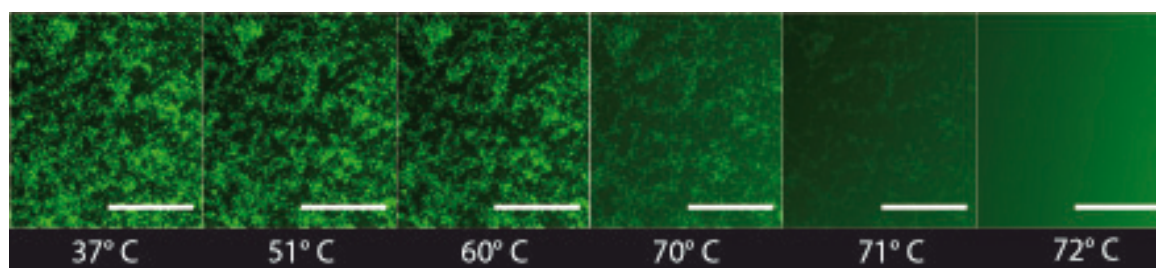


Figure 9.8: Low magnification fluorescence microscopy images of DNA nanotube solution. Individual tubes cannot be made out at this magnification – however, bulk behaviour of many tubes can be observed. The solution was heated in situ at  $8^{\circ}\text{C h}^{-1}$  and images were captured at the labelled temperatures. The scale bar is  $200\ \mu\text{m}$ . The tubes appear stable until approximately  $70^{\circ}\text{C}$ , and then melt within a few degrees of this temperature. Thus supports the results of the ultraviolet absorption and atomic force microscopy measurements [5].

[160]. These results show hysteresis but do not show a fundamental difference (as seen by the different shapes of the formation and melting curves supported by the atomic force microscopy results) between formation and melting observed in the nanotube structure.

The reason for this difference is thought to result from a co-operative effect. Once the nanotubes are formed there are few non-paired strands exposed, only those at the ends of the nanotubes and those in any defects. The nanotubes are a ‘closed’ structure apart from the ends. In two-dimensional structures, the relative portion of non-paired strands is higher because of the relatively larger edges and because the structure is ‘open’. This higher portion of paired strands in an almost closed structure suggests that it is significantly more stable (i.e. melting occurs at much higher temperatures) than open two-dimensional structures.

We have shown that a single, short and apparently simple DNA sequence can exhibit a rich spectrum of self-assembly phenomena. Accurate thermodynamic predictions for DNA nano-assemblies are difficult due to the presence of multi-strand interactions. In the case of the DNA nanotubes studied here an additional complication arises from palindromic subsequences and pseudoknotted higher-order structures. Rather than fitting experimental data to standard thermodynamic and kinetic theories, we have correlated ultraviolet absorption measurements with atomic force microscopy and fluorescence microscopy. This has demonstrated the formation and melting of DNA nanotubes, illustrating important differences between these processes. The differences can be understood in terms of cooperativity between segments of the sequence and their binding and, when contrasted with results from two-dimensional self-assembly, indicate that closed three-dimensional structures may be significantly more thermodynamically stable.

# Chapter 10

## Conclusion and outlook for self-assembly with DNA and self-assembly itself...

### Contents

---

<b>10.1 Overview</b>	<b>131</b>
<b>10.2 Future experiments</b>	<b>133</b>
<b>10.3 The future of understanding self-assembly</b>	<b>135</b>

---

The examples presented in this work demonstrate that DNA is a useful molecule for self-assembly. I hope that I have been able to give you an insight into the physical properties of DNA molecules, the experimental techniques that one can use, the wide variety of structures that one can assemble, and some of their potential uses.

Here I would like to give an overview of this work, discuss potential further experiments and applications, and look at what the future might bring for understanding both self-assembly with DNA and self-assembly itself.

### 10.1 Overview

We began with the idea that the study of self-assembly is the science of learning about how things put themselves together. Self-assembly processes occur throughout nature, from assembly of molecules at the nanoscale, the organisation of cellular structures into living organisms such as leaves, and the development of structure within the universe up to scales between galaxies.

More strictly, we defined self-assembly as requiring pre-existing structured components, reversible binding forces, an environment and a driving force.

DNA molecules can provide complex structure via sequences of the four base molecules, Watson-Crick base pairing via hydrogen bonds provides the binding forces, and these

are reversible within temperature ranges of 0-100 °C. Aqueous buffers with mono- and divalent salts and controlled pH provide a suitable environment. And thermal movement via Brownian motion provides a driving force.

Mechanical properties give DNA molecules their structural integrity, and optical (ultra-violet) properties provide a means for indirectly measuring its structure. Kinetics and thermodynamics provide methods for predicting or calculating particular properties and rates of structures assembled.

DNA self-assembly forms structures at energy minimums. As such, they are generally static equilibrium structures once formed. Both algorithmic (e.g. lattices) and templated (e.g. origami) structures can form, and current examples are considered single-level of assembly, with more complex multi-level structures aimed for in the future, particularly three-dimensional structures.

Assembly yield and the occurrence of defects created because of experimental stoichiometry challenges have been a problem. Use of methods such as sequence-symmetry in 'design', or templating via long strands in origami can reduce this.

We examined previously developed self-assembled DNA structures that are one, two, or three-dimensional, including chains, lattices, and helix bundles that can have designed tensions, twists, and curves.

Some of the common experimental equipment and methods along with detailed protocols are presented. These include absorption spectroscopy, gel electrophoresis, fluorescence, total internal reflection and super-resolution microscopy, and atomic force microscopy.

We give a review of self-assembled DNA structures that can be used as molecular devices. These couple information processing to mechanical action and/or sensing functions, allowing the generation of novel motors, walkers and biological sensors. Moreover, these can be now controlled via natural genetic mechanisms.

Examples of DNA self-assembly that were demonstrated in the laboratory during this work are given. Lattices comprising of just two sequences and nanotubes composed of a single sequence are shown. Long strands of DNA are stretched and aligned on atomically flat surfaces. Carbon nanotubes, DNA structures and colloidal quantum dots are combined, creating composites of these nanoscale materials.

Self-assembly of DNA structures has previously involved thermal heating and cooling, we demonstrate here an isothermal technique using dilution of denaturants. This allows incorporation of temperature-sensitive components.

Using DNA origami structures as supramolecular platforms, we attach fluorescent molecules in defined geometries and at defined distances from each other. With the aid of super-resolution microscopy techniques, we identify the fluorescent molecules below the diffraction limit with nanometer resolution. This makes these structures useful as nanoscopic rulers and calibration standards.

Finally, the stability of DNA structures and their assembly and melting properties are examined using DNA nanotubes. The assembly process is determined to be hierarchical, involving formation of tiles, lattices and then tubes, whereas melting occurs in a single step with a breaking open and melting of the tubes at high temperature. This indicates that the three-dimensional tubes have a high structural stability in contrast to two-dimensional

lattices. This stability will make them useful as components for DNA nanotechnology.

## 10.2 Future experiments

Two ideas that have been initially explored are presented here for future work.

The first involves a technique known as ‘Förster resonant energy transfer’ spectroscopy. Briefly, this makes use of ‘non-radiative’ transfer of energy from one fluorescent molecule to another via ‘dipole-dipole’ interactions. This process is dependent on the distance between the fluorescent molecules, and is optimal at ranges of 2-10 nm for particular pairs of fluorescent molecules. Changes in intensity of the molecule reflect this distance. By binding the fluorescent molecules to particular locations on a DNA structure, conformational changes in the structure can be measured.

One application of this is the measurement of the effect of proteins on DNA molecules. Particular proteins bind to double-stranded DNA at particular recognition sequences, and in doing so bend and twist the DNA. This is important in processes in cells such as transcription of DNA into RNA. One such protein is the TATA-box protein, so called because it binds to the sequence TATA. Limited measurements in two dimensions have been made of this process using Förster resonant energy transfer techniques, however, more detailed information in three dimensions is needed to fully understand this process.

Collecting this information may be possible by using an advanced form of the technique involving three different fluorescent molecules and fast successive pulsing of three different light sources (lasers) used to stimulate the fluorescent molecules. By assembling two-dimensional (rectangular) structures at the ends of the double-stranded TATA sequence and attaching fluorescent molecules at the corners, one should be able to measure the conformational changes of binding and unbinding of the TATA-box protein, and enhance our understanding of this process and more generally the transcription process.

The second idea involves the further development of DNA walkers, stemming from a combination of three ideas. Natural molecular walkers such as the protein kinesin can be attached to flat surfaces with their ‘legs’ projecting from the surface. ‘Microtubules’ placed on top of these can be propelled across the surface by the motion of the legs of many walkers. The proteins have a fuel source in the molecule ‘ATP’ and can achieve significant speed of the microtubules by making use of conversion of this molecule.

DNA walkers in comparison rely on DNA hybridisation processes, DNzyme activity, and Brownian motion. This results in very slow motion with considerably lower forces generated in comparison to the natural kinesin protein. However, electrophoresis can be used to direct the motion of DNA molecules, as discussed in Section 4.1.2. Moreover, by creating electrodes in a two- or three-dimensional configuration around a buffer solution containing DNA structures, and attaching voltage sources that can change the amplitude and polarity of the applied voltages, one can direct the DNA motion in multiple directions.

The challenge is to combine this with DNA walkers. I propose a system similar to that of the kinesin attached to a surface and microtubules. Here high concentrations of short single- or multiple-stranded DNA molecules bound at one end to the surface would

provide binding opportunities and act as walkers with legs projecting away from the surface. DNA nanotubes or other self-assembled DNA structures with additional extended single strands protruding from them would act in place of microtubules. Hybridisation between the extensions would provide binding to the surface (assisted perhaps by application of a suitable voltage in a suitable direction between electrodes). The hybridisation would be chosen to be such that it is weak enough to be intermittent, for example by changing the complementary sequence length, temperature, and perhaps denaturant concentration. By applying suitable voltages between electrodes, directed motion across the surface should be possible as the hybridisation between DNA strands form and break.

Initial experiments that I have completed demonstrate circular motion of long ( $\lambda$ ) DNA molecules and also of DNA nanotubes. These are fluorescently labelled and in weak buffer solution without salt. Four thin platinum electrode wires and voltages up to several volts were used. The voltages were applied with a slow sinusoidal (frequency approximately 1 Hz) and with appropriate phase differences between electrode pairs to achieve the circular motion. Care has to be taken that 'electroosmosis' does not have a significant effect.

These experiments thus could be advanced by attaching DNA molecules to the surface and adding appropriate single-stranded extensions to the molecular structures in solution so that they can intermittently bind to those on the surface. Additional binding sites on the DNA structures in solution might be used to bind and offload cargo such as nanoparticles on proteins that are in solution or on the surface, thus providing possibilities for cargo transport.

The two examples of experiments that could be completed in the future are just two of many:

- assembling origami structures into lattices, using either single or multiple types of origami structures
- assembling complex three-dimensional structures and 'crystals' of DNA
- achieving multiple levels of DNA self-assembly to create structures comprised of multiple components
- using DNA to organise other nano-objects such as carbon nanotubes on surfaces, possibly in order to create networks of transistors or other devices.
- combining DNA with other polymers such as 'block copolymers' to enhance assembly possibilities.
- using self-assembled DNA structures for biological sensing or as medical drugs or drug delivery systems
- using self-assembled DNA structures in systems and synthetic biology - a rapidly advancing field aiming to understand and reproduce the functional properties of living organisms that result from interactions of molecular complexes.

### 10.3 The future of understanding self-assembly

The last experiment mentioned above brings us back to the beginning. In the motivation I wrote about my childhood (and continued) wondering about why things in the natural world are as they are. Leaves, as an example. And leaves on trees are living organisms. Which are what systems and synthetic biology are trying to understand and reproduce.

We have learnt that self-assembly is also present in many other forms and at many other scales. DNA is not the only useful building block (structured particle) for self-assembly. As a scientist in this field of research, one often has to ask oneself if DNA molecules are really the best option for understanding the question we ask or assembling the structure we would like. In some cases the answer is yes, in others it is no. In those in which no is the answer, this is not a bad thing, it means that we as scientists have to learn more about other types of structured particles, environments, binding and driving forces that occur in the natural world. And in doing so work with other chemists, biologists, mathematicians, physicists and so forth on new sets of self-assembly problems. And one day we might be able to answer our wonderings about leaves...



# Bibliography

- [1] Sobey, T. L. In *Protocols in DNA Nanotechnology*; Humana Press (submitted), 2010.
- [2] Liedl, T.; Sobey, T.; Simmel, F. C. *Nano Today* **2007**, *2*, 36; 2.
- [3] Jungmann, R.; Liedl, T.; Sobey, T. L.; Shih, W.; Simmel, F. C. *Journal of the American Chemical Society* **2008**, *130*, 10062–10063.
- [4] Steinhauer, C.; Jungmann, R.; Sobey, T. L.; Simmel, F. C.; Tinnefeld, P. *Angewandte Chemie International Edition* **2009**, *48*, 8870–8873; 47.
- [5] Sobey, T. L.; Renner, S.; Simmel, F. C. *Journal of Physics-Condensed Matter* **2009**, *21*, art. no. 034112; 3.
- [6] Pelesko, J. A. *Self Assembly The Science of Things That Put Themselves Together*; Chapman & Hall, 2007.
- [7] Garrett, R. H.; Grisham, C. M. *Biochemistry*, 2nd ed.; Brooks/Cole, 1999.
- [8] ImageFromWikipedia [http://en.wikipedia.org/wiki/File:A-DNA,\\_B-DNA\\_and\\_Z-DNA.png](http://en.wikipedia.org/wiki/File:A-DNA,_B-DNA_and_Z-DNA.png), 2010.
- [9] Pierce, N. A. <http://www.nupack.org/>, 2010.
- [10] Dickerson, R. *Nucleic Acids Research* **1998**, *26*, 1906–1926.
- [11] Hugel, T.; Rief, M.; Seitz, M.; Gaub, H. E.; Netz, R. R. *Physical Review Letters* **2005**, *94*, 048301.
- [12] Storm, C.; Nelson, P. C. *Physical Review E* **2003**, *67*, 051906.
- [13] Kratky, O.; Porod, G. *Rec. Trav. Chim. Pays-Bas* **1949**, *68*, 1106–1123.
- [14] Poon, W. C. K.; Andelman, D. *Soft condensed matter physics in molecular and cell biology*; CRC Press, 2006.
- [15] Peyrard, M. *Nature Physics* **2006**, *2*, 13–14.
- [16] Beyer, S. *DNA-based molecular templates and devices*; Ludwig-Maximilians-Universitaet Muenchen, 2005.

- [17] Reuter, A. *DNA-basierte molekulare Maschinen und Aktuatoren*; Ludwig-Maximilians-Universitaet Muenchen, 2007.
- [18] IntegratedDNATechnologies <http://eu.idtdna.com/analyzer/applications/Instructions/Default.aspx?AnalyzerDefinitions=true#ExtinctionCoefficient>, 2010.
- [19] Cavaluzzi, M. J.; Borer, P. N. *Nucleic Acids Research* **2004**, *32*, e13.
- [20] Cantor, C. R.; Warshaw, M. M.; Shapiro, H. *Biopolymers* **1970**, *9*, 1059–1077.
- [21] Wartell, R. M.; Benight, A. S. *Physics Reports* **1985**, *126*, 67–107.
- [22] Pörschke, D. *Biophysical Chemistry* **1974**, *2*, 83–96.
- [23] Pack, G. R.; Lamm, G. *International Journal of Quantum Chemistry* **1993**, *48*.
- [24] OShaughnessy, B.; Yang, Q. *Physical Review Letters* **2005**, *94*.
- [25] Friedrichs, E. *Synthetische Transkriptionsnetzwerke*; Technische Universitaet Muenchen, 2009.
- [26] Bloomfield, V. A.; Crothers, D. M.; Tinoco, I. *Nucleic Acid Structures, Properties and Functions*; University Science Books, 2000.
- [27] Reynaldo, L. P.; Vologodskii, A. V.; Neri, B. P.; Lyamichev, V. I. *Journal of Molecular Biology* **2000**, *297*, 511–520.
- [28] Turberfield, A. J.; Mitchell, J. C.; Yurke, B.; Mills, A. P.; Blakey, M. I.; Simmel, F. C. *Physical Review Letters* **2003**, *90*, 118102.
- [29] Green, S. J.; Lubrich, D.; Turberfield, A. J. *Biophysical Journal* **2006**, *91*, 2966–2975.
- [30] SantaLucia, J.; Hicks, D. *Annual Review of Biophysics and Biomolecular Structure* **2004**, *33*, 415–440.
- [31] SantaLucia, J.; Hicks, D. *Annual Review of Biophysics and Biomolecular Structure* **2004**, *33*, 415–440.
- [32] Dirks, R. M.; Bois, J. S.; Schaeffer, J. M.; Winfree, E.; Pierce, N. A. *SIAM Review* **2007**, *49*, 65–88; 1.
- [33] ImageFromWikipedia [http://en.wikipedia.org/wiki/Holliday\\_junction](http://en.wikipedia.org/wiki/Holliday_junction), 2010.
- [34] Chen, J.; Seeman, N. C. *Nature* **1991**, *350*, 631–633.
- [35] Park, S. H.; Yin, P.; Liu, Y.; Reif, J. H.; LaBean, T. H.; Yan, H. *Nano Letters* **2005**, *5*, 729–733.

- [36] Liu, D.; Wang, M.; Deng, Z.; Walulu, R.; Mao, C. *Journal of the American Chemical Society* **2004**, *126*, 2324–2325.
- [37] He, Y.; Tian, Y.; Chen, Y.; Deng, Z. X.; Ribbe, A. E.; Mao, C. D. *Angewandte Chemie-International Edition* **2005**, *44*, 6694; 41.
- [38] Fujibayashi, K.; Hariadi, R.; Park, S. H.; Winfree, E.; Murata, S. *Nano Letters* **2008**, *8*, 3554.
- [39] Andersen, E. S.; Dong, M.; Nielsen, M. M.; Jahn, K.; Subramani, R.; Mamdouh, W.; Golas, M. M.; Sander, B.; Stark, H.; Oliveira, C. L. P.; Pedersen, J. S.; Birkedal, V.; Besenbacher, F.; Gothelf, K. V.; Kjems, J. *Nature* **2009**, *459*, 73–76.
- [40] He, Y.; Ye, T.; Su, M.; Zhang, C.; Ribbe, A. E.; Jiang, W.; Mao, C. D. *Nature* **2008**, *452*, 198–202; 7184.
- [41] Liedl, T.; Hogberg, B.; Tytell, J.; Ingber, D. E.; Shih, W. M. *Nat Nano* **2010**, *5*, 520–524.
- [42] Dietz, H.; Douglas, S. M.; Shih, W. M. *Science* **2009**, *325*, 725–730; 5941.
- [43] Liu, H. P.; Chen, Y.; He, Y.; Ribbe, A. E.; Mao, C. D. *Angewandte Chemie-International Edition* **2006**, *45*, 1942–1945; 12.
- [44] Soloveichik, D.; Cook, M.; :10.1007/s11047-007-9036-x Winfree, E. D. *Natural Computing* **2008**, *7*, 203–218; 2.
- [45] Shih, W. M.; Quispe, J. D.; Joyce, G. F. *Nature* **2004**, *427*, 618–621.
- [46] Rothmund, P. W. K. *Nature* **2006**, *440*, 297–302.
- [47] Tataurov, A. V.; You, Y.; Owczarzy, R. *Biophysical Chemistry* **2008**, *133*, 66–70; 1-3.
- [48] Lu, M.; Guo, Q.; Marky, L. A.; Seeman, N. C.; Kallenbach, N. R. *Journal of Molecular Biology* **1992**, *223*, 781–789; 3.
- [49] ImageFromWikipedia [http://en.wikipedia.org/wiki/Beer-Lambert\\_law](http://en.wikipedia.org/wiki/Beer-Lambert_law), 2010.
- [50] ImageFromScienceofspectroscopy <http://scienceofspectroscopy.info/>, 2010.
- [51] Sambrook, J.; Russel, D. W. *Molecular cloning - A laboratory manual*; Cold Spring Harbor, 2001.
- [52] ImageFromUgent [http://www.aquaculture.ugent.be/coursmat/online20courses/ATA/img/e\\_phor.jpg](http://www.aquaculture.ugent.be/coursmat/online20courses/ATA/img/e_phor.jpg), 2010.
- [53] Viovy, J. *Reviews of Modern Physics* **2000**, *72*, 813.

- [54] Olympus *Shining Fluorescent Details - Basics of Light Microscopy and Imaging*, 2010.
- [55] MolecularExpressions <http://micro.magnet.fsu.edu/primer/lightand-color/fluoroexcitation.html>, 2010.
- [56] Axelrod, D. *Traffic* **2001**, *2*, 764–774.
- [57] Tirftechnologies <http://www.tirftechnologies.com/>, 2010.
- [58] Nikon <http://www.microscopyu.com/articles/fluorescence/tirf/tirfintro.html>, 2010.
- [59] Olympus <http://www.olympusmicro.com/primer/techniques/fluorescence/tirf/tirfintro.html>, 2010.
- [60] Hell, S. W. *Science* **2007**, *316*, 1153–1158.
- [61] Hell, S. W. *Nat Meth* **2009**, *6*, 24–32.
- [62] Heilemann, M.; van de Linde, S.; Schüttpelz, M.; Kasper, R.; Seefeldt, B.; Mukherjee, A.; Tinnefeld, P.; Sauer, M. *Angewandte Chemie International Edition* **2008**, *47*, 6172–6176.
- [63] DigitalInstruments *Scanning Probe Microscopy Training Notebook*; Veeco, 2001.
- [64] Prater, C. B.; Maivald, P. G.; Kjoller, K. J.; Heaton, M. J. *Tapping Mode Imaging Applications and Technology - application note*, 2008.
- [65] Sugimoto, N.; Nakano, S.; Yoneyama, M.; Honda, K. *Nucleic Acids Research* **1996**, *24*, 4501–4505; 22.
- [66] SantaLucia, J.; Allawi, H. T.; Seneviratne, A. *Biochemistry* **1996**, *35*, 3555–3562; 11.
- [67] Breslauer, K. J.; Frank, R.; Blocker, H.; Marky, L. A. *Proceedings of the National Academy of Sciences of the United States of America* **1986**, *83*, 3746–3750; 11.
- [68] Doyle, P. S.; Ladoux, B.; Viovy, J. L. *Physical Review Letters* **2000**, *84*, 4769–4772; 20.
- [69] DigitalInstruments *Guidelines for Fluid Operation with a MultiMode AFM Support Note No. 290*; Veeco, 2001.
- [70] Balzani, V.; Venturi, M.; Credi, A. *Molecular devices and machines: a journey into the nano world*; Wiley-VCH, 2003.
- [71] Finer, J. T.; Simmons, R. M.; Spudich, J. A. *Nature* **1994**, *368*, 113–119.

- [72] Howard, J. *Mechanics of Motor Proteins and the Cytoskeleton*; Sinauer Associates, 2001.
- [73] Svoboda, K.; Schmidt, C. F.; Schnapp, B. J.; Block, S. M. *Nature* **1993**, *365*, 721–727.
- [74] Beissenhirtz, M. K.; Willner, I. *Organic & Biomolecular Chemistry* **2006**, *4*, 3392.
- [75] Lakowicz, J. R. *Principles of Fluorescence Spectroscopy*, 2nd ed.; Springer, Berlin, 1999.
- [76] Hazarika, P.; Ceyhan, B.; Niemeyer, C. M. *Angewandte Chemie International Edition* **2004**, *43*, 6469–6471.
- [77] Liedl, T.; Olapinski, M.; Simmel, F. C. *Angewandte Chemie International Edition* **2006**, *45*, 5007–5010.
- [78] Liu, D.; Bruckbauer, A.; Abell, C.; Balasubramanian, S.; Kang, D.; Klenerman, D.; Zhou, D. *Journal of the American Chemical Society* **2006**, *128*, 2067–2071.
- [79] Buranachai, C.; McKinney, S. A.; Ha, T. *Nano Letters* **2006**, *6*, 496–500.
- [80] Müller, B. K.; Reuter, A.; Simmel, F. C.; Lamb, D. C. *Nano Letters* **2006**, *6*, 2814–2820.
- [81] Feng, L.; Park, S. H.; Reif, J. H.; Yan, H. *Angewandte Chemie International Edition* **2003**, *42*, 4342–4346.
- [82] Yan, H.; Zhang, X.; Shen, Z.; Seeman, N. C. *Nature* **2002**, *415*, 62–65.
- [83] Endo, M.; Sugiyama, H. *Nucleic Acids Symposium Series* **2009**, *53*, 81–82.
- [84] Shu, W.; Liu, D.; Watari, M.; Riener, C. K.; Strunz, T.; Welland, M. E.; Balasubramanian, S.; McKendry, R. A. *Journal of the American Chemical Society* **2005**, *127*, 17054–17060.
- [85] Yang, X.; Vologodskii, A. V.; Liu, B.; Kemper, B.; Seeman, N. C. *Biopolymers* **1998**, *45*, 69–83.
- [86] Yurke, B.; Turberfield, A. J.; Mills, A. P.; Simmel, F. C.; Neumann, J. L. *Nature* **2000**, *406*, 605–608; PMID: 10949296.
- [87] Simmel, F. C.; Yurke, B. *Physical Review E* **2001**, *63*, 041913.
- [88] Chen, Y.; Wang, M.; Mao, C. *Angewandte Chemie International Edition* **2004**, *43*, 3554–3557.
- [89] Chhabra, R.; Sharma, J.; Liu, Y.; Yan, H. *Nano Letters* **2006**, *6*, 978–983.

- [90] Seeman, N. *Trends in Biochemical Sciences* **2005**, *30*, 119–125.
- [91] Li, J. J.; Tan, W. *Nano Letters* **2002**, *2*, 315–318.
- [92] Makita, N.; Inoue, S.; Akaike, T.; Maruyama, A. *Nucleic Acids Symposium Series* **2004**, *48*, 173–174.
- [93] Ackermann, D.; Schmidt, T. L.; Hannam, J. S.; Purohit, C. S.; Heckel, A.; Famulok, M. *Nature Nanotechnology* **2010**, *5*, 436–442.
- [94] Niemeyer, C. M.; Adler, M.; Lenhert, S.; Gao, S.; Fuchs, H.; Chi, L. *Chembiochem: A European Journal of Chemical Biology* **2001**, *2*, 260–264; PMID: 11828453.
- [95] Chen, Y.; Lee, S.; Mao, C. *Angewandte Chemie International Edition* **2004**, *43*, 5335–5338.
- [96] Chen, Y.; Mao, C. *Journal of the American Chemical Society* **2004**, *126*, 13240–13241.
- [97] Liu, D.; Balasubramanian, S. *Angewandte Chemie International Edition* **2003**, *42*, 5734–5736.
- [98] Liedl, T.; Simmel, F. C. *Nano Letters* **2005**, *5*, 1894–1898.
- [99] Seela, F.; Budow, S. *Helvetica Chimica Acta* **2006**, *89*, 1978–1985.
- [100] Schlossbauer, A.; Warncke, S.; Gramlich, P. M. E.; Kecht, J.; Manetto, A.; Carell, T.; Bein, T. *Angewandte Chemie International Edition* **2010**, *49*, 4734–4737.
- [101] Shin, J.; Pierce, N. A. *Journal of the American Chemical Society* **2004**, *126*, 10834–10835.
- [102] Sherman, W. B.; Seeman, N. C. *Nano Letters* **2004**, *4*, 1203–1207.
- [103] Tian, Y.; Mao, C. *Journal of the American Chemical Society* **2004**, *126*, 11410–11411.
- [104] Yin, P.; Yan, H.; Daniell, X. G.; Turberfield, A. J.; Reif, J. H. *Angewandte Chemie* **2004**, *116*, 5014–5019.
- [105] Tian, Y.; He, Y.; Chen, Y.; Yin, P.; Mao, C. *Angewandte Chemie International Edition* **2005**, *44*, 4355–4358.
- [106] Pei, R.; Taylor, S. K.; Stefanovic, D.; Rudchenko, S.; Mitchell, T. E.; Stojanovic, M. N. *Journal of the American Chemical Society* **2006**, *128*, 12693–12699.
- [107] Lund, K.; Manzo, A. J.; Dabby, N.; Michelotti, N.; Johnson-Buck, A.; Nangreave, J.; Taylor, S.; Pei, R.; Stojanovic, M. N.; Walter, N. G.; Winfree, E.; Yan, H. *Nature* **2010**, *465*, 206–210.

- [108] Gu, H.; Chao, J.; Xiao, S.; Seeman, N. C. *Nature* **2010**, *465*, 202–205.
- [109] Jhaveri, S.; Rajendran, M.; Ellington, A. D. *Nature Biotechnology* **2000**, *18*, 1293–1297.
- [110] Potyrailo, R. A.; Conrad, R. C.; Ellington, A. D.; Hieftje, G. M. *Analytical Chemistry* **1998**, *70*, 3419–3425.
- [111] Stojanovic, M. N.; de Prada, P.; Landry, D. W. *Journal of the American Chemical Society* **2001**, *123*, 4928–4931.
- [112] Tsai, D. E.; Kenan, D. J.; Keene, J. D. *Proceedings of the National Academy of Sciences of the United States of America* **1992**, *89*, 8864–8868.
- [113] Xu, W.; Ellington, A. D. *Proceedings of the National Academy of Sciences of the United States of America* **1996**, *93*, 7475–7480.
- [114] Dittmer, W. U.; Reuter, A.; Simmel, F. C. *Angewandte Chemie International Edition* **2004**, *43*, 3550–3553.
- [115] Lin, C.; Katilius, E.; Liu, Y.; Zhang, J.; Yan, H. *Angewandte Chemie International Edition* **2006**, *45*, 5296–5301.
- [116] Liu, Y.; Lin, C.; Li, H.; Yan, H. *Angewandte Chemie International Edition* **2005**, *44*, 4333–4338.
- [117] Stojanovic, M. N.; Kolpashchikov, D. M. *Journal of the American Chemical Society* **2004**, *126*, 9266–9270.
- [118] Beyer, S. *Nucleic Acids Research* **2006**, *34*, 1581–1587.
- [119] Stojanovic, M. N.; de Prada, P.; Landry, D. W. *Chembiochem: A European Journal of Chemical Biology* **2001**, *2*, 411–415; PMID: 11828471.
- [120] Weizmann, Y.; Beissenhirtz, M. K.; Cheglakov, Z.; Nowarski, R.; Kotler, M.; Willner, I. *Angewandte Chemie International Edition* **2006**, *45*, 7384–7388.
- [121] Alberts, B.; Johnson, A.; Walter, P.; Lewis, J.; Raff, M.; Roberts, K. *Molecular Biology of the Cell*, 5th ed.; Taylor & Francis, 2007.
- [122] Noireaux, V. *Proceedings of the National Academy of Sciences* **2003**, *100*, 12672–12677.
- [123] Noireaux, V. *Proceedings of the National Academy of Sciences* **2004**, *101*, 17669–17674.
- [124] Dittmer, W. U.; Kempfer, S.; Rädler, J. O.; Simmel, F. C. *Small* **2005**, *1*, 709–712.

- [125] Hamada, S.; Murata, S. *Angewandte Chemie International Edition* **2009**, *48*, 6820–6823.
- [126] Zheng, M.; Jagota, A.; Semke, E. D.; Diner, B. A.; Mclean, R. S.; Lustig, S. R.; Richardson, R. E.; Tassi, N. G. *Nat Mater* **2003**, *2*, 338–342.
- [127] Blake, R.; Delcourt, S. *Nucl. Acids Res.* **1996**, *24*, 2095–2103.
- [128] McConaughy, B. L.; Laird, C. D.; McCarthy, B. J. *Biochemistry* **1969**, *8*, 3289–3295; PMID: 4980190.
- [129] Mathieu, F.; Liao, S.; Kopatsch, J.; Wang, T.; Mao, C.; Seeman, N. C. *Nano Letters* **2005**, *5*, 661–665.
- [130] SantaLucia, J. *Proceedings of the National Academy of Sciences of the United States of America* **1998**, *95*, 1460–1465.
- [131] Hutton, J. R. *Nucleic Acids Research* **1977**, *4*, 3537–3555; PMID: 928068 PMCID: 342670.
- [132] Liu, H.; Chen, Y.; He, Y.; Ribbe, A. E.; Mao, C. *Angewandte Chemie International Edition* **2006**, *45*, 1942–1945.
- [133] Hell, S. W. *Nature Methods* **2009**, *6*, 24–32.
- [134] Gordon, M. P. *Proceedings of the National Academy of Sciences* **2004**, *101*, 6462–6465.
- [135] Heinlein, T.; Biebricher, A.; Schlueter, P.; Roth, C. M.; Herten, D.; Wolfrum, J.; Heilemann, M.; Mueller, C.; Tinnefeld, P.; Sauer, M. *ChemPhysChem* **2005**, *6*, 949–955.
- [136] Qu, X. *Proceedings of the National Academy of Sciences* **2004**, *101*, 11298–11303.
- [137] Rust, M. J.; Bates, M.; Zhuang, X. *Nature Methods* **2006**, *3*, 793–796.
- [138] Wiggins, P. A.; van der Heijden, T.; Moreno-Herrero, F.; Spakowitz, A.; Phillips, R.; Widom, J.; Dekker, C.; Nelson, P. C. *Nature Nanotechnology* **2006**, *1*, 137–141.
- [139] Steinhauer, C.; Forthmann, C.; Vogelsang, J.; Tinnefeld, P. *Journal of the American Chemical Society* **2008**, *130*, 16840–16841.
- [140] Vogelsang, J.; Kasper, R.; Steinhauer, C.; Person, B.; Heilemann, M.; Sauer, M.; Tinnefeld, P. *Angewandte Chemie International Edition* **2008**, *47*, 5465–5469.
- [141] van de Linde, S.; Endesfelder, U.; Mukherjee, A.; Schüttpelz, M.; Wiebusch, G.; Wolter, S.; Heilemann, M.; Sauer, M. *Photochemical & Photobiological Sciences* **2009**, *8*, 465.

- [142] Vogelsang, J.; Cordes, T.; Forthmann, C.; Steinhauer, C.; Tinnefeld, P. *Proceedings of the National Academy of Sciences* **2009**, *106*, 8107–8112.
- [143] Thompson, R. E.; Larson, D. R.; Webb, W. W. *Biophysical Journal* **2002**, *82*, 2775–2783.
- [144] Heilemann, M.; Margeat, E.; Kasper, R.; Sauer, M.; Tinnefeld, P. *Journal of the American Chemical Society* **2005**, *127*, 3801–3806.
- [145] Douglas, S. M.; Dietz, H.; Liedl, T.; Högberg, B.; Graf, F.; Shih, W. M. *Nature* **2009**, *459*, 414–418.
- [146] Shen, W.; Zhong, H.; Neff, D.; Norton, M. L. *Journal of the American Chemical Society* **2009**, *131*, 6660–6661.
- [147] Andronescu, M.; Zhang, Z. C.; Condon, A. *Journal of Molecular Biology* **2005**, *345*, 987–1001.
- [148] Bois, J. S. *Nucleic Acids Research* **2005**, *33*, 4090–4095.
- [149] Dimitrov, R.; Zuker, M. *Biophysical Journal* **2004**, *87*, 215–226.
- [150] Dirks, R. M.; Pierce, N. A. *Journal of Computational Chemistry* **2004**, *25*, 1295–1304.
- [151] Dirks, R. M.; Bois, J. S.; Schaeffer, J. M.; Winfree, E.; Pierce, N. A. *SIAM Review* **2007**, *49*, 65.
- [152] Atkins, P. W.; Höpfner, A. *Physikalische Chemie*, 3rd ed.; Wiley-VCH, 2002.
- [153] Hou, S.; Wang, J.; Martin, C. R. *Journal of the American Chemical Society* **2005**, *127*, 8586–8587.
- [154] Kuzuya, A.; Wang, R.; Sha, R.; Seeman, N. C. *Nano Letters* **2007**, *7*, 1757–1763.
- [155] Liu, D.; Park, S. H.; Reif, J. H.; LaBean, T. H. *Proceedings of the National Academy of Sciences of the United States of America* **2004**, *101*, 717–722.
- [156] Mitchell, J. C.; Harris, J. R.; Malo, J.; Bath, J.; Turberfield, A. J. *Journal of the American Chemical Society* **2004**, *126*, 16342–16343.
- [157] O'Neill, P.; Rothmund, P. W. K.; Kumar, A.; Fygenson, D. K. *Nano Letters* **2006**, *6*, 1379–1383.
- [158] Rothmund, P. W. K.; Ekani-Nkodo, A.; Papadakis, N.; Kumar, A.; Fygenson, D. K.; Winfree, E. *Journal of the American Chemical Society* **2004**, *126*, 16344–16352.
- [159] Lin, C.; Ke, Y.; Liu, Y.; Mertig, M.; Gu, J.; Yan, H. *Angewandte Chemie International Edition* **2007**, *46*, 6089–6092.

- [160] Schulman, R.; Winfree, E. *Proceedings of the National Academy of Sciences* **2007**, *104*, 15236–15241.

## Acknowledgements

My sincere thanks go to those who have helped me with this project:

- Professor Friedrich Simmel for taking me on unseen and giving me this opportunity. It has been a challenge and I believe we have both benefited and learnt from the experience. Thank you very much!
- Professor Philip Tinnefeld for co-supervising my work, helping out with our collaboration and publication, and supporting my IDK membership, thank you.
- Helene Budjarek and Erika Bischofs, für Eure unschätzbare Hilfe und Begleitung, ohne Euch wäre es alles nichts!
- The Arbeitsgruppe, Stefan Beyer, Tim Liedl, Andreas Reuter, Michael Olapinski, Ralf Jungmann, Stefan Renner and all the others that have been around, for the collegial atmosphere, putting up with my German, and the occasional beer. Eike I would especially like to thank, it hasn't always been easy, but I appreciate your support. Danke.
- Marie-Christine Blüm, Marilena Pinto, and Evelyn Morgenroth for helping out an Aussie in need and sharing the Bavarian weather...
- The IDK colleagues, for being in it together.
- The International Doctorate Program NanoBioTechnology and Elite Network of Bavaria, for the valuable financial support and workshops.
- Professor Jörg Kotthaus, for initially forwarding on my doctoral application, and for his welcome after I arrived and the words of support.
- Martina Jüttner, für Deine immer freundliche Unterstützung und Lächeln.
- Burkhard Lewerich, Lokman Ho, Anton Belikov and Diliانا Belikova, André Hedler and Family Hedler, Torsten Frosch, Alexandra Wark, Annabelle Burian, and the others, for the most important things: the little things.
- Herr Domanov und Frau Domanova, dass Sie mich herzlich willkommen in Ihrer Familie geheißen haben!
- Westa, es wäre für mich die größte Freude überhaupt, wenn wir noch weiter machen können. Drücken wir mal die Daumen.
- Mum and Dad, El and Dave, and Mops, for letting me come to Europe but still answering my telephone calls and welcoming me when I come home. . .



# Résumé

Thomas Leslie Sobey

Single, Australian nationality

02/03/1981 Born in Albury, Australia  
1986-1991 Albury West Public School  
1992-1998 Albury High School  
1999-2004 Bachelor of Science with Honours Class 1(Physics),  
Bachelor of Commerce with Merit (Finance),  
University of New South Wales  
2005-2006 Scientist, Australian Defence Science and Technology Organisation  
2006-2010 Doctoral candidate, Ludwig-Maximilians-Universität, München  
Supervisor: Professor Friedrich Simmel

Munich 15/07/2010